BROADBAND FIBRE PARAMETRIC AMPLIFIERS

VLADIMIR GORDIENKO

Doctor of Philosophy

ASTON UNIVERSITY

April 2018

Aston University

Broadband fibre parametric amplifiers

Gordienko Vladimir

Doctor of Philosophy

2018

Summary

This thesis explores the broadband fibre optical parametric amplifiers (FOPAs) to develop the FOPA ability to provide broadband amplification anywhere in the low-loss transmission window and to make FOPA an enabling technology for future ultra-wide bandwidth high-speed optical communications. A number of techniques have been implemented to demonstrate an exceptionally wide and flat FOPA gain of 10.5±0.5 dB over 102 nm bandwidth on a single side of the FOPA pump. A flat gain spectrum is targeted here because FOPA is prone to large gain variation which has a particularly strong negative impact on amplified signals in FOPA. The FOPA dependence on gain fibre length, pump wavelength and pump power has been experimentally investigated. The parametric gain bandwidth enhancement by a forward Raman gain invoked by the same pump has been demonstrated. Gain spectrum shaping by pump polarisation tuning has been explored and has allowed for a significant gain spectrum flatness improvement. A concept of cascading low gain stages has been introduced as a way to achieve a high gain with low variation across a wide bandwidth. It is envisaged that gain of ~20±1.5 dB over >100 nm can be achieved using this approach. Additionally, a reliance of the FOPA on Erbium doped fibre amplifiers (EDFAs) for pump amplification, which restricts the FOPA operating range, has been addressed by demonstrating a high pump power (>1 W) EDFA-free FOPA for the first time. In this experiment a Raman amplification was used instead of an EDFA to amplify the FOPA pump and thus to grant a required flexibility for FOPA operation anywhere in the low-loss transmission window. In summary, this thesis has demonstrated the FOPA ability to provide an ultra-wide amplification and has highlighted a way towards obtaining an optical gain in arbitrary spectral regions.

Keywords: fibre optical parametric amplifier, fibre optical amplification, optical phase conjugation, Raman amplification, fibre optical communications.

ACKNOWLEDGEMENTS

I would like to thank my supervisor Prof Nick Doran for giving me the opportunity to study for PhD at Aston University. I am deeply grateful to him for the highly-competent guidance, the remarkable patience and the great support.

I would like to express my gratitude to my associate supervisor Dr Marc Stephens for everything I learnt from him and the enormous assistance in the lab and with the writing. His cheerfulness and friendly advises have also helped me a lot.

I would like to thank the II-VI and Dr Ian McClean for the financial support which clearly made a difference.

I would like to thank the Furukawa Electric and particularly Dr Shigehiro Takasaka and Dr Ryuichi Sugizaki for provision of the fibre which allowed for my best experimental results.

I would like to thank Dr Filipe Ferreira for the code he provided for my simulations and readily adapted for my needs.

I would like to thank Dr Ian Phillips for his general support in the lab and particularly for setting up signals for my experiment.

I would like to thank Prof Keith Blow for lessons on fundamental fibre optics and Dr Vladislav Dvoyrin for useful discussions on topics adjacent to my research.

I also would like to thank Asif Iqbal, Mohammad Al-Khateeb, Auro Perego, Morteza Kamalian Kopae and Dr Srikanth Sugavanam for their help and advices when I needed it.

Finally, a special thanks to my wife Tetyana Gordienko for continuous support and to my sons Artem and Kirill for inspiration.

TABLE OF CONTENTS

LIST OF ABBREVIATIONS

ASE	amplified spontaneous emission
B2B	back-to-back
DCF	dispersion compensating fibre
DSF	dispersion shifted fibre
EDFA	Erbium-doped fibre amplifier
FBG	fibre Bragg grating
FOPA	fibre optical parametric amplifier
FWM	four wave mixing
GV	gain variation
GVD	group velocity dispersion
HNLF	highly nonlinear fibre
NF	noise figure
NLSE	nonlinear Schrodinger equation
OPC	optical phase conjugation
OSA	optical spectrum analyser
OSNR	optical signal-to-noise ratio
PBS	polarisation beam splitter
PC	polarisation controller
PM	phase modulator
PMD	polarisation mode dispersion
QPSK	quadrature phase shift keying
RA-OPC	Raman-assisted optical phase conjugation
RF	radio frequency
RIN	relative intensity noise
SBS	stimulated Brillouin scattering
SC	supercontinuum
SPM	self-phase modulation
SRS	stimulated Raman scattering
SSMF	standard single mode fibre
TL	tuneable laser
VOA	variable optical attenuator
WDM	wavelength division multiplexer

XPM	cross-phase modulation
YDFA	Ytterbium-doped fibre amplifier
ZDW	zero dispersion wavelength
ZMDW	zero material dispersion wavelength

LIST OF FIGURES

LIST OF TABLES

LIST OF PUBLICATIONS

Peer-reviewed

1. M. F. C. Stephens, M. Tan, **V. Gordienko**, P. Harper, and N. J. Doran, "In-line and cascaded DWDM transmission using a 15dB net-gain polarization-insensitive fiber optical parametric amplifier," *Opt. Express*, vol. 25, no. 20, pp. 24312–24325, Oct. 2017.
2. **V. Gordienko**, M. F. C. Stephens, and N. J. Doran, "Broadband gain-spectrum measurement for fiber optical parametric and Raman amplifiers," *IEEE Photonics Technol. Lett*, vol. 29, no. 16, pp. 1399–1402, Aug. 2017.
3. M. F. C. Stephens, **V. Gordienko**, and N. J. Doran, "20 dB net-gain polarization-insensitive fiber optical parametric amplifier with >2 THz bandwidth," *Optics Express*, vol. 25, no. 9, pp. 10597–10609, May 2017.
4. **V. Gordienko**, M. F. C. Stephens, A. E. El-Taher, and N. J. Doran, "Ultra-flat wideband single-pump Raman-enhanced parametric amplification," *Optics Express*, vol. 25, no. 5, pp. 4810–4818, Mar. 2017.
5. A. D. Ellis, M. Tan, M. A. Iqbal, M. A. Z. Al-Khateeb, **V. Gordienko**, G. Saavedra, S. Fabbri, M. F. C. Stephens, M. E. McCarthy, A. Perentos, I. D. Phillips, D. Lavery, G. Liga, R. Maher, P. Harper, N. J. Doran, S. K. Turitsyn, S. Sygletos, and P. Bayvel, "4 Tb/s transmission reach enhancement using 10 × 400 Gb/s super-channels and polarization insensitive dual band optical phase conjugation," *J. Lightw. Technol.*, vol. 34, no. 8, pp. 1717–1723, Apr. 2016.

Conference proceedings

1. M. F. C. Stephens, **V. Gordienko**, and N. J. Doran, "Reduced crosstalk, polarization insensitive fiber optical parametric amplifier (PI FOPA) for WDM applications," in *Optical Fiber Commun. Conf. and Exhibition (OFC)*, San Diego, CA, 2018, paper W3D.4.
2. **V. Gordienko**, M. F. C. Stephens, F. M. Ferreira, and N. J. Doran, "Gain spectrum shaping technique for one-pump fibre optical parametric amplifier (FOPA)," in *43nd European Conf. on Optical Commun. (ECOC)*, Gothenburg, Sweden, 2017, paper P1.SC1.16.

3. **V. Gordienko**, M. F. C. Stephens, and N. J. Doran, "Towards wide-bandwidth ultra-flat FOPAs," in *19th Int. Conf. on Transparent Optical Networks (ICTON)*, Girona, Spain, 2017, paper We.D5.1 (invited).
4. M. F. C. Stephens, **V. Gordienko**, and N. J. Doran, "20dB net-gain fiber optical parametric amplification of 18× 120Gb/s polarization-multiplexed signals," in *Optical Fiber Commun. Conf. and Exhibition (OFC)*, Los Angeles, CA, 2017, paper Th4A.1.
5. **V. Gordienko**, M. F. C. Stephens, A. E. El-Taher, and N. J. Doran, "Novel broadband gain-spectrum measurement technique for Raman and parametric amplifiers," in *Optical Fiber Commun. Conf. and Exhibition (OFC)*, Los Angeles, CA, 2017, paper W2A.11.
6. **V. Gordienko**, M. F. C. Stephens, S. Takasaka, A. E. El-Taher, I. D. Phillips, W. Forysiak, R. Sugizaki, and N. J. Doran, "Demonstration of an ultra-flat Raman-enhanced fibre optical parametric amplifier (FOPA) with >110nm gain-bandwidth," in *42nd European Conf. on Optical Commun. (ECOC)*, Dusseldorf, Germany, 2016, paper Th.2.P2.SC1.1.
7. A. E. El-Taher, M. F. C. Stephens, **V. Gordienko**, W. Forysiak, P. Harper, and N. J. Doran, "Performance characterization and limitations of high-gain discrete Raman amplification," in *Conf. on Lasers and Electro-Optics (CLEO)*, San Jose, CA, 2016, paper STu1F.6.
8. A. D. Ellis, I. D. Phillips, M. Tan, M. F. C. Stephens, M. E. McCarthy, M. A. Z. Al-Khateeb, M. A. Iqbal, A. Perentos, S. Fabbri, **V. Gordienko**, D. Lavery, G. Liga, G. Saavedra, R. Maher, S. Sygletos, P. Harper, N. J. Doran, P. Bayvel, and S. K. Turitsyn, "Enhanced superchannel transmission using phase conjugation," in *41st European Conf. on Optical Commun. (ECOC)*, Valencia, Spain, 2015, paper We.2.6.4.

1 INTRODUCTION

This thesis is about the development of fibre optical parametric amplifier's (FOPA) ability to expand the available transmission bandwidth restricted by capabilities of modern amplifiers via providing an ultra-wide gain bandwidth and operating in spectral ranges lacking high gain broadband amplifiers suitable for high speed optical communications.

1.1.1 Motivation

The invention of the Erbium-doped fibre amplifier (EDFA) in early 1980's revolutionised fibre optical communications by enabling wavelength division multiplexing (WDM). WDM is a technique whereby multiple signals can be transmitted in parallel, with each signal having different carrier frequency. The use of WDM allowed a doubling of fibre transmission capacity every year in the 1990's [1]. However, a complete utilisation of EDFA operation range and a spectral efficiency saturation due to approaching the nonlinear Shannon limit [2] have slowed down the WDM capacity per fibre growth to only 20% a year. Such lagging behind a long-term trend of the capacity demand growth by 60% a year is predicted to result in a capacity crunch [1].

Technological developments aimed to improve spectral efficiency via noise figure decrease, nonlinearity mitigation and compensation, etc. have been significant over the past decade. All these advancements are essentially to increase an optical signal-to-noise ratio (OSNR). However, an impact of OSNR improvement on the achievable capacity is scaled down by a logarithm as shown in the simple form of the linear Shannon limit for capacity C [2, 3]:

$$C = B \cdot \log_2\left(1 + \frac{S}{N}\right), \tag{1.1}$$

where B is the bandwidth, S is the average signal power and N is the noise power, so S/N denotes OSNR. Therefore, the overall capacity increase due to S/N improvement was not sufficient. On the contrary, the transmission bandwidth is a pre-logarithm factor, so in practice it allows for almost a linear scaling of the capacity. Therefore, in this thesis it is viewed much more promising to focus on a transmission bandwidth increase to allow for a significant boost of the transmission capacity per fibre.

A potential of transmission bandwidth increase lies in a ~44 THz wide transparency window (1310 – 1625 nm) of modern 'dry' fibres, which utilisation is limited by EDFA gain bandwidth to only ~20%. Therefore, the development of amplifiers capable of providing amplification over the full transmission band at once would offer a fivefold transmission capacity increase. Additionally, a development of microstructured fibres could allow for a further expansion of the low-loss transmission window [4], which would allow for a further capacity increase given that amplification technologies would offer an appropriate gain bandwidth scalability.

Recent development of doped fibre amplifiers relying on Thulium [5] and Holmium [6] has suggested >100 nm gain bandwidth. However, the demonstrated gain spectra were restricted to wavelength range where transmission loss of modern fibres is high. Additionally, the doped fibre amplifiers have poor scalability due to the dopant-imposed limitations on position and bandwidth of their gain spectra. Fibre Raman amplifiers are more advantageous due to their ability to operate in arbitrary wavelength range. However, the gain bandwidth of Raman amplifiers has so far been limited to ~100 nm, and requires multiple (>5) pumps [7]. Conversely, a single pump FOPA with a continuous gain bandwidth of 270 nm (>30 THz) has been demonstrated [8]. In fact, FOPAs suggest an ultimate scalability of the available transmission bandwidth supplied by gain due to its arbitrary gain position and virtually unlimited gain bandwidth [9]. Therefore, FOPA is viewed in this thesis as the main candidate to lead bandwidth expansion beyond C and L bands and to breach the capacity limits.

1.1.2 FOPA overview

The FOPA underlying process is a four wave mixing (FWM) involving one or two pump waves, a signal and an idler [10]. An idler is the signal's phase conjugate symmetric with the signal around the so called FOPA central frequency. The FOPA central frequency is either the frequency of a single pump wave or an average of two pump waves' frequencies. The emergence of the idler is inevitable to satisfy energy and momentum conservation laws when power is transferred from the pump(s) to the signal. These conservation laws essentially lead to following equations:

$$\omega_{p1} + \omega_{p2} = \omega_s + \omega_i, \tag{1.2}$$

$$\beta_{p1} + \beta_{p2} = \beta_s + \beta_i, \tag{1.3}$$

where ω is the optical frequency and β is the propagation constant, whilst indices $p1, p2, s$ and i correspond to two pump, signal and idler respectively. It can be viewed from the quantum mechanical of view as the conversion of two pump photons to signal and idler photons [11]. Single-pump FOPA corresponds to the case when $\omega_{p1} = \omega_{p2}$ and two-pump FOPA corresponds to $\omega_{p1} \neq \omega_{p2}$. This work focuses on single-pump FOPA development.

The FOPA gain does not rely on transitions between energy states, so the key requirement for the gain occurrence is satisfying a phase-matching condition between signal, idler and pump(s), which arises from the momentum conservation [11]. The phase-matching is defined by phase shifts due to nonlinear refractive index change and dispersion parameters, so gain can in principle be obtained in any spectral range by choosing a fibre with suitable dispersion parameters. In addition, the FOPA gain bandwidth increases with pump power [9].

FOPA does not have a spontaneous emission so the main sources of noise in FOPA are amplification of quantum noise, the pump noise transfer and the Raman amplified spontaneous emission (ASE) noise invoked by the FOPA pump [12–14]. Note, another effect degrading signal quality, the nonlinear crosstalk, is typically not considered a part of noise figure because it immensely depends on input signal. Therefore, the nonlinear crosstalk is discussed separately. FOPA can operate in two regimes: phase-sensitive, when an idler phase-matched with signal is injected at the FOPA input along with the signal [15], and phase-insensitive, when an idler is absent at the input. In phase-sensitive FOPA the quantum noise figure (NF) limit of 3 dB is mitigated and NF down to 1.1 dB has been demonstrated [16]. In phase-insensitive operation NF ~4 dB has been demonstrated [13, 17, 18]. Overall, FOPA can allow for ultra-low NFs, but accordingly to Equation (1.1) it is viewed that the transmission bandwidth improvement suggested by FOPA is more beneficious for the transmission capacity than the NF improvement. Therefore, this thesis considers phase-insensitive FOPAs only.

Another FOPA feature is the ability to deliver very high gain. The FOPA gain coefficient is ~2-3 times higher than its of Raman amplifiers [11]. For example, a FOPA gain of up to 70 dB has been demonstrated [19]. It should be noted that the FOPA unidirectional gain and absence of spontaneous emission allow for a high single-pass gain whilst avoiding amplification of reflections, high ASE level, lasing, etc. [20].

The signal modulation is transferred to the idler with an opposite phase. This has found an implementation for optical phase conjugation (OPC) to perform nonlinearity and dispersion compensation [21] or for wavelength conversion to change the signal frequency [22]. Additionally, wavelength conversion can be used to generate waves in regions without suitable sources. The power of generated waves can be very high owing to possibility of high FOPA gain [20].

FOPA also faces a few serious challenges on its way towards practical implementation. First, FOPA exhibits gain strongly depending on polarisations of both pump and signal [23]. However, a very promising solution of this issue has been suggested recently [24] and has immediately led to demonstration of polarisation-multiplexed WDM signals amplification with net gain of 15 dB [25]. This thesis demonstrates only single-polarisation FOPAs and their implementation in a polarisation-insensitive way is the next step for future work.

Second, the stimulated Brillouin scattering (SBS) limits FOPA pump power prohibiting any significant FOPA gain without SBS mitigation [26]. A number of techniques has been suggested to mitigate SBS, but those providing a sufficient SBS threshold increase have a negative impact on either dispersion properties of a gain fibre or the FOPA NF [26]. Therefore, a further advancement of SBS mitigation techniques for FOPA would be needed.

Finally, an unwanted FWM between WDM signals also known as nonlinear crosstalk can have a detrimental impact on signals because FOPA operation itself requires a creation of conditions for efficient FWM, namely high nonlinearity and low dispersion. It has been shown in [27] that the nonlinear crosstalk scales as

$$XT \sim \left(\frac{P_{s,out}}{P_{p,in}}\right)^2, \tag{1.4}$$

where XT is the power ratio between unwanted FWM products and signals, $P_{s,out}$ is the total output signal power and $P_{p,in}$ is the input signal power. Therefore, the nonlinear crosstalk becomes a particular issue in high gain and wide bandwidth applications. On the other hand, the nonlinear crosstalk can be mitigated by employing high pump powers. Additionally, it has been experimentally demonstrated that the crosstalk scales approximately with a fibre length L squared ($XT \sim L^2$) [28]. Although this thesis does not perform an experimental assessment of the nonlinear crosstalk in the demonstrated FOPAs, an employment of the ultra-short fibre lengths and high pump powers will minimise this effect. Additionally, this thesis specifically

targets low gain variation across gain bandwidth of developed FOPAs, because any gain excessive over the minimum gain level within a reported gain bandwidth essentially causes an excessive output signal power which leads to a quadratic boost of the nonlinear crosstalk.

1.1.3 Thesis structure

Chapter 2 covers theoretical and practical aspects relevant to the developed FOPA. First, an underlying fibre optics theory is provided. Second, the FOPA principle of operation is described through derivation of key equations. Resulting FOPA gain spectrum concepts are discussed. Third, an origin of FOPA polarisation dependent gain is illustrated and state-of-the-art techniques to obtain polarisation-independent gain are discussed. Finally, an impact of stimulated Brillouin scattering and stimulated Raman scattering on FOPA performance is examined.

Chapter 3 describes an experiment on broadband FOPA gain spectrum optimisation targeting an ultra-wide FOPA gain spectrum with low gain variation across it. A methodology of broadband gain measurement employing a broadband probe (published in [29, 30]) is explained and verified. Then, FOPA gain spectrum optimisation in terms of gain bandwidth and gain variation (published in [31, 32]) resulted in Raman-enhanced FOPA gain spectrum of 9.2±0.7 dB over 104 nm with a potential for further gain variation decrease and gain bandwidth increase. This result is shown to strongly outperform the previous achievements' trend of gain variation increase with gain bandwidth.

Chapter 4 introduces two techniques for further FOPA gain spectrum engineering. A novel gain spectrum shaping technique (published in [33]) is demonstrated to provide an experimental gain of 10.5±0.5 dB over 102 nm. It is also shown that in principle this technique allows to achieve a targeted gain spectrum shape with a deviation of as low as 0.2 dB. Besides, a concept of cascaded FOPA (introduced in [34]) is shown to enable gain >20 dB with gain variation <3 dB over bandwidth >100 nm.

Chapter 5 is devoted to development of EDFA-free FOPA and OPC to realise FOPA potential of arbitrary wavelength range operation which is currently restricted by reliance of the FOPA pump amplification on EDFA. A pump power of 1.5 W is achieved by implementing a high gain Raman amplifier. The pump quality is characterised in terms of linewidth, OSNR and relative intensity noise to ensure its suitability for FOPA. Then, a FOPA employing this Raman-amplified pump is demonstrated. Additionally, an EDFA-free Raman-assisted OPC has been demonstrated allowing for

OPC implementation outside of EDFA bands for future optical communication networks and granting a pump wavelength flexibility for wavelength conversion.

Chapter 6 summarises results of this work and proposes directions of future FOPA research and development to achieve a practical ultra-wide high gain amplifier suitable to replace EDFAs.

2 STATE-OF-THE-ART

2.1 Fibre optics background

Fibre optical parametric amplifiers (FOPAs) are implemented using optical fibres as it is stated in their name. Therefore, this section covers areas of fibre optics relevant to FOPA operation such as fibre loss, dispersion, birefringence and nonlinearity. Additionally, a propagation of optical waves along fibre is considered and corresponding equations are derived.

2.1.1 Optical fibre

The simplest optical fibre design is called step-index [35]. Step-index fibres consist of a circular core and a cladding with refractive indices n_{co} and n_{cl} respectively. The fibre core in step-index fibres has a slightly higher refractive index: $n_{co} > n_{cl}$. Propagation of light along fibre can be explained in simple by a full internal reflection. The core and the cladding of low-loss optical fibres consist of pure silica glass (SiO_2), whereas the core is doped typically by GeO_2 to increase its refractive index n_{co} as compared to the cladding refractive index n_{cl}.

The normalised frequency for step-index fibres is defined as

$$V = \frac{a\omega}{c}\sqrt{n_{co}^2 - n_{cl}^2}, \tag{2.1}$$

where a is the radius of the core and ω is the angular frequency. A step-index fibre supports only one transverse mode as long as $V < 2.405$. The frequency/wavelength where $V = 2.405$ is called a cut-off frequency/wavelength. Single-mode fibres are designed so that $V = 2 \ldots 2.4$ in its wavelength range of operation (the lower boundary of V is defined by bend loss as discussed in Subsection 2.1.2). Modern standard single mode fibres (SSMF) have a core radius $a \sim 4$ μm and a cut-off wavelength <1260 nm [36, 37]. This work mainly uses highly nonlinear fibres (HNLF) possessing a much smaller core and therefore a higher difference between the core and the cladding refractive indices.

2.1.2 Fibre loss

Fibre attenuation (loss) is a decrease of transmitted optical power along fibre [38]. Main sources of fibre attenuation are material absorption (intrinsic and extrinsic), Rayleigh scattering and bend loss. In optical fibre communications, the fibre

attenuation α is typically expressed as a decrease of transmitted optical power in dB per unit length:

$$\alpha = \frac{P_{in}^{dB} - P_{out}^{dB}}{L}, \tag{2.2}$$

where P_{in}^{dB} and P_{out}^{dB} are optical powers at the input and the output of the fibre length L. A linear attenuation constant α_{lin} is related to the fibre attenuation α expressed in dB as:

$$\alpha_{lin} = \alpha/(10\log_{10} e) = \alpha/4.343. \tag{2.3}$$

The intrinsic absorption is caused by major components of a fibre, e.g. silica and its dopants. The absorption of germanium-doped silica glass is low (0.01 – 0.3 dB/km) in a wavelength range from ~800 nm to ~1700 nm. The boundaries of this window are defined by tails of significant (≫10 dB/km) absorption peaks in ultraviolet and infrared bands.

Rayleigh scattering is caused by imperfections of a scale much smaller than the wavelength of the light. In modern fibres used for transmission in optical communications Rayleigh scattering produces attenuation of ~0.3 dB/km at 1310 nm which scales with wavelength λ as $\alpha_{lin} \sim \lambda^{-4}$. Therefore, Rayleigh scattering limits low loss transmission window from the short wavelength side. In speciality fibres, for example dispersion shifted fibres (DSF) or HNLFs, Rayleigh scattering is significantly increased due to an increased concentration of GeO_2 dopants.

The extrinsic absorption is caused by impurities within a fibre. It can be a major source of attenuation. It is typically caused by metallic or OH (water) ions dissolved in the glass. Absorption bands of the most common metallic ions and the OH group are situated between ~400 nm and ~1400 nm. The water absorption peak at 1380 nm has the most impact on fibres for optical communications, because it is situated within the transparency window defined by Rayleigh scattering and intrinsic loss. Depending on manufacturing process the water absorption peak can introduce from a few dB per km (modern fibres) to virtually no (modern 'dry' fibres) attenuation.

Fibre bend loss occurs via radiation due to the wavefront tilt at fibre bends and curves. Fibre bend loss increase with a decrease of bend radius or normalised frequency V. Bend loss becomes substantial when $V < 2$. The normalised frequency V of particular wave frequency can be tuned by changing the difference between core and cladding refractive indices (equation (2.1)).

Overall, fibre attenuation strongly depends on wavelength. The low-loss transmission window is defined by Rayleigh scattering, infrared intrinsic absorption and water absorption. Modern SSMFs have two transparency windows around the water peak with loss ~0.3 dB/km around 1310 nm and ~0.2 dB km around 1550 nm, while 'dry' (low water peak) SSMFs feature α < 0.3 dB/km in a range from ~1310 nm to ~1625 nm. In special fibres, for example, HNLF loss can reach ~1 dB/km at 1550 nm due to higher concentration of dopants and smaller core radius.

2.1.3 Optical wave propagation in fibre

Propagation of an optical wave through a non-magnetic charge-free medium can be described by a following equation derived from Maxwell's equations [39]:

$$\nabla^2\vec{E} - \frac{1}{c^2}\frac{\delta^2\vec{E}}{\delta t^2} = \mu_0\frac{\delta^2\vec{P}}{\delta t^2}, \tag{2.4}$$

where $\vec{E}$ and $\vec{P}$ are electric field and polarisation density vectors. The polarisation density $\vec{P}$ reflects an interaction between electric field $\vec{E}$ and a medium in equation (2.4). In general case a relation between the polarisation density and the electric field is set using a power series expansion:

$$\vec{P} = \varepsilon_0\left(\chi^{(1)}\vec{E} + \chi^{(2)}\vec{E}\vec{E} + \chi^{(3)}\vec{E}\vec{E}\vec{E} + \cdots\right), \tag{2.5}$$

where $\chi^{(i)}$ $(i = 1, 2, \ldots)$ is i-th order electric susceptibility represented by a three-dimensional tensor with a rank $i + 1$. All terms $\chi^{(i)}$ describing an electric susceptibility have a frequency dependency. In general, terms $\chi^{(i)}$ are complex values. It can be shown that their imaginary part represent absorption. Here absorption is neglected for analysis of wave propagation along fibre and occurring linear and nonlinear effects, so only real part of electric susceptibility $\chi^{(i)}$ is considered below.

Polarisation vector $\vec{P}$ can be presented as a sum of linear and nonlinear components $\vec{P} = \vec{P}_L + \vec{P}_{NL}$. The linear response of the medium $\vec{P}_L = \varepsilon_0\chi^{(1)}\vec{E}$ has the dominant contribution especially for low electric field and hence is used to describe optical wave propagation in a fibre. The nonlinear response $\vec{P}_{NL} = \varepsilon_0\left(\chi^{(2)}\vec{E}\vec{E} + \chi^{(3)}\vec{E}\vec{E}\vec{E} + \cdots\right)$ is then viewed as a perturbation caused by high electric field (power) of an optical wave.

An optical wave consisting of a single frequency ω component can be represented in space (x and y are transverse coordinates of a fibre and z is the distance along a

fibre) and time as $\vec{E}(x,y,z,t) = \vec{E}_s(x,y,z) \cdot \exp(-i\omega t)$. A spatial distribution of electric field $\vec{E}_s(x,y,z)$ of an optical wave guided by an optical fibre is derived in a linear case $\vec{P} = \varepsilon_0 \chi^{(1)} \vec{E}$. Additionally, the coefficient $\chi^{(1)}$ can be treated as a scalar value in isotropic fibre, so polarisation and electric field vectors $\vec{P}$ and $\vec{E}$ are collinear and can be referred to as P and E respectively. Substitution of equation (2.5) into equation (2.4) with these considerations leads to

$$(\nabla^2 + K^2)E_s = 0, \tag{2.6}$$

where $K = n_0\omega/c$ is the local (at point x,y,z) propagation constant and $n_0 = \sqrt{1+\chi^{(1)}}$ is the weak-field refractive index at frequency ω.

It can be shown that if $E_s(x,y,z)$ is represented as $E_s(x,y,z) = \psi(x,y)\exp(i\beta z)$, where β is the propagation constant of the mode and $\psi(x,y)$ is the transverse mode profile, which does not change along a fibre, equation (2.6) can be rewritten as

$$\left(\frac{\partial^2}{\partial x^2} + \frac{\partial^2}{\partial y^2}\right)\psi + \left(K^2 - \beta^2\right)\psi = 0. \tag{2.7}$$

Equation (2.7) can be solved to find ψ and β for modes guided by an optical fibre (note, Cartesian coordinates are used here, but cylindrical coordinates are more suitable for optical fibre). For example, in a step-index fibre with the cladding and the core refractive indices of n_{cl} and n_{co} respectively and a core radius a, the local propagation constant K in equation (2.7) is defined as follows:

$$\begin{aligned} K(x,y,z) &= \frac{n_{cl}\omega}{c}, \text{if } x^2 + y^2 > a^2, \\ K(x,y,z) &= \frac{n_{co}\omega}{c}, \text{if } x^2 + y^2 < a^2. \end{aligned} \tag{2.8}$$

It should be noted that as $\chi^{(1)}$ is frequency dependent, all derived values: n_0, K, ψ, β are frequency dependent too.

Overall, an electric field of single frequency wave propagated along an optical fibre in a linear regime (low electric field approximation) with no attenuation is expressed as follows:

$$E(x,y,z,t) = \psi(x,y)\exp(i\beta z - i\omega t). \tag{2.9}$$

2.1.4 Propagation constant and dispersion

In contrast to the local propagation constant K, which is the property of a medium in a particular point, the mode propagation constant β considers a transverse refractive index profile of an optical fibre ($n(x,y)$) and its overlap with a transverse mode

profile ($\psi(x,y)$) as shown by equations (2.7) and (2.8). The effective refractive index $n_{eff} = \beta c/\omega$ and the phase velocity $v_{ph} = \omega/\beta = c/n_{eff}$ are defined for a mode based on its propagation constant β.

However, as it was noted in the previous subsection, β is frequency dependent. It is often accounted for by expanding β in a Taylor series about the frequency ω_0:

$$\beta(\omega) = \beta(\omega_0) + \beta^{(1)}(\omega_0) \cdot (\omega - \omega_0) + \frac{1}{2}\beta^{(2)}(\omega_0) \cdot (\omega - \omega_0)^2 + \cdots, \quad (2.10)$$

where $\beta^{(m)} = d^m\beta/d\omega^m$, $m = 1,2,3,\ldots$ and ω_0 is typically chosen as a central frequency of a pulse, wave, combination of waves, etc.

In practice waves consist of multiple frequency components for many reasons – non-zero linewidth of sources, modulation, etc. [40]. These frequency components propagate with different velocities due to frequency dependency of the propagation constant $\beta(\omega)$ and, consequently, the phase velocity $v_{ph}(\omega)$. Therefore, the envelope formed by close frequency components travels with a group velocity $v_g = d\omega/d\beta = 1/\beta^{(1)}$. The group velocity has a great importance as it defines the propagation velocity of waveforms, for example, pulses or modulated signals.

However, the transmitted envelope is distorted by frequency dependency of the group velocity v_g described by a so called group velocity dispersion (GVD) $\beta^{(2)}$ [41]. An interpretation of GVD is that pulses with close carrier frequencies ω_1 and ω_2 propagated along a fibre length L accumulate a separation in time by the group delay difference $\Delta\tau = L\beta^{(2)}(\omega_1) \times (\omega_1 - \omega_2)$. Therefore, a distortion of the transmitted envelope due to dispersion is increasing with propagated distance, frequency separation and GVD. The group delay difference can also be presented in a wavelength domain in a similar way. In this case a chromatic dispersion coefficient $D(\lambda) = -\beta^{(2)}(\omega) \times \omega/\lambda$ is used instead of GVD. Dispersion slope is usually given in a wavelength domain as $S = dD/d\lambda$.

GVD can cause a significant distortion if signals and pulses are transmitted over long distance. This can be avoided if $\beta^{(2)} = 0$ as there is no group delay difference in this case. A wavelength and a frequency where $\beta^{(2)} = 0$ are called a zero-dispersion wavelength (ZDW) and a zero-dispersion frequency. A group of waves propagating near ZDW maintain phase synchronism required for a four wave mixing (FWM) [41] discussed in Subsection 2.1.6. This is beneficial for applications relying on FWM, like

FOPA, but is detrimental to transmitted signals. Therefore, ZDW is an important parameter for fibres used in FOPA.

The dominating effects defining GVD in single-mode fibres are material dispersion and waveguide dispersion (intermodal dispersion occurring in multi-mode fibres is not considered) [38]. The material dispersion results from the different group velocities v_g of the various spectral components in the fibre core material. The material dispersion is defined by $d^2n_{co}/d\omega^2$. The waveguide dispersion results from the group velocity v_g variation with frequency for a particular mode and is defined by normalized frequency V and refractive index difference $n_{co} - n_{cl}$.

Zero material dispersion wavelength (ZMDW) of silica is ~1276 nm and can be shifted in a wavelength range ~1200 – 1400 nm by adding dopants [42]. The material dispersion $D_M(\lambda)$ of silica has a positive slope and is positive on the longer wavelength side of ZMDW. In contrast, the waveguide dispersion $D_W(\lambda)$ is typically negative in the silica transmission window and has a negative slope [38]. As total dispersion is approximately a sum of $D_M(\lambda)$ and $D_W(\lambda)$, a fibre ZDW is typically located on the longer wavelength side of the ZMDW and has a positive slope ($d(D_M + D_W)/d\lambda > 0$). It has been shown that the fibre ZDW can be selected in a wavelength range 1300 – 2000 nm by controlling waveguide dispersion through fibre core radius [43]. In general, ZDW can be shifted to longer wavelengths (e.g. to C band for DSFs) through decreasing the core radius and increasing the refractive index difference $n_{co} - n_{cl}$ (both change waveguide dispersion) or suitable doping of silica (changes material dispersion) [38]. Importantly, a ZDW change with the core radius means that if a fibre core radius has to be small, e.g. in HNLF, it might be difficult to get this fibre ZDW close to 1300 nm.

It should be noted that a core diameter fluctuates along fibre due to manufacturing process limitations. This leads to longitudinal fluctuations of ZDW, because waveguide dispersion depends on core diameter. It should be noted that ZDW of small core fibres (e.g. HNLF) is more susceptible to core radius variation, so ZDW variation can be as high as 20 nm in 1.7 km long HNLF [44]. Additionally, fibre tension or stretch can modify ZDW. However, fibre designs and fabrication technologies to reduce ZDW fluctuation are being developed and implemented to create so called dispersion stable fibres [45, 46]. ZDW also exhibits temperature dependency up to 0.06 nm/°C for DSF-HNLF [47, 48].

2.1.5 Fibre birefringence

An electric field $\vec{E}$ was assumed to be linearly polarised in Subsection 2.1.3 to derive a propagation constant of a fundamental mode. However, a linearly polarised electric field can have various orientation in axes x and y. Any such wave can be represented as a superposition of waves linearly polarised along axes x and y: $\vec{E}_x$ and $\vec{E}_y$ respectively. Therefore, even single mode fibre supports two modes of orthogonal polarisations [49]. They have the same propagation constant in an ideal isotropic fibre. However, real fibres are anisotropic due to deviations of the core geometry (e.g. ellipticity), bends and stress. Therefore, in general case propagation constants for orthogonal modes β_x and β_y are different and a fibre exhibit birefringence B:

$$B = \frac{\beta_x - \beta_y}{2\pi/\lambda}. \tag{2.11}$$

Light polarised along one of the principal axes of a birefringent fibre retains its polarisation. However, a wave polarised at an angle with the principal axes passes through various states of polarisation, because such wave is a superposition of orthogonal modes with different phase velocities leading to phase retardation between them $\Phi(z) = (\beta_x - \beta_y) \times z$. The length $L_B = \lambda/B$ is called a beat length as this is a period of polarisation state evolution, i.e. $\Phi(L_B) = 2\pi$.

2.1.6 Fibre nonlinearity

Nonlinear response of a medium arises due to high order terms of electric susceptibility $\chi^{(2)}$, $\chi^{(3)}$, etc. These terms are grouped together as $\vec{P}_{NL} = \varepsilon_0(\chi^{(2)}\vec{E}\vec{E} + \chi^{(3)}\vec{E}\vec{E}\vec{E} + \cdots)$. However, the second order nonlinearity $\chi^{(2)}$ does not make a contribution in glass due to an inversion symmetry at the molecular level. Therefore, the lowest order nonlinear effects in optical fibres originate from the third-order electric susceptibility $\chi^{(3)}$ and are known as the third-order nonlinearity.

It can be shown that the real part of the third-order susceptibility $\chi^{(3)}$ invokes the Kerr effect representing a refractive index change due to a presence of a strong light wave [35]:

$$n = n_0 + n_2|E|^2, \tag{2.12}$$

where n_0 is the weak-field refractive index (see Subsection 2.1.3), $|E|^2$ is the optical intensity inside the fibre and n_2 is the nonlinear refractive index coefficient which relation to $\chi^{(3)}$ can be derived from (2.4) [35]:

$$n_2 = \frac{3}{8n_0}\mathrm{Re}\left(\chi^{(3)}\right). \tag{2.13}$$

The third-order nonlinearity combines up to four waves as follows. If E consists of multiple frequency components, any two of them, for example ω_1 and ω_2, cause together a refractive index modulation at frequencies $\pm\omega_1 \pm \omega_2$ (equation (2.12)). Another frequency component, for example ω_3, is then phase modulated by the refractive index distortion to produce a new frequency component at frequency $\pm\omega_1 \pm \omega_2 \pm \omega_3$. The process is called FWM because three frequency components produce a new (or amend an existing) frequency component at frequency $\omega_4 = \pm\omega_1 \pm \omega_2 \pm \omega_3$. The process is called a degenerate FWM if two frequencies are equal (e.g. $\omega_1 = \omega_2$) and essentially only three frequency components are interacting. Other third-order nonlinear effects are the cross phase modulation (XPM) (e.g. $\omega_1 = \omega_2 \neq \omega_3 = \omega_4$) and the self-phase modulation (SPM) ($\omega_1 = \omega_2 = \omega_3 = \omega_4$) also play an important role and are discussed in more details in Subsection 2.2.2.

2.2 Single-polarisation FOPA

This section explores in details the FOPA principle of operation, emergence of gain due to the third-order nonlinearity and key principles defining FOPA gain spectrum. All waves are considered co-polarised for simplification of the discussion whilst allowing for important conclusions. In Subsection 2.2.1 the propagation equation for FOPA is derived. It governs an impact of the third-order nonlinearity on the evolution along fibre of four waves which frequencies satisfy energy conservation to allow power transfer between them (equation (1.2)). In particular, effects of SPM, XPM and FWM appear as separate terms in the propagation equation. In Subsection 2.2.2 it is demonstrated how the FWM enables signal gain and an equation for the signal gain is derived as a function of phase-matching. The key role of the SPM and XPM terms for phase-matching is illustrated. In Subsection 2.2.3 the dependence of FOPA gain spectrum on dispersion parameters is explored and the typical gain spectrum shape is analysed. Consequently, main principles allowing for ultra-wide FOPA gain spectrum are defined. Subsection 2.2.4 presents a powerful tool for further FOPA analysis, the generalised nonlinear Schrodinger equation (NLSE). It allows to consider a combined effect of the third-order nonlinearity and other phenomena taking place in fibre such as loss and the Raman interaction for arbitrary optical spectra.

2.2.1 FOPA propagation equation

A FOPA propagation equation defines evolution along fibre of all waves participating in parametric amplification, namely, two pump waves, a signal wave and an idler wave, and is therefore a foundation for FOPA analysis. The FOPA propagation equation is derived in this subsection based on [39]. Routine transformations are omitted here, instead a few points critical for understanding of FOPA principle of operation are discussed in more detail.

Waves of different frequencies are defined by equation (2.9) so that there is no interaction between them in the linear case: any linear combination of the solutions of the equation (2.6) of is also a solution of the equation (2.6). In contrast, in the nonlinear case ($\chi^{(3)} \neq 0$) equation (2.6) obtains an extra term on the right-hand side:

$$(\nabla^2 + K^2)E = \frac{\chi^{(3)}}{c^2}\frac{\delta^2 E^3}{\delta t^2} \tag{2.14}$$

which introduces products of interaction of different frequency components to the equation (electric field E is assumed to consist of close frequencies so the third-order electric susceptibility term $\chi^{(3)}$ can be considered to be the same for all of them). Indeed, if an electric field E is a superposition of a few waves, they will be combined in all possible combinations of three on the right-hand side of equation (2.14). The third-order nonlinearity allows therefore a mixing of up to four frequency components and the solution of equation (2.14) for each frequency depends on electric field at other frequencies. An evolution of the electric field E due to nonlinear response of a medium can be addressed by adding a coefficient (slowly varying envelope) $B(z)$ to equation (2.9):

$$E = B(z)\psi(x, y)\exp(i\beta z - i\omega t). \tag{2.15}$$

In general case, parametric amplification involves four frequency components satisfying a relation (1.2). A real electric field E_Σ comprising four single-frequency waves E_k, where k = 1…4 and E_k is given by equation (2.15), can be expressed as

$$E_\Sigma = \frac{1}{2}\sum_{k=1}^{4}[E_k + E_k^*] \tag{2.16}$$

Upon substitution of equation (2.16) into equation (2.14), the term E_Σ^3 produces 56 unique terms (3-combinations from a set of 8 terms). There is no need to write down all of them, instead to get an equation for one of frequency components, for

example E_1, only terms with the resulting frequency ω_1 are kept on both sides of the equation:

$$(\nabla^2 + K_1^2)E_1 = \\ = \frac{\chi^{(3)}}{4c^2}\frac{\delta^2(3E_1E_1E_1^* + 6E_1E_2E_2^* + 6E_1E_3E_3^* + 6E_1E_4E_4^* + 6E_2^*E_3E_4)}{\delta t^2} \quad (2.17)$$

The terms of form $E_1E_kE_k^*$ have the same resulting frequency as the term E_1 because the exponential part of $E_kE_k^*$ is cancelled out. The frequency of the term $E_2^*E_3E_4$ equals to $-\omega_2 + \omega_3 + \omega_4 = \omega_1$ according to equation (1.2). Coefficients before each term reflect a number of occurrences of each term when performing an exponentiation E_Σ^3. It is shown in the following subsection that terms of form $E_1E_kE_k^*$ cause phase shift only to E_1. Therefore, a nonlinear effect of the term $E_1E_1E_1^*$ is called SPM, and a nonlinear effect of the terms $E_1E_kE_k^*$ $(k \neq 1)$ is called XPM. The term $E_2^*E_3E_4$ describing an evolution of E_1 denotes a FWM.

The left-hand side of equation (2.17) is essentially equation (2.6), which equals to zero, except that the electric field E_1 in equation (2.17) includes an additional coefficient $B_1(z)$. Therefore, upon substitution of equation (2.15) into equation (2.17) all terms on the left-hand side except derivatives with respect to z vanish. Additionally, the term $d^2B_1(z)/dz^2$ can be neglected using a slowly varying envelope approximation [39]. Assuming also that the transverse mode profile ψ is the same for all frequency components as long as they have close frequencies, a following equation for the envelope describing an evolution of the electric field due to nonlinear interaction B_1 is obtained from equation (2.17):

$$-i\psi\frac{dB_1}{dz} = \frac{3\chi^{(3)}\psi^3\omega_1^2}{8\beta_1c^2} \times \\ \times [(B_1B_1B_1^* + 2B_1B_2B_2^* + 2B_1B_3B_3^* + 2B_1B_4B_4^*) + 2B_2^*B_3B_4\exp(i\Delta\beta z)] \quad (2.18)$$

Note, the sum of propagation constants of the FWM term does not necessary equals β_1, so to remove the term $\exp(i\beta_1 z)$ from equation (2.18), the propagation constant mismatch $\Delta\beta$ has been introduced:

$$\Delta\beta = \beta_3 + \beta_4 - \beta_1 - \beta_2 \quad (2.19)$$

Equation (2.18) is then to be integrated in transverse coordinates to introduce the nonlinear coefficient γ:

$$\gamma = \frac{3\mu_0 \omega \chi^{(3)}}{8 n_{eff}^2 A_{eff}} = \frac{\mu_0 \omega n_2}{n_{eff} A_{eff}} = \frac{\omega n_2'}{c A_{eff}} \tag{2.20}$$

where A_{eff} is the effective area of the mode and n_2 is the nonlinear refractive index coefficient in accordance with equation (2.12) and n_2' is the nonlinear refractive index satisfying a different form of equation (2.12) [41]; and to replace coefficients B_k with scaled field amplitudes A_k such that $A_k A_k^* = P_k$ is the average power at the frequency ω_k:

$$\frac{dA_1}{dz} = i\gamma\left(A_1 |A_1|^2 + 2A_1 \sum_{k=2}^{4} |A_k|^2 + 2A_2^* A_3 A_4 \exp(i\Delta\beta z) \right) \tag{2.21}$$

Equation (2.21) is the FOPA propagation equation describing evolution of complex amplitude A_1 of one of four co-propagating frequency components due to third-order nonlinearities. Equations for amplitudes of other frequency components A_2, A_3 and A_4 are identical to equation (2.21), except the exponential term for A_3 and A_4 changes the argument sign due to definition of $\Delta\beta$ (equation (2.19)) and becomes $\exp(-i\Delta\beta z)$. The general form of the equation is provided in [39]. Following equation (2.17) it should be clear that the three terms on the right-hand side of equation (2.21) define an impact of SPM, XPM and FWM on the wave complex amplitude.

It also should be noted that the nonlinear coefficient γ depends on the frequency, but assuming it to be a constant within a small frequency range greatly simplifies equations. It is important though to be aware that this approximation may lead to inaccurate results when investigating FOPAs operating over very wide frequency range.

2.2.2 Signal gain in FOPA

Equation (2.21) allows to deduce the origin and key features of parametric gain as well as to derive corresponding equations. A derivation and a discussion in this section is based on [39] but presented in a different way, providing a clearer physical representation of equations' transformations and introduced variables. For this discussion frequencies of the four waves participating in parametric amplification ω_1, ω_2, ω_3 and ω_4 are named as ω_{p1}, ω_{p2}, ω_s and ω_i respectively, where ω_{p1}, ω_{p2} are the frequencies of two pump waves, ω_s is the signal frequency and ω_i is the idler frequency. The subscript k is used when a relation is equally correct for any of these waves.

Considering that terms $|A_k|^2$ and γ in equation (2.21) are scalar values, an impact of SPM and XPM can be presented as follows:

$$\left(\frac{dA_k}{dz}\right)_{SPM,XPM} = i \times A_k \times scalar \tag{2.22}$$

which means that the change of the complex amplitude due to SPM and XPM $(dA_k/dz)_{SPM,XPM}$ and the complex amplitude A_k itself are always orthogonal on the complex plane (Figure 2.1(a)). Therefore, SPM and XPM can only rotate a vector A_k on the complex plane (change its phase) without changing its amplitude.

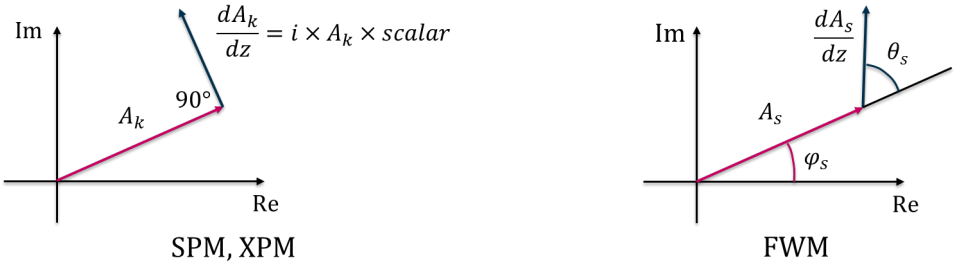

(a) (b)

Figure 2.1. Impact of (a) SPM, XPM and (b) FWM on a wave's complex amplitude.

FWM is different from SPM and XPM, because the angle between the complex amplitude change due to FWM $(dA_k/dz)_{FWM}$ and the complex amplitude A_k itself depends on phases of all waves and a phase mismatch $\Delta\beta z$ accumulated due to dispersion. For example, for a signal in FOPA:

$$\left(\frac{dA_s}{dz}\right)_{FWM} = i \times 2\gamma A_i^* A_{p1} A_{p2} \exp(-i\Delta\beta z) \tag{2.23}$$

If each complex amplitude in equation (2.33) is represented as $A_k(z) = |A_k(z)| \times \exp[i\varphi_k(z)]$, where $\varphi_k(z)$ is the phase of the wave, then the angle θ_s between vectors $(dA_s/dz)_{FWM}$ and A_s in the complex plane (Figure 2.1(b)) is

$$\theta_s(z) = \varphi_s(z) + \varphi_i(z) - \varphi_{p1}(z) - \varphi_{p2}(z) + \Delta\beta z - \frac{\pi}{2} \tag{2.24}$$

Figure 2.1(b) shows that depending on the angle $\theta_s(z)$, both the phase and the amplitude of signal or any other wave can be modified by FWM. This makes FWM the key interaction for parametric amplification. The maximum signal gain, called phase-matched, is obtained when the signal wave complex amplitude and its derivative are codirected (phase-matched), i.e. $\theta_s(z) = 0$ for any z. There is no idler at the input of

phase-insensitive FOPA (except for noise), so an idler wave with the most favourable phase, i.e. satisfying this condition, is generated at the input as a result of phase-matched signal amplification:

$$\varphi_i(0) = \varphi_{p1}(0) + \varphi_{p2}(0) - \varphi_s(0) + \frac{\pi}{2} \tag{2.25}$$

Therefore, there phase matching is always satisfied at the input of phase-insensitive FOPA: $\theta_s(0) = 0$ for any signal frequency. However, the angle $\theta_s(z)$ changes with distance z as follows:

$$\frac{d\theta_s}{dz} = \frac{d\varphi_s}{dz} + \frac{d\varphi_i}{dz} - \frac{d\varphi_{p1}}{dz} - \frac{d\varphi_{p2}}{dz} + \Delta\beta \tag{2.26}$$

where $d\varphi_k/dz$ is the phase derivative representing an impact of SPM and XPM on kth wave and can be derived from equation (2.21):

$$\frac{d\varphi_k}{dz} = \gamma\left(P_k(z) + 2\sum_{j=1\neq k}^{4} P_j(z)\right) \tag{2.27}$$

A few assumptions applicable in most practical cases need to be made to significantly simplify a further derivation. Fibre loss are neglected, which is usually a good approximation, because typically FOPA gain fibres are no longer than a few hundred meters, so distributed fibre loss are typically below 0.2 dB. Signal and idler powers are considered negligibly small as compared to pump power (typically, signal power is >30 dB smaller than pump power). Pump depletion can be neglected if an output signal power is <10 dB smaller than a pump power (under certain conditions pump depletion can be neglected for higher signal power too) [12, 13]. Overall, signal and idler powers can be neglected in equation (2.27) and pump powers can be considered constant along fibre, so equation (2.27) can be rewritten for each wave as follows:

$$\begin{aligned} d\varphi_s/dz &= 2\gamma(P_{p1} + P_{p2}); \quad d\varphi_i/dz = 2\gamma(P_{p1} + P_{p2}); \\ d\varphi_{p1}/dz &= \gamma(P_{p1} + 2P_{p2}); \quad d\varphi_{p2}/dz = \gamma(2P_{p1} + P_{p2}). \end{aligned} \tag{2.28}$$

Equation (2.28) shows that signal and idler are affected only by XPM with pumps and pumps are affected only by SPM and XPM with each other. The phase derivatives $d\varphi_k/dz$ do not depend on z with the assumptions made, so the nonlinear wavevector mismatch $\Delta\beta_{NL}$ can be introduced to describe a total impact of SPM and XPM on phase-matching condition:

$$\Delta\beta_{NL} = \frac{d\varphi_s}{dz} + \frac{d\varphi_i}{dz} - \frac{d\varphi_{p1}}{dz} - \frac{d\varphi_{p2}}{dz} = \gamma\left(P_{p1} + P_{p2}\right) = \gamma P_0, \tag{2.29}$$

where $P_0 = P_{p1} + P_{p2}$ is the total pump power. Then, equation (2.26) can be rewritten as follows:

$$\frac{d\theta_s}{dz} = \Delta\beta_{NL} + \Delta\beta = \kappa, \tag{2.30}$$

where κ is the total wavevector mismatch describing how the angle θ_s changes over distance. Phase-matched gain requires $\kappa = 0$ to obtain phase-matching along all fibre ($\theta_s(z) = 0$ for any z). This means that the phase-mismatch accumulated with distance due to dispersion and due to SPM/XPM has to be mutually compensated. Conditions for this are discussed in the next subsection. At this point it is important to note that if $\kappa \neq 0$, the vector $(dA_s/dz)_{FWM}$ is rotating relatively A_s. Therefore, an effect of FWM on signal is changing over distance causing an amplification decrease, phase rotation or even attenuation (i.e. if $\theta_s = \pi$ the power is transferred from signal to pumps). A solution of equation (2.21) as a function of the total wavevector mismatch κ is provided in [39]. The parametric gain coefficient g is given by

$$g^2 = r^2 - \left(\frac{\kappa}{2}\right)^2, \tag{2.31}$$

where $r = 2\gamma\left|A_{p1}(0)\right|\left|A_{p2}(0)\right| = 2\gamma\sqrt{P_{p1}P_{p2}}$ is the amplitude of FWM coupling. Signal gain G_s and a signal-to-idler conversion efficiency G_i (further, conversion efficiency) defined as a ratio between output idler and input signal powers are given as

$$G_i(z) = \left|\frac{r}{g}\sinh(gz)\right|^2, \tag{2.32}$$

$$G_s(z) = G_i(z) + 1. \tag{2.33}$$

It can be shown that both signal gain $G_s(z)$ and conversion efficiency $G_i(z)$ increase with gain coefficient g. The highest gain is therefore obtained when the gain coefficient is at its maximum. Equation (2.31) shows that the maximum gain coefficient value $g_{max} = r$ is achieved when the total wavevector mismatch $\kappa = 0$, which also follows from the discussion above. If assume an equality of pumps' powers: $P_{p1} = P_{p2} = P_0/2$, then the maximum gain coefficient is $g_{max} = r = \gamma P_0$ and the maximum idler and signal gain have the simple forms

$$G_{i,max}(z) = [\sinh(\gamma P_0 z)]^2 \quad \text{and} \quad G_{s,max}(z) = [\cosh(\gamma P_0 z)]^2, \tag{2.34}$$

which can be approximated for large gains ($x > 1 \Rightarrow \sinh^2(x) \approx \cosh^2(x) \approx e^{2x}/4$; $10\log_{10} e \approx 4.34$) as follows:

$$G_{s,max}^{dB}(z) \approx G_{i,max}^{dB}(z) \approx 8.69\Phi - 6 \text{ dB}. \tag{2.35}$$

where $\Phi = \gamma P_0 z$ is the nonlinear phase shift. Figure 2.2 shows peak FOPA gain as a function of the nonlinear phase shift plotted using equations (2.34) and (2.35). It shows that the signal gain G_s increases very slowly when the nonlinear phase shift is low ($\Phi < 1$) and grows exponentially (linearly in dB scale) when $\Phi > 1$. The reason for this is that an impact of the FWM term on a signal is scaled by an idler amplitude (equation (2.23)). Therefore, the signal receive little gain until an idler power is comparable with a signal power ($G_i \sim 0$). For the same reason, the conversion efficiency G_i increases quickly when idler power is low and then the conversion efficiency is practically equal to the signal gain. It can also be explained from another point of view: as a result of FWM a signal and an idler are incremented by the same amount of power. A signal and an idler experience therefore very different gain unless their powers are of the same order.

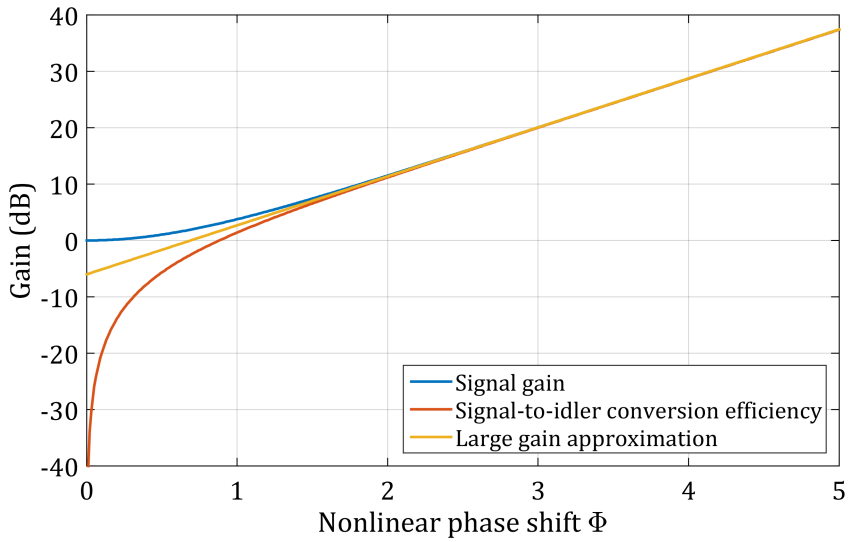

Figure 2.2. The maximum FOPA gain as a function of the nonlinear phase shift. Signal gain (blue) and conversion efficiency (orange) are calculated using an analytic solution (2.34). The large gain approximation (yellow) is calculated using an approximation of this solution (2.35).

Figure 2.2 shows also that to achieve gain of 20 dB a nonlinear phase of shift of 3 is required. Thus, for a modern HNLF (e.g. $\gamma = 14$ W^{-1}·km^{-1}) a length of 100 m and a pump power of just over 2 W is required to obtain a peak gain of 20 dB.

For a single pump FOPA, two pumps are considered to have the same frequency: $\omega_{p1} = \omega_{p2} = \omega_p$. In this case, the only difference for a whole subsection is that in equation (2.28): $d\varphi_{p1}/dz = d\varphi_{p2}/dz = \gamma P_0$ due to SPM only. Therefore, for a single pump FOPA the nonlinear wavevector mismatch in equation (2.29) is: $\Delta\beta_{NL} = 2\gamma P_0$.

2.2.3 Single pump FOPA gain spectrum

Since this thesis is devoted to single pump FOPAs, this subsection examines gain spectrum of a single pump FOPA only. This subsection is based on [51] and supplied with additional discussion. FOPA gain for every frequency can be derived using equations (2.32) and (2.33). The frequency dependent parameter in these equations is a gain coefficient g:

$$g^2 = r^2 - \left(\frac{\Delta\beta_{NL} + \Delta\beta}{2}\right)^2 \tag{2.36}$$

defined through the propagation constant mismatch $\Delta\beta$ representing a difference between propagation constants at three (four) different frequencies.

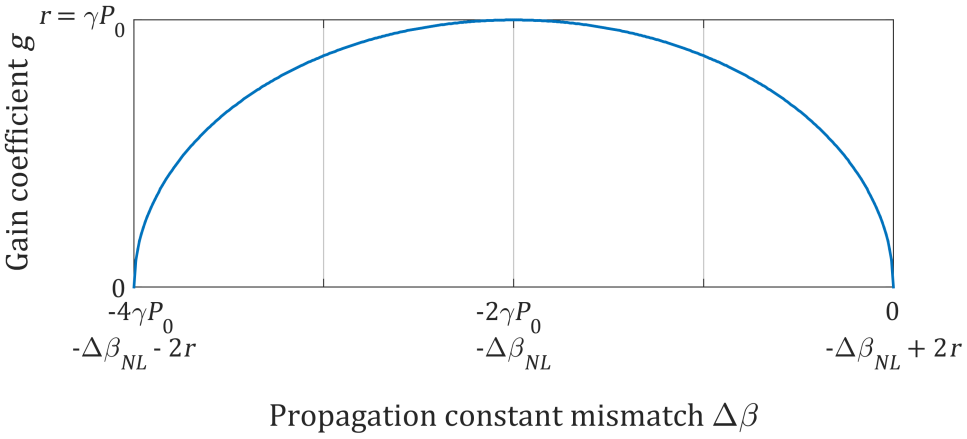

Figure 2.3. Gain coefficient g calculated as a function of propagation constant mismatch $\Delta\beta$ for a single pump FOPA. The horizontal axis is labelled in two ways: in terms of γP_0 and in terms of $\Delta\beta_{NL}$ and r.

Equation (2.36) describes an ellipse in axes of the propagation constant mismatch $\Delta\beta$ and the gain coefficient g (Figure 2.3). It can be seen that the gain coefficient is not a real value when the total wavevector mismatch $\kappa = |\Delta\beta_{NL} + \Delta\beta| > 2r$, which

means that rotation of the vector $(dA_s/dz)_{FWM}$ (Figure 2.1(b)) causes signal power fluctuations rather than amplification, i.e. no substantial gain. Real gain in a scalar case of a single pump FOPA is obtained when the propagation constant mismatch $\Delta\beta$ is within a range from $-4\gamma P_0$ to 0. Often a normalised mismatch parameter $K = -\Delta\beta/2\gamma P_0$ is used to describe the state of phase matching. The gain coefficient is real when $2 \geq K \geq 0$, and the phase-matched gain is observed when $K = 1$.

The propagation constant mismatch $\Delta\beta$ defined in equation (2.19) can be calculated using a series expansion of signal, idler and pump propagation constants around the pump frequency ω_p as shown in equation (2.10). In this case all propagation constants are defined via derivatives of the propagation constant β at the pump frequency ω_p, and due to a symmetry of signal and idler frequencies all odd derivatives are being cancelled. Then keeping only two the highest-order terms, the propagation constant mismatch $\Delta\beta$ can be presented as:

$$\Delta\beta(\Delta\omega_s) = \beta^{(2)}(\omega_p) \cdot \Delta\omega_s^2 + \frac{\beta^{(4)}(\omega_p) \cdot \Delta\omega_s^4}{12}, \tag{2.37}$$

where $\Delta\omega_s = \omega_s - \omega_p = -(\omega_i - \omega_p)$ is the signal frequency detuning from the pump.

Equation (2.37) demonstrates that the FOPA signal gain is symmetric around the pump frequency ω_p and allows to find the propagation constant mismatch $\Delta\beta$ as a function of signal detuning from the pump. The value of the group velocity dispersion at the pump frequency $\beta^{(2)}(\omega_p)$ can be modified by tuning the pump frequency ω_p:

$$\beta^{(2)}(\omega_p) \approx \beta^{(3)}(\omega_0) \cdot (\omega_p - \omega_0). \tag{2.38}$$

Conversely, the value of the fourth-order propagation constant $\beta^{(4)}$ has little frequency dependency within a practical pump frequency tuning range. Additionally, the fourth-order propagation constant is difficult to measure or manufacture with a high accuracy. Therefore, the fourth-order propagation constant is commonly characterized by its sign and an order of magnitude.

Figure 2.4 shows the propagation constant mismatch $\Delta\beta(\Delta\omega_s)$ calculated using equation (2.37) for all combinations of $\beta^{(2)}$ and $\beta^{(4)}$ signs. Each plot contains two curves for different values of the group velocity dispersion $\beta^{(2)}$ to demonstrate how its change affects the propagation constant mismatch $\Delta\beta$. Orange curves are calculated for a four times smaller value of $\beta^{(2)}$ than blue curves. Lines are highlighted by thickness to demonstrate the range, where the gain coefficient g is a real, positive

number in scalar case, i.e. $-4\gamma P_0 < \Delta\beta < 0$. The value of gain coefficient as a function of the propagation constant mismatch can be looked up at Figure 2.3.

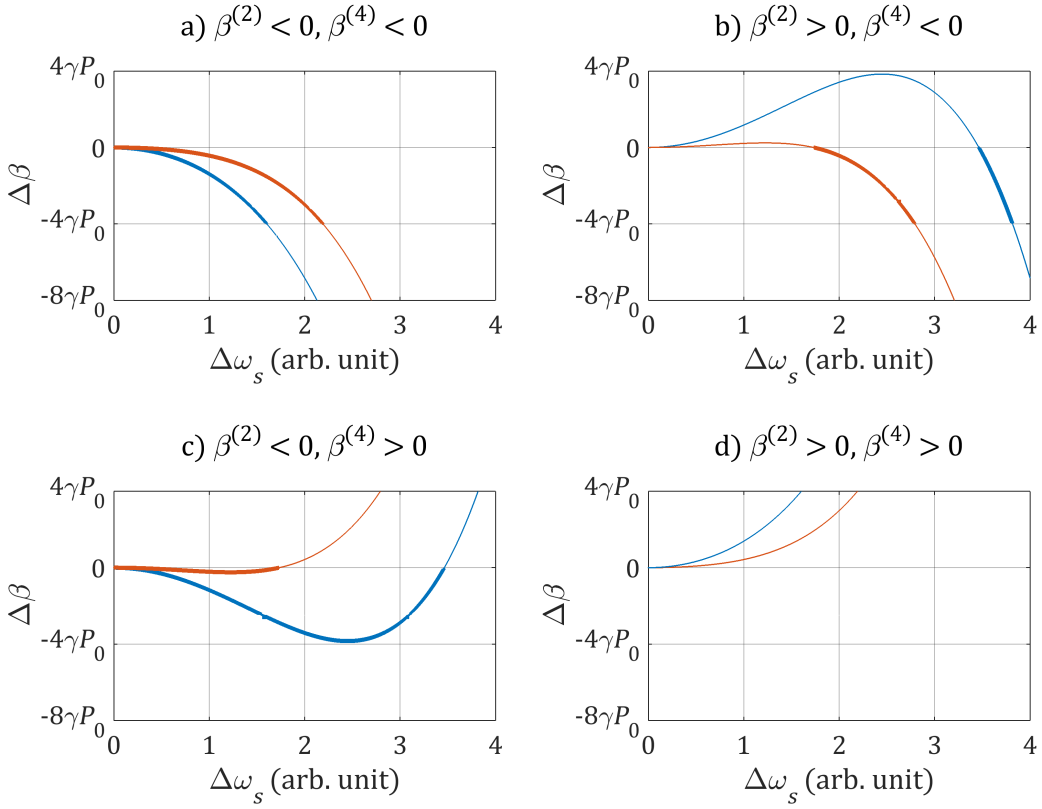

Figure 2.4. Propagation constant mismatch $\Delta\beta$ as a function of signal detuning from the pump $\Delta\omega_s$ for various dispersion parameters at the pump frequency. Curves are thick in the range implying a real gain coefficient in scalar case. The absolute value of the group velocity dispersion $\beta^{(2)}$ is four times smaller for orange curves as compared to blue curves.

Figure 2.4(a) is the basic case for a single pump FOPA operation: the pump dispersion is anomalous and $\beta^{(4)} < 0$. Gain is formed near the pump and smaller moduli of $\beta^{(2)}$ and $\beta^{(4)}$ allow for a wider gain bandwidth. This case is the most robust against dispersion parameters fluctuations as is demonstrated by only a little change of the propagation constant mismatch $\Delta\beta(\Delta\omega_s)$ curve with a four-fold change of $\beta^{(2)}$, but on the other hand does not give much freedom for a FOPA gain spectrum optimisation.

Pump dispersion at Figure 2.4(b) is normal in contrast to Figure 2.4(a). This allows for a special operation regime when gain can be obtained at very large detuning from the pump, but over relatively narrow bandwidth. Importantly, the frequency range

where gain exists can be modified by a little tuning of the pump frequency. This operation regime can be used for amplification in bands where no sources/amplifiers are available or for wavelength conversion. This operation regime is discussed in details in [52].

The case shown at Figure 2.4(c) provides the most freedom for FOPA gain spectrum optimisation as $\beta^{(2)}$ and $\beta^{(4)}$ have opposite signs and gain is real for low $\Delta\omega_s$ (unlike Figure 2.4(b)). Large values of $\beta^{(2)}$ in this case lead to gain near the pump similarly to Figure 2.4(a) and narrow gain far from the pump similarly to Figure 2.4(b) at the same time. Additionally, $\beta^{(2)}$ and $\beta^{(4)}$ can compensate for each other to keep a value of $\Delta\beta$ within the range of interest over a wide continuous bandwidth allowing the broadest (blue curve) and/or the flattest gain spectra (orange curve) among all discussed cases. Note, that the flat gain spectrum predicted by the orange curve has nearly zero propagation constant mismatch $\Delta\beta \approx 0$, so predicted gain is phase-mismatched (relatively low) but nearly constant over wide bandwidth. A flat phase-matched gain has been predicted for this case too (when the $\Delta\beta(\Delta\omega_s)$ curve vertex is just below $-2\gamma P_0$) [9], but it has never been experimentally demonstrated with a single pump FOPA (although this is the best performing operation regime for a two-pump FOPA [53, 54]).

In case of positive $\beta^{(2)}$ and $\beta^{(4)}$ (Figure 2.4(a)), $\Delta\beta$ is positive and adds constructively to the nonlinear wavevector mismatch $\Delta\beta_{NL}$ for all signal frequencies. Gain coefficient is therefore imaginary and there is no persistent gain but rather low gain fluctuations decaying with detuning from the pump. However, as it will be shown in Subsection 2.3.1 the nonlinear wavevector mismatch $\Delta\beta_{NL}$ can be negative for some combinations of pump and signal states of polarisation. Therefore, in general (vector) case a real gain coefficient is possible for positive $\beta^{(2)}$ and $\beta^{(4)}$ under certain conditions.

Figure 2.5 shows an example single pump FOPA signal gain spectrum featuring the most common single pump FOPA gain spectrum shape. The gain spectrum was calculated using equation (2.34) for signal gain. Following parameters were used: the pump power $P = 5$ W, the fibre length $L = 200$ m, the nonlinearity coefficient $\gamma = 14$ W^{-1}·km^{-1} and the dispersion slope $S = 43$ s^{-1}·m^{-3}. Pump offset from the zero dispersion frequency was 200 GHz to introduce a significant anomalous dispersion at the pump frequency. Large $\beta^{(2)}$ makes gain spectrum practically independent of $\beta^{(4)}$

for relatively low signal detuning from the pump, so $\beta^{(4)}$ was set to zero and the calculated gain spectrum is relevant for cases (a) and (c) of Figure 2.4.

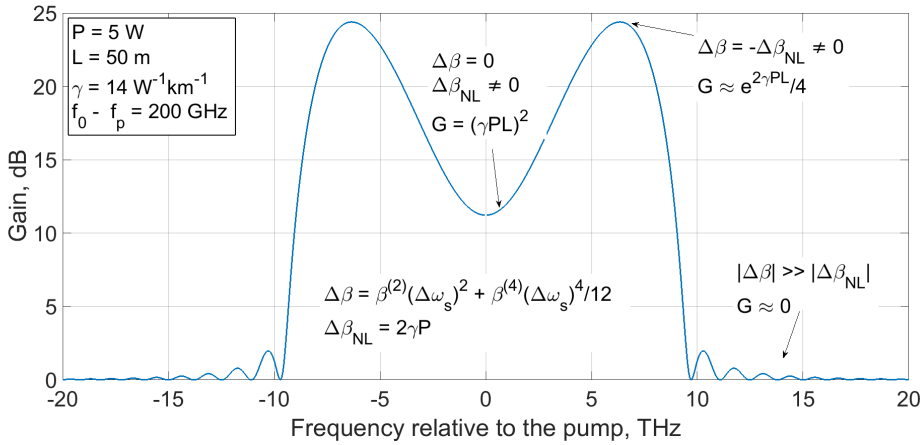

Figure 2.5. Example of a single pump FOPA gain spectrum calculated using analytic equations.

Near the pump the propagation constant mismatch $\Delta\beta$ is close to zero, so a moderate quadratic gain $G_{\Delta\beta=0} = (\gamma PL)^2 + 1$ is observed. As signal detuning from the pump increases the propagation constant mismatch $\Delta\beta$ reaches a value of $-2\gamma P$ and gain increases up to its maximum featuring an exponential gain growth. Further increase of signal detuning from the pump leads to a quick increase of a total wavevector mismatch κ and causes a gain decrease to near zero.

Overall, even though FOPA can provide high gain value and wide bandwidth, typically gain variation across the gain spectrum is very high. Therefore, significant penalties can be induced due to nonlinear crosstalk between excessively amplified signal channels near the gain peak. The suggested approach to obtain a broadband flat gain is to use a fibre with a small positive value of $\beta^{(4)}$ and to tune pump wavelength to proximity of ZDW to obtain a small negative value of $\beta^{(2)}$. In this case a contribution of $\beta^{(2)}$ and $\beta^{(4)}$ is mutually compensated to provide nearly constant propagation constant mismatch $\Delta\beta \approx 0$ for the widest bandwidth.

2.2.4 Generalised Nonlinear Schrodinger equation for FOPA

The preceding subsections have illustratively described the FOPA principle of operation. The performed analysis is convenient for FOPA gain spectrum analysis. However, this approach considers an interaction of only up to four frequency components. Therefore, it is insufficient to describe a behaviour of a large number of

frequency components co-propagating in FOPA, which is typical for WDM systems, phase-modulated pumps (see Subsection 2.4.2), etc. In contrast, a NLSE can describe a propagation of essentially arbitrary optical spectra passing through HNLF.

First, it can be shown [55] that a complex slowly varying envelope $A(z,t)$ of an arbitrary combination of frequency components evolve along a linear isotropic fibre as follows:

$$\begin{aligned}\frac{\partial A(z,t)}{\partial z} &= -\alpha_{lin}\frac{A(z,t)}{2} + \sum_{n=1}^{\infty}\frac{i^{n+1}\beta^{(n)}}{n!}\frac{\partial^n A(z,t)}{\partial t^n} = \\ &= -\alpha_{lin}\frac{A(z,t)}{2} - \beta^{(1)}\frac{\partial A(z,t)}{\partial t} - i\frac{\beta^{(2)}}{2}\frac{\partial^2 A(z,t)}{\partial t^2} + \cdots,\end{aligned} \tag{2.39}$$

where $\beta^{(n)}$ are the derivatives of the propagation constant β arising from the power series expansion as shown in Equation (2.10) and α_{lin} is the power loss coefficient in linear units. In this equation the term $-\alpha_{lin}\,A(z,t)/2$ describes fibre loss, the first term of the summation ($n=1$) describes the envelope propagation with a group velocity v_g, the second term of the summation ($n=2$) describes an impact of the group velocity dispersion on the envelope and the consecutive terms ($n \geq 3$) describe high order dispersion.

Then, an impact of the third-order nonlinearity is introduced as a perturbation of Equation (2.39):

$$\frac{\partial A}{\partial z} = \frac{-\alpha_{lin}A}{2} + \sum_{n=1}^{\infty}\frac{i^{n+1}\beta^{(n)}}{n!}\frac{\partial^n A}{\partial t^n} + i\gamma|A|^2A, \tag{2.40}$$

where A implies $A(z,t)$ and γ is the nonlinear coefficient (Equation (2.20)). In fact, the FOPA propagation equation (Equation (2.21)) is essentially Equation (2.40) neglecting fibre loss and written for four frequency components, while only terms with one particular frequency are kept in the equation. If loss are neglected and only the group velocity disperison is considered for linear propagation, then Equation (2.40) takes the standard NLSE form [56]:

$$i\frac{\partial A}{\partial z} - \frac{\beta^{(2)}}{2}\frac{\partial^2 A}{\partial t^2} + \gamma|A|^2A = 0. \tag{2.41}$$

Finally, the Raman response is introduced as a fraction f_R of the total nonlinear response of the medium [57]. Therefore, considering the third-order nonlinearity only, the Raman response is added to Equation (2.40) as follows [58]:

$$\frac{\partial A(z,t)}{\partial z} = \frac{-\alpha_{lin} A(z,t)}{2} + \sum_{n=1}^{\infty} \frac{i^{n+1}\beta^{(n)}}{n!} \frac{\partial^n A(z,t)}{\partial t^n} + \\ + i\gamma \left[(1 - f_R)|A(z,t)|^2 + f_R \int_{-\infty}^{t} \chi_R^{(3)}(t - t')|A(z,t')|^2 dt' \right] A(z,t), \tag{2.42}$$

where $\chi_R^{(3)}(t)$ is the temporal Raman response function. Equation (2.42) is the single-polarisation generalised NLSE (further referred to as NLSE) showing an evolution along fibre of the group of waves envelope due to the loss, the linear propagation, the third-order nonlinearity and the Raman response.

The important feature of the NLSE is that it separates terms corresponding to different phenomena. One consequence is that the analysis of the NLSE can be simplified by keeping only the terms requiring consideration. Thus, terms describing dispersion up to the fourth order only ($n \leq 4$) are typically kept for FOPA analysis. The Raman contribution and the fibre loss terms are also added if they need to be considered. Another consequence is that NLSE allows to separate linear and nonlinear effects. This is the key idea of NLSE-based split step Fourier method used for FOPA simulations. For every elementary segment of a fibre this method processes at first linear effects in the frequency domain and then nonlinear effects in the time domain.

The NLSE is a powerful tool for FOPA analysis both analytically and through simulations. It allows to investigate a propagation of arbitrary optical spectra, which is useful for study of dithering, nonlinear crosstalk, etc. Unlike the FOPA propagation equation (Equation (2.21)), the NLSE can be used to consider fibre loss, longitudinal fluctuations of fibre parameters, Raman contribution, pump depletion, etc. Additionally, a dual polarisation NLSE for birefringent fibres can be derived.

2.3 An impact of polarisation on FOPA

In previous section it has been assumed that all waves has the same linear state of polarisation, so all vectors could have been handled as scalars. This subsection considers a general case of interacting waves with arbitrary states of polarisation.

2.3.1 Vector FOPA theory

Equation (2.14) has been written for a scalar case under assumptions of a fibre being isotropic and frequencies of an electric field E being close to each other. This equation can be rewritten for a vector electric field $\vec{E}$ as follows:

$$(\nabla^2 + K^2)\vec{E} = \frac{\chi^{(3)}}{c^2}\frac{\delta^2(\vec{E}\vec{E})\vec{E}}{\delta t^2} \tag{2.43}$$

A solution of this equation in the vector case is much more difficult than in the scalar case, consequently a relatively simple illustrative non-scalar example is discussed. A case of a single pump FOPA with linearly polarised but orthogonal pump and signal is considered for demonstration of FOPA involving waves with different polarisation states. In this case an idler has the same polarisation as a signal [23]. Therefore, the products $\vec{E}_p\vec{E}_s$ and $\vec{E}_p\vec{E}_i$ vanish, where $\vec{E}_p$, $\vec{E}_s$ and $\vec{E}_i$ represent the vector electric field of pump, signal and idler respectively. Then, equation (2.17) can be rewritten as follows for a signal frequency:

$$\begin{gathered}(\nabla^2 + K_s)\vec{E}_s = \\ = \frac{\chi^{(3)}}{4c^2}\frac{\delta^2\left(3(\vec{E}_s\vec{E}_s^*)\vec{E}_s + 2(\vec{E}_p\vec{E}_p^*)\vec{E}_s + 6(\vec{E}_i\vec{E}_i^*)\vec{E}_s + 2(\vec{E}_p\vec{E}_p)\vec{E}_i^*\right)}{\delta t^2}\end{gathered} \tag{2.44}$$

The main difference between equations (2.17) and (2.44) is that coefficients for terms causing XPM and FWM and including the pump has been decreased from 6 to 2 (i.e. scaled by $1/3$). The reason for this is that some terms contributing to XPM and FWM between co-polarised waves are turning to zero for orthogonally polarised waves. For example, in the scalar case the term $E_pE_sE_p^*$ is contributing to XPM, but in the vector case the term $(\vec{E}_p\vec{E}_s)\vec{E}_p^*$ equals to zero due to orthogonality of vectors $\vec{E}_p$ and $\vec{E}_s$.

A solution of equation (2.44) is the same as in the scalar case (equations (2.31) – (2.33)), but a change of coefficients for terms causing XPM and FWM has two consequences. First, the FWM coupling coefficient r is decreased by a factor of three as compared to scalar (co-polarised) case, which means that the maximum gain coefficient $g_{max} = r = \gamma P_0/3$ is decreased too. Second, the nonlinear phase shift of the signal and the idler caused by XPM with pump is scaled by $1/3$ so equation (2.28) can be rewritten as follows (the second line is the same as for a single pump FOPA in the scalar case):

$$\begin{gathered}d\varphi_s/dz = d\varphi_i/dz = 2\gamma P_0/3\,; \\ d\varphi_{p1}/dz = d\varphi_{p2}/dz = \gamma P_0.\end{gathered} \tag{2.45}$$

Therefore, the nonlinear phase shift for orthogonal linearly polarised pump and signal is:

$$\Delta\beta_{NL} = \frac{d\varphi_s}{dz} + \frac{d\varphi_i}{dz} - \frac{d\varphi_{p1}}{dz} - \frac{d\varphi_{p2}}{dz} = -\frac{2\gamma P_0}{3}. \quad (2.46)$$

Then, the propagation constant mismatch $\Delta\beta$ range where the gain coefficient is real is $0 < \Delta\beta < 4\gamma P_0/3$. Therefore, in contrast to the scalar case, in the case of orthogonal linearly polarised signal and pump, a gain will be observed for positive $\beta^{(2)}$ and $\beta^{(4)}$ (Figure 2.4(d)), but not for negative ones (Figure 2.4(a)). However, gain bandwidth and peak gain are much smaller for orthogonally polarized waves due to low FWM coupling coefficient.

Overall, following coefficients have been introduced to calculate the maximum gain coefficient g_{max} and the nonlinear wavevector mismatch $\Delta\beta_{NL}$ for arbitrary polarisation states of pump(s) and signal in FOPA:

$$b = \frac{g_{max}}{\gamma P_0}, \quad u = \frac{\Delta\beta_{NL}}{\gamma P_0}. \quad (2.47)$$

These coefficients have been calculated for 12 principal combinations of linear and circular polarisations of pump and signal for birefringent and non-birefringent cases in [23, 59]. For example, in the case discussed above $b = 1/3$ and $u = -2/3$, while in the co-polarised (scalar) case: $b = 1$ and $u = 2$. These coefficients show that a relation between signal and pump polarisation states defines not only an amplitude of FOPA gain, but also a frequency range where a FOPA gain exist. Probably, the most important values derived in [59] are $b = 8/9$ and $u = 16/9$ for co-polarised signal and pump in case of random birefringence. A coefficient of $8/9$ arises due to averaging over the Poincare sphere.

2.3.2 Polarisation independent FOPA gain

A number of techniques have been investigated to achieve the same gain for signals with arbitrary polarisation and polarisation multiplexed signals. One of them is using orthogonally polarised pumps in two-pump FOPA [60]. An on-off gain of ~10 dB over 0.4 THz with polarisation dependent gain of 0.4 dB has been demonstrated using this approach [61]. Therefore, it can be used for optical phase conjugation and low gain FOPA. However, achieving high gain is difficult with orthogonally polarised pumps because in this case the coefficient $b = 1/3 \ldots 4/9$ depending on polarisation averaging [59], which means that gain coefficient is reduced by a factor of 2 ... 3 as compared to a co-polarised case.

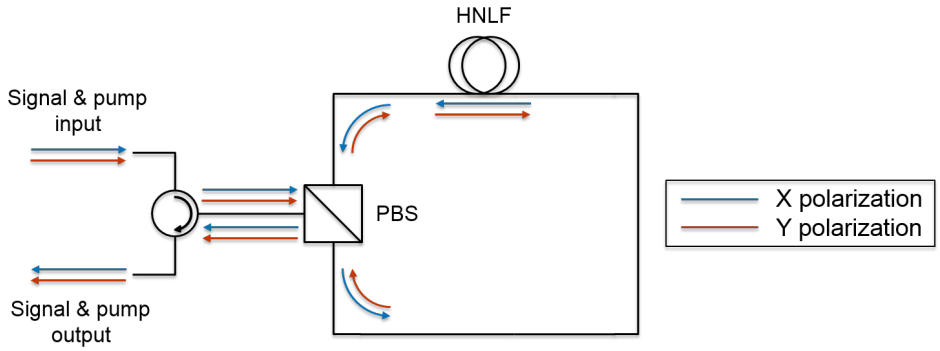

Figure 2.6. Schematic of an example loop architecture for polarisation-independent FOPA [62].

For a single pump FOPA it has been suggested to split a signal with arbitrary polarisation into two orthogonal linear polarisations using a polarisation beam splitter (PBS) and to amplify each of them independently by a corresponding co-polarised pump. It can be done in a Mach-Zehnder interferometer arrangement using two HNLF lengths in parallel, but an active optical path alignment is required in this case [63]. Therefore, it has been realised in a Sagnac interferometer (loop) arrangement using a single length of HNLF [62]. This approach takes advantage of unidirectional FOPA gain (a signal is not amplified by a counter propagating pump) and ensures the same optical path length (an example scheme is shown at Figure 2.6). This approach has shown good performance for optical phase conjugation [64], but it has been proved to be unsuitable for high gain FOPA due to interaction of counter propagating high power pumps through stimulated Brillouin scattering (see Subsection 2.4.2), which leads to significant signal distortion [65].

The polarisation-diversity loop configuration was therefore upgraded by employing two lengths of HNLF [24] and passing only one pump through each fibre length as shown at Figure 2.7. Each signal polarisation therefore passes an 'active' section of HNLF where it obtains an amplification and then a 'passive' section of HNLF where orthogonal polarisation is amplified. In this case there is no counter-propagating pumps and the setup resembles a Mach-Zehnder interferometer with looped output. An amplification by >20 dB of polarisation multiplexed-signals over a range of 2.3 THz has demonstrated a viability of this scheme for broadband high gain FOPA [63]. However, performance was strongly limited by nonlinear crosstalk arising due to propagation of amplified signals through an additional HNLF section. An effective length was used to assess nonlinear crosstalk accumulation and it was found

that the effective length of a passive section was 6 times higher than the effective length of an active section.

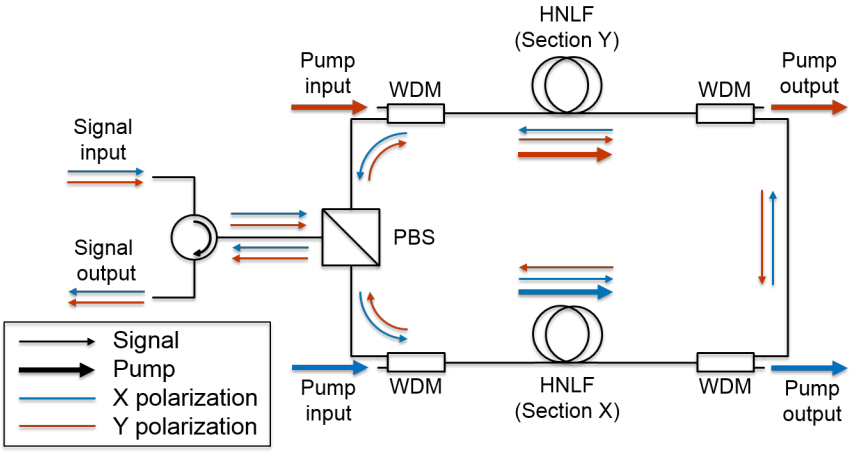

Figure 2.7. Schematic of an example two-fibre loop architecture for a polarisation-independent FOPA [24].

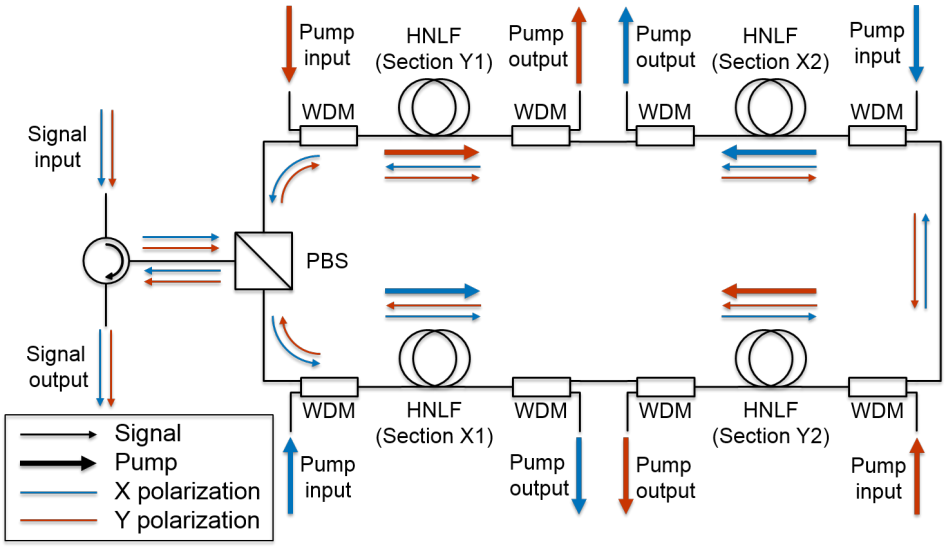

Figure 2.8. Schematic of an example four-fibre loop architecture for a polarisation-independent FOPA [66].

Nonlinear crosstalk in the two-fibre loop could be tackled by changing direction of pumps, which means that signals at first pass the 'passive' section accumulating little crosstalk due to low power and then get amplified in the 'active' section [63]. However, this would have a major impact on the noise figure due to significant upfront loss [67]. Therefore, a four-fibre loop has been suggested [66]. In this configuration signal passes through sections in a following way: 'active', 'passive',

'active' and 'passive' (Figure 2.8). The first 'active' section is to compensate for upcoming loss and thus to minimise a noise figure penalty. On the other hand, since this section is relatively short, the nonlinear crosstalk accumulation in the last 'passive' section (the first and the last sections have the same fibre length due to symmetry) is also reduced as compared to the two-fibre loop. Simulations have shown that the four-fibre loop configuration allows to optimise a combined impact of noise figure and nonlinear crosstalk [66], but it is yet to be proved experimentally.

2.4 Nonlinear scattering

Previously considered nonlinear effects are elastic as no energy was exchanged between the optical field and the medium. This section considers inelastic nonlinear effects in which the optical field transfers a part of its energy to the medium. They are called stimulated Raman scattering (SRS) and stimulated Brillouin scattering (SBS) and can have a crucial impact on FOPA due to high optical intensities targeted in FOPA to invoke the third-order nonlinearity [35].

SBS and SRS from the quantum mechanical point of view consist in annihilation of an incident photon to create a lower frequency photon (Stokes wave) and a phonon. The main difference between SRS and SBS is that SRS is an interaction with optical phonons and SBS is an interaction with acoustic phonons. This defines other differences between them: SBS introduces a much smaller frequency shift than SRS, SBS is much more efficient process than SRS, and SBS occurs only in backward direction, while SRS can occur in both directions.

2.4.1 Stimulated Raman scattering

An effect of Raman in frequency domain can be analysed by introducing the complex Raman susceptibility $\tilde{\chi}_R^{(3)}(\Delta f)$ which is a Fourier transform of the delayed Raman response $\chi_R^{(3)}(t)$ (Subsection 2.2.4) and is normalised such that $\tilde{\chi}_R^{(3)}(0) = 1$ [58]. Figure 2.9 shows an imaginary and a real part of the nomralised complex Raman susceptibility $\tilde{\chi}_R^{(3)}$ in silica as a function of a frequency detuning Δf from the pump. An imaginary part of the Raman susceptibility was extracted from the files of the VPI simulation software, a real part of the Raman susceptibility was calculated using Kramers-Kronig relations [68].

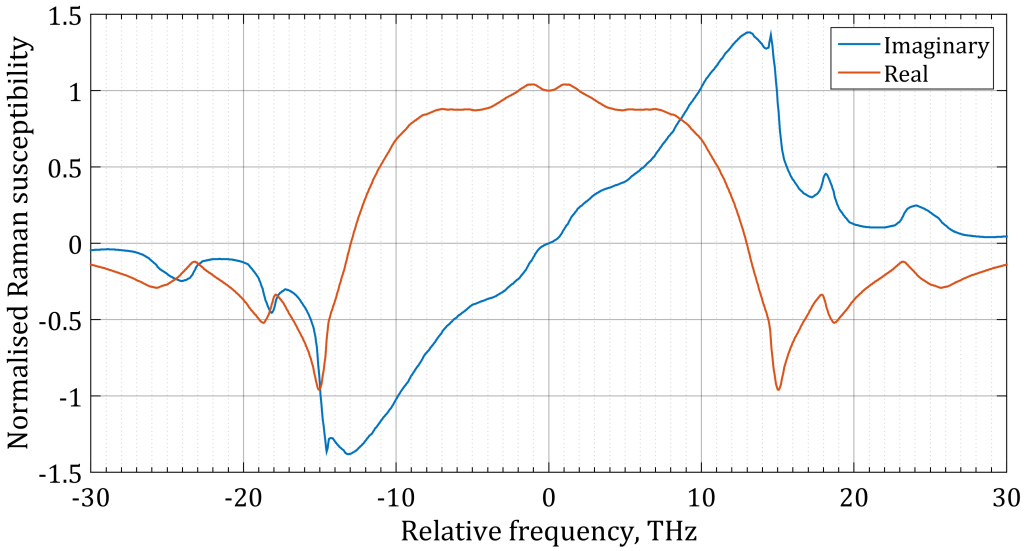

Figure 2.9. Imaginary and real parts of the normalised Raman susceptibility in silica.

The imaginary part of the Raman susceptibility $Im\left(\tilde{\chi}_R^{(3)}(\Delta f)\right)$ is responsible for power transfer between frequency components (Raman gain). Thus, a small-signal Raman gain (no pump depletion, no signal-signal interaction) in a lossless fibre can be calculated as follows [69]:

$$G(z,\Delta f) = \exp[g_R(\Delta f)Pz] = \exp\left[\gamma f_R Im\left(\tilde{\chi}_R^{(3)}(\Delta f)\right)Pz\right], \qquad (2.48)$$

where $g_R(\Delta f)$ is the Raman gain coefficient as a function of the frequency detuning from the pump. High power pump in FOPA inevitably invokes Raman gain. For large gains, the Raman gain and the phase-matched parametric gain ($\exp(2\gamma Pz)/4$) differ in scaling of gain coefficient by $f_R Im\left(\tilde{\chi}_R^{(3)}\right)$ and have a fixed shift by 6 dB. The Raman fractional strength f_R is typically ~0.18 [70], but also can be as high as ~0.3 [71], so the Raman gain peak is typically 2-3 times smaller than the phase-matched parametric gain [11]. However, an impact of Raman gain on FOPA gain spectrum in silica fibres can be substantial for frequency detuning >5 THz and peaks ~13 THz away from the pump (Figure 2.9). Thus, Raman gain was producing a ripple on the top of flat FOPA gain spectrum in [54]. Therefore, it must be considered in broadband FOPA.

The real part of the Raman susceptibility $Re\left(\tilde{\chi}_R^{(3)}\right)$ describes a phase shift introduced by the Raman effect. Note, since Raman contribution is included to the NLSE (Subsection 2.2.4) as a fraction of the third order nonlinearity, the Raman-

induced phase-shift is in a deviation of the real Raman susceptibility from 1, i.e. there is no phase-shift when $Re\left(\tilde{\chi}_R^{(3)}\right) = 1$. The phase shift introduced by the real Raman susceptibility affects phase-matching condition in FOPA (Subsection 2.2.2), which is demonstrated in [58]. In fact, the decrease of the real Raman susceptibility well below 1 for detuning >10 THz essentially means that the nonlinear coefficient for XPM and FWM between distant frequency components (>10 THz) is decreased by the amount of the Raman fractional strength. Therefore, the real part of Raman susceptibility can also affect FOPA gain spectrum, especially for gain bandwidth >10 THz.

2.4.2 Brillouin scattering

The process of SBS can be viewed as follows. The pump generates an acoustic wave via electrostriction, and the acoustic wave modulates the refractive index. The formed refractive index grating moves with the acoustic velocity and reflects the pump back through Bragg diffraction. The frequency of the reflected light is shifted due to the Doppler effect. The Brillouin frequency shift is $\nu_B \sim 11$ GHz in silica [72].

The power backscattered due to SBS increases exponentially due to Brillouin gain until the pump is depleted. Therefore, the SBS essentially limits the maximum power P_{th} that can be injected into the fibre within the SBS interaction linewidth $\Delta\nu_B$ (typically, lying in the range from 20 to 100 MHz) [73]:

$$P_{th} \approx \frac{21kA_{eff}}{g_B L_{eff}}\left(1 + \frac{\Delta\nu_p}{\Delta\nu_B}\right), \tag{2.49}$$

where k is the coefficient between 1 and 2 depending on polarisation and birefringence [74], A_{eff} is the effective area, g_B is the Brillouin gain coefficient, L_{eff} is the effective length and $\Delta\nu_p$ is the pump linewidth. Assuming a long span of a standard single-mode fibre ($L_{eff} = 20$ km) and a narrow linewidth ($\Delta\nu_p \ll \Delta\nu_B$) pump, the P_{th} is of the order of a few mW [73], which is clearly not enough to invoke significant SRS or the third-order nonlinearity and thus makes SBS a dominant nonlinear effect for narrow linewidth pumps in long fibres.

HNLFs used in FOPA typically have a small core (small A_{eff}), so SBS threshold for them is even lower than e.g. for standard single mode fibres. However, a relatively short fibre lengths (an order of ~100 m) are used in FOPA, so their effective length essentially equals a fibre length L. In this case the SBS threshold scales inversely with a fibre length, and it is convenient to refer to the SBS threshold as $(PL)_{th}$.

It has been shown that the SBS causes significant instabilities to the pump in presence of counter-propagating wave (e.g. Rayleigh backscattering, backreflection from connectors, etc.) at much lower power than the critical power P_{th} [75]. Additionally, SBS converts the pump phase noise to the pump intensity noise with significant amplification [76]. Therefore, an impact of SBS on the pump quality might be the most important for definition of the SBS threshold in FOPA.

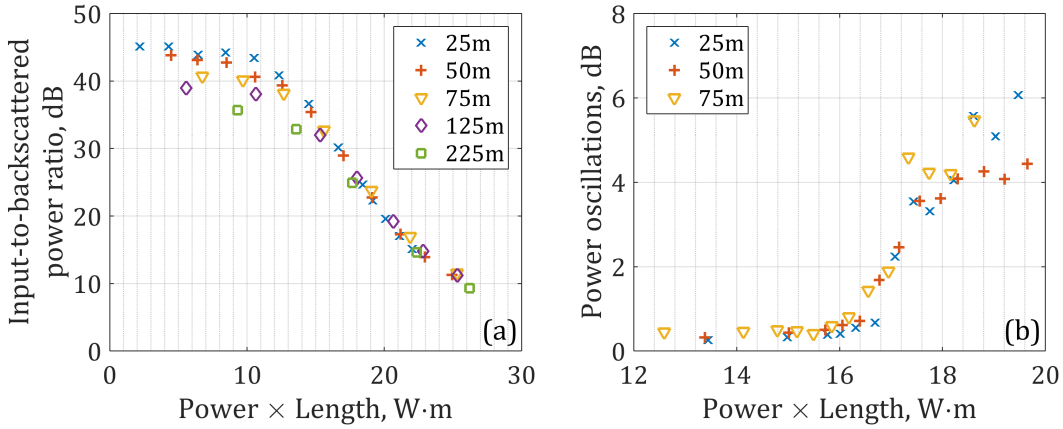

Figure 2.10. Experimental characterisation of (a) backscattered power and (b) oscillations of backscattered power due to SBS in various lengths (named in corresponding legends) of the same HNLF.

Figure 2.10 shows results of experimental SBS measurements for a range of lengths of the same HNLF. A narrow linewidth pump source boosted by an Erbium-doped fibre amplifier and a HNLF employed in experiments throughout this work (described in Subsection 3.1.1) were used. Figure 2.10 (a) demonstrates that the backscattered fraction of the pump power is indeed an exponential function (looks linear when dB are plotted versus linear units) of a pump power and a fibre length product PL for a range of fibre lengths from 25 to 225 m. A common SBS threshold definition is when 1% of the pump power is backscattered, i.e. the ratio between the input and the backscattered powers is 20 dB. The 1% SBS threshold was $(PL)_{th,1\%} = 20$ W·m. This definition allows to neglect power loss due to SBS below the threshold. Additionally, Figure 2.10(b) shows an amplitude of the backscattered power oscillations detected by a power meter. There is a rapid growth of oscillations at $PL \sim 16$ W·m for all three examined fibre lengths. Since backscattered power is subtracted from the input pump power, these power oscillations are transferred to the pump. Pump intensity noise can strongly degrade the FOPA performance, so $(PL)_{th,int.noise} = 16$ W·m can be considered the SBS threshold for intensity noise in

this fibre in this setup. However, the value of threshold defined in such way strongly depends on system parameters so it is not universal.

It can be noted that the nonlinear coefficient scales inversely with the effective area ($\gamma \sim 1/A_{eff}$), so the SBS threshold scales proportionally with the effective area: $(PL)_{th} \sim A_{eff}$. Therefore, the nonlinear phase shift limited by the SBS $\Phi_{th} = \gamma(PL)_{th}$ is expected to be nearly the same for all silica fibres unless SBS is mitigated in some way. It has been experimentally confirmed that two different HNLFs available in the lab and possessing different nonlinear coefficients γ of $0.014\ \mathrm{W^{-1}{\cdot}m^{-1}}$ and $0.008\ \mathrm{W^{-1}{\cdot}m^{-1}}$ had the same value of $\Phi_{th,1\%} = \gamma(PL)_{th,1\%}$. However, the SBS threshold, especially if it is defined via power fluctuations, also depends on the pump source properties and the amount of backscattered/backreflected light in the setup. Overall, SBS essentially limits (with minor reservations) the nonlinear phase shift and consequently the maximum FOPA gain in silica fibres:

$$G_{max,th} = [\cosh(\Phi_{th})]^2 \quad \text{or} \quad G_{max,th}^{dB} \approx 8.69\Phi_{th} - 6. \tag{2.50}$$

Using the measured 1% SBS threshold of $(PL)_{th,1\%} = 20\ \mathrm{W{\cdot}m}$ and the corresponding nonlinear coefficient $= 0.014\ \mathrm{W^{-1}{\cdot}m^{-1}}$, it can be derived that the nonlinear phase shift limited by not mitigated SBS is $\Phi_{th,1\%} = 0.28$. This corresponds to the maximum FOPA gain of $G_{max,th} = 0.34$ dB and means that SBS do not allow any reasonable FOPA gain unless SBS is mitigated. Since the nonlinear phase shift of 3 is required to reach a peak FOPA gain of 20 dB (Figure 2.2), the SBS threshold needs to be increased by a factor of at least 10 to allow for high gain FOPA.

There are two general approaches to mitigate SBS. One is to disrupt an acoustic wave propagation along fibre, typically via amending the Brillouin frequency shift ν_B longitudinally. This can be done by introducing a longitudinal variation of temperature [47], strain [77, 78], core radius [79, 80] or dopant concentration [81]. However, only one of these works has demonstrated the required SBS threshold increase of at least 10 dB [78] and only one of them has allowed for a uniform dispersion profile [80].

Therefore, another approach is typically used in FOPA: the SBS threshold scales proportionally with the pump linewidth $\Delta\nu_p$ as shown in equation (2.49), so the latter is being increased. Pump phase modulation is typically used to broaden the pump in FOPA and this process is called a dithering. Pump phase modulation with five harmonics up to 10 GHz has been used to increase the SBS threshold by ~20 dB [19].

Besides, a bandwidth efficient pump phase modulation driven by a 1.5 GHz noise source has been demonstrated to increase the SBS threshold by 19 dB [26]. Although this approach is highly efficient to mitigate SBS, its drawbacks include signal gain fluctuations degrading signal quality [82, 83] and a transfer of phase-modulation to idlers [84]. This work uses dithering with three harmonics up to 1 GHz which provides the SBS threshold increase by ~13 dB. Therefore, the maximum nonlinear phase shift in this work is $\Phi_{th,1\%} \times 20 = 5.6$ corresponding to the maximum FOPA gain of 42 dB.

3 BROADBAND FLAT FOPA GAIN SPECTRUM

FOPA is viewed as the main candidate to significantly improve an utilisation by high-speed optical communications of the 44 THz wide low-loss transmission window, because FOPA in principle can provide a virtually unlimited gain bandwidth in arbitrary wavelength range [11]. However, although a continuous band of net gain >30 THz wide has been demonstrated with FOPA [8], it was found difficult to achieve a low gain variation (GV) gain spectrum spanning >9 THz on one side of the FOPA central frequency.

Low unfiltered GV is important in a FOPA because nonlinear crosstalk scales as the square of the output signal power [85]. FOPAs with high GV are therefore likely to suffer from signal quality degradation arising from both higher crosstalk and additional noise associated with overcoming gain flattening filter loss. Signal amplification within a FOPA is in general case constraint to one side of the FOPA central frequency due to the emergence of phase conjugate idlers possessing symmetry around the FOPA central frequency with any amplified signals [9] (see Subsection 3.2.2 for details). Therefore, gain bandwidth only at one (the best performing) side of the central frequency is considered and implied further in this work. Note that for single pump FOPAs considered in this chapter, the central frequency coincides with the pump frequency [9].

Some of the broadest low GV FOPA gain spectra have been obtained in two-pump FOPAs by designing a so called Chebyshev gain spectrum [53]. Following gains have been experimentally demonstrated in this way: 25±1.5 dB over 7.1 THz (59 nm) [86], 23.5±1.5 dB over 8.6 THz (73.5 nm) [54] or 38.5±1 dB over 4.9 THz (39 nm) [87] (these gain bandwidths consider gain only at one side of the central frequency, so they differ from those claimed in the original sources). However two-pump FOPAs can be considered experimentally complex, suffer from significant 'unwanted' four wave mixing (FWM), and require high power pump generation in unfavourable parts of the spectrum to obtain wide bandwidth.

Single pump FOPAs conversely can provide a wide gain bandwidth using a pump placed in the C or L band where high power is easily obtainable. The achievable bandwidth is additionally not bound by the wavelength location of the pump, and the 'unwanted' FWM is substantially lower than the two-pump case [27]. The most notable single pump FOPA gain spectrum achievements obtained with standard

highly nonlinear fibre (HNLF) include gains of 12.3±0.6 dB over 6 THz (50 nm) [88] and 16.8±2.8 dB over 12.5 THz (110 nm) [8]. Although the latter result suggests an exceptional gain bandwidth, the GV of >5 dB is considered to be intolerably high as it can cause up to 10 dB higher nonlinear crosstalk due to its quadratic scaling with the signal power [27]. Advanced dispersion management techniques have been suggested to enable low GV across wide gain spectrum provided by a single pump FOPA [89–93]. Among them, the most notable experimental result is quasi phase matched gain of 23.7±1.3 dB over 6.4 THz (50 nm) [94]. An impressive pulsed gain of 63±3.5 dB over 12 THz bandwidth in the 1100 nm region was obtained in dispersion-varying HNLF [91], but a viability of such approach for optical communications is yet to be confirmed.

Overall, experimental results with single pump FOPAs demonstrate possibility of a wider gain spectrum than with two-pump FOPAs, but on the cost of increased GV. In this chapter a capability of a single pump FOPA to provide low GV over wide bandwidth is re-examined. An ultra-short dispersion-stabilized HNLFs are implemented to improve the dispersion parameters stability and increase the stimulated Brillouin scattering (SBS) threshold allowing an employment of high pump power, and consequently to improve the gain bandwidth. Then, a fine tuning of pump wavelength around the zero-dispersion wavelength (ZDW) is performed to find an optimal pump wavelength in terms of gain bandwidth and GV. An impact of pump power on GV is examined too.

In Section 3.1 an experimental setup allowing a diverse single pump FOPA optimisation and characterisation is described. In Section 3.2 a methodology of a quick broadband FOPA gain spectrum using a broadband supercontinuum is presented and verified. In Section 3.3 a single pump FOPA gain spectrum is experimentally optimised to maximise low GV gain bandwidth. As a result of this optimisation a record wide flat gain of 9.2±0.7 dB in a range of 104 nm (12.2 THz) is obtained.

3.1 Experimental setup

This section describes an experimental setup employed in Chapters 3 and 4. Subsection 3.1.1 describes the whole system including a single pump FOPA and means of its characterisation. Subsection 3.1.2 describes a supercontinuum source, which is an essential module used for broadband FOPA gain spectrum measurement.

3.1.1 Broadband FOPA

Figure 3.1 shows the experimental setup for broadband FOPA optimisation and characterisation. The experimental setup is based on the one described in [95]. A continuous pump generated from a 100 kHz linewidth tuneable laser (TL) was passed through a phase modulator (PM) driven by radio frequency (RF) tones at 100 MHz, 320 MHz and 980 MHz to mitigate stimulated Brillouin scattering [26]. The pump was amplified by a high-power EDFA and filtered using a circulator and a stretchable reflective fibre Bragg grating (FBG) tuned to the pump wavelength to remove amplified spontaneous emission (ASE) noise, and to combine the filtered pump with a FOPA input of choice. Polarisation controllers (PC) PC1 and PC2 were used to control a polarisation of the input and the pump respectively.

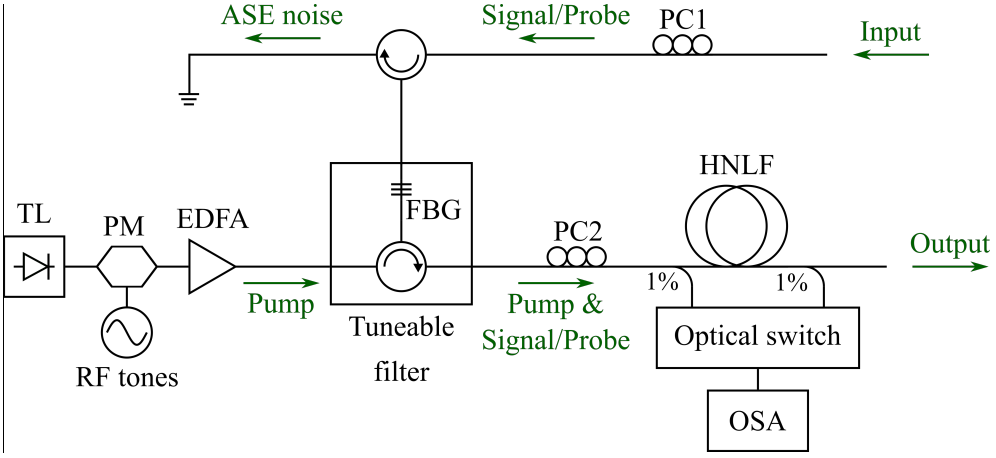

Figure 3.1. Experimental setup for broadband FOPA optimisation and characterisation.

Three variants of the FOPA input sources were used with this setup. First, a supercontinuum source described in Subsection 3.1.2 was used to generate a broadband probe ranging from 1520 nm to 1700 nm to perform broadband gain measurements in Chapters 3 and 4. Second, lasers tuneable across C and L bands were used to generate polarised 100 kHz linewidth probes for conventional gain measurements in a range 1550 – 1625 nm. These measurements are performed in Section 3.2 to verify a broadband gain measurement technique. Due to unavailability of laser sources in a wavelength range 1625 – 1682 nm, polarised narrow linewidth probes in this range were generated using a wavelength conversion from 1460 – 1510 nm where a suitable tuneable laser was available. Third, a wavelength-

tuneable 60 Gbps quadrature phase shift keying (QPSK) signal was used for assessment of signal penalties occurring in the FOPA in Subsection 3.3.5.

The pump and the input were guided into one of lengths of dispersion-stable HNLF [96]. All available lengths: 25, 50, 75 and 100 m, were derived from the same parent spool. The key datasheet parameters of the parent spool were: ZDW of 1550.5±0.5 nm, nonlinear coefficient $\gamma = 21.4$ W^{-1}·km^{-1} and dispersion slope $S = 0.043$ ps·nm^{-2}·km^{-1} measured at 1550 nm. The fourth order propagation constant $\beta_4 \sim 10^{-56}$ s^4·m^{-1} was estimated from the fibre dispersion profile measured by the manufacturer. Due to variation of dispersion parameters along the parent spool these values may be used for reference only. Additionally, a matching of experimental results with simulations in Subsection 3.3.1 has shown that $\gamma \sim 14$ W^{-1}·km^{-1} is the most suitable to describe FOPA gain spectrum occurring in this HNLF.

Two 1% couplers were placed at the ends of the HNLF and connected to an optical spectrum analyser (OSA) via an optical switch. They allowed to non-intrusively take optical power spectra and to perform power measurements across wide wavelength range (~1460 – 1700 nm) before and after amplification. Additionally, a set of calibrated couplers and power meters (not shown at Figure 3.1) were used to control pump power across the setup and particularly to measure input and backscattered pump powers. Calibration factors of all monitor paths were accurately measured.

Amplified probes were guided to a beam dump. Amplified QPSK signals were passed through filters to remove the pump and then guided to a coherent receiver. Details on the signal amplification experiment are provided in Subsection 3.3.5.

3.1.2 Broadband supercontinuum source for FOPA gain measurement

The broadband probe for the amplifier characterisation in this work was generated using a supercontinuum (SC) source as described in [97]. A setup of a broadband SC source used in this experiment is shown at Figure 3.2. A 5 km long TrueWave© fibre was pumped by a Raman laser operating at 1455 nm with the maximum output power of 5.4 W. A broadband SC source was connected to the input of the broadband FOPA experimental setup shown at Figure 3.1.

Figure 3.3 shows an adjustable spectral shape of the SC measured at the input of the HNLF (Figure 3.1) for various Raman laser powers. It can be seen that the Raman laser power >4 W is sufficient to generate a SC in a range 1520 – 1700 nm. A ripple at ~1562 nm is caused by FBG (shown at Figure 3.1) meant to couple a probe (a SC in this case) and a FOPA pump (turned off during this measurement). A sharp edge of

the SC at ~1520 is caused by a 1455/1550 WDM coupler. The total output SC power reaching HNLF could have been >1 W for Raman laser power >3 W. Therefore, the SC power was attenuated using a 10% coupler followed by a digital variable optical attenuator (VOA).

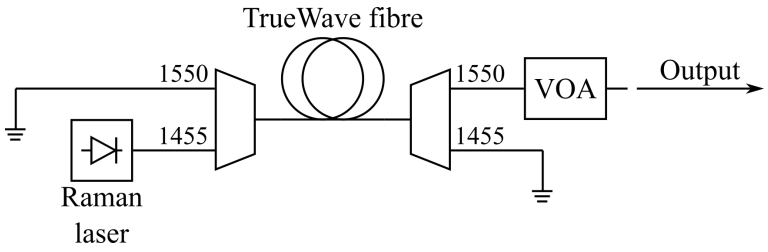

Figure 3.2. Schematic setup of the broadband SC source.

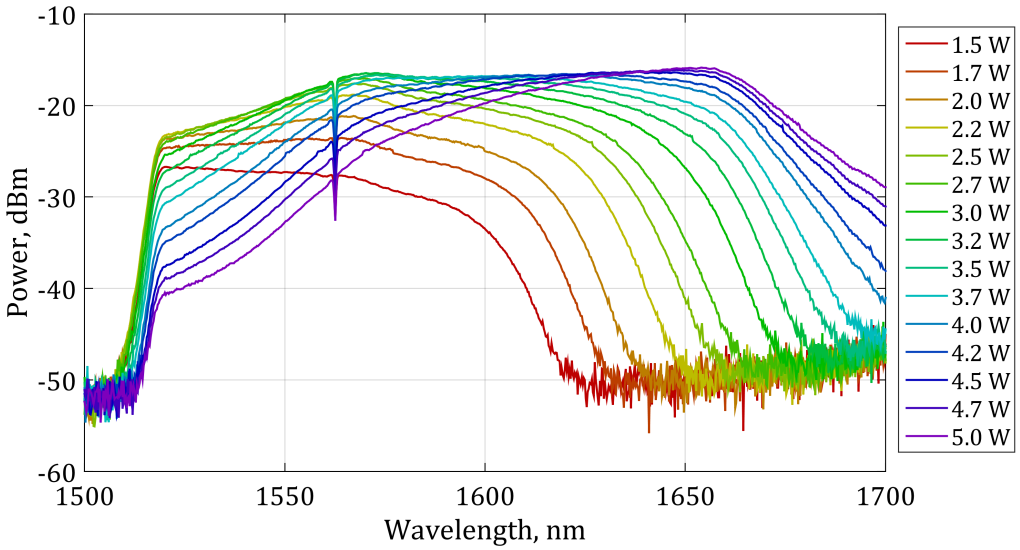

Figure 3.3. SC spectra measured at the input of HNLF for various Raman laser powers (named in the legend).

The SC supposedly inherited random polarisation from the Raman pump laser used for SC generation. Polarisation properties of the SC were tested using a polariser added after the PC1 (Figure 3.1). It has been confirmed that the measured SC spectrum at the input of the HNLF was fluctuating by less than 0.1 dB while the SC polarisation before the polariser was being changed using the PC1. Therefore, it was assumed that this SC source can be considered to be depolarised as instantaneous state of polarisation of the SC was distributed evenly over the Poincare sphere within the OSA response time.

3.2 Methodology of broadband gain spectrum measurement

Demonstration and experimental optimisation of broadband FOPA (>100 nm gain bandwidth was aimed) requires ability to quickly and accurately measure broadband gain spectra. Reports of similar gain bandwidths involving Raman or doped fibre amplifiers demonstrate that gain spectrum characterisation over such a wide bandwidth using a comb of fixed lasers or a tuneable laser is difficult due to the availability of sources and/or measurement time [7, 98–100]. This is exacerbated if the amplifier possesses polarisation dependent gain requiring probe polarisation control.

It has been demonstrated that a broadband probe can be used to roughly evaluate FOPA gain spectra over wide bandwidth [8, 84]. However, it has been noted in [84] that the FOPA has unique features which can skew the raw measurement results obtained with a broadband probe such as idler generation [9] and significant FWM between frequency components of the broadband probe [101]. Additionally, FOPA polarisation-dependent gain needs to be accounted for when a broadband probe is used (see Subsections 3.2.4 and 3.2.5 for details). These issues therefore need to be investigated before a broadband probe can be used for an accurate ultra-wide gain FOPA characterisation. Raman gain is also to be considered since it inevitably mixes with FOPA gain spanning over 100 nm.

The broadband gain measurement technique described in this section has been published in [29, 30]. This section relies on the same set of experimental data and supplements [29] with extra details and discussion.

3.2.1 Gain spectrum measurement using a broadband probe

Broadband gain spectrum measurement consists in finding the difference between the power spectra of a broadband probe measured at the input and the output of the amplifier under test. The gain can be measured at every frequency where the broadband probe exists. A broadband probe does not need to be spectrally flat as the gain is calculated independently at each frequency. However, determining the correct gain at all frequencies of a broadband probe requires to eliminate or to account for such issues as signal-idler mixing, nonlinear interaction between frequency components of a broadband probe, gain saturation and polarisation dependent gain. All of these issues are considered in this section by developing a measurement methodology and deriving relations for numerical processing of raw results. Note, an analysis of raw experimental results is complicated in the general case of an amplifier

comprising both Raman and parametric amplification, because the gain spectrum consists of parametric-only and Raman-only regions as well as regions with substantial Raman and parametric gain occurring together.

3.2.2 Signal-idler mixing

Parametric gain is symmetric around its central frequency [9]. If the broadband probe straddles the central frequency at the input then the output spectrum will unavoidably represent a mix of signals and idlers, where 'signals' refer to amplified frequency components where signal gain is being measured, and 'idlers' are copies of amplified frequency components symmetric with 'signals' around the central frequency. Mixing of signals and idlers does not allow the gain to be calculated as a ratio between output and input powers because in this case the output power at some frequencies is a sum of the amplified signal and an idler [84]. Therefore, gain calculation requires either the signal-idler mixing to be resolved or the input broadband probe to be restricted to strictly one side of the central frequency per measurement. The latter is difficult to achieve experimentally without a 'blind-spot' occurring around the central frequency, so it is preferable for a broadband probe to straddle the central frequency and to resolve occurring signal-idler mixing.

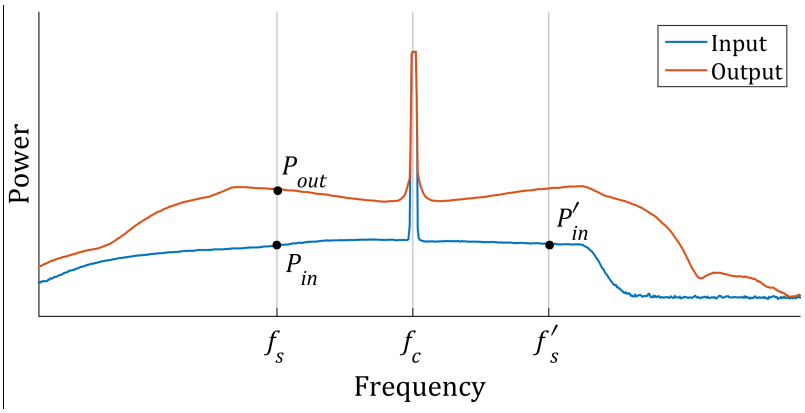

Figure 3.4. Illustration for signal-idler mixing consideration depicting example power spectra of a broadband probe at the input and the output of the FOPA.

Whilst performing gain measurement using a broadband probe, for every frequency where signal gain is to be found, the signal-idler mixing results in output power to equal:

$$P_{out} = P_{in} \times G_s + P'_{in} \times G_i, \tag{3.1}$$

where P_{in} and P_{out} are measured input and output powers at the signal frequency f_s, P'_{in} is the measured input power at the frequency $f'_s = 2f_c - f_s$ symmetric to signal around the central frequency f_c, G_s and G_i are the signal gain and the conversion efficiency at the signal frequency (Figure 3.4).

The unknown conversion efficiency G_i has to be substituted or removed from the equation (3.1) to find the signal gain G_s. The substitution can be done by using the relation $G_s = G_i + 1$ (equation (2.33)) applicable if Raman gain at both the signal frequency and the frequency symmetric to the signal can be neglected, i.e. the signal gain G_s and the conversion efficiency G_i are defined by parametric gain only. In this case the signal gain can be calculated as follows:

$$G_s = (P_{out} + P'_{in})/(P_{in} + P'_{in}). \tag{3.2}$$

However, equation (2.33) is skewed in presence of Raman gain at the signal frequency and/or the corresponding symmetric frequency [58]. The relation between the signal gain and the conversion efficiency becomes complex in this case, so it is suggested to avoid signal-idler mixing as follows: if Raman gain is noticeably present (~5-15 THz away from the pump in silica [71]) at least at one of two frequencies symmetric around the central frequency, the broadband probe power has to be negligibly low at one of these frequencies to allow a signal gain measurement at another frequency of this pair, i.e. gain measurement at frequency f_s requires $P'_{in} \ll P_{in}$ (Figure 3.4). Then, the term $P'_{in} \times G_i$ in equation (3.1) can be neglected and signal gain can be found using a simple relation:

$$G_s = P_{out}/P_{in}. \tag{3.3}$$

Note, that equations (3.2) and (3.3) are equivalent in case of negligible P'_{in}, so equation (3.2) can be used to process results in frequency ranges where preconditions for equations (3.2) or (3.3) are satisfied.

The Raman gain is localised in the range ~5-15 THz away from the pump in single pump FOPAs. A broadband signal gain measurement of an entire single side of the central frequency can then be performed by using a broadband probe spanning one side of the central frequency plus up to ~5 THz (~40 nm) on the other side of the central frequency where Raman gain susceptibility can be neglected. An importance of this 5 THz is to allow an accurate gain measurement near the central frequency without a 'blind-spot'. This is demonstrated at Figure 3.5 where the input probe spans in range 1515–1620 nm around the central wavelength of 1550 nm. The raw gain

calculated as a ratio between input and output overestimates the gain processed using equation (3.2) by ~3 dB at 1520-1590 nm due to the idler generation. When there is no probe at symmetric frequencies (i.e. wavelength >1590 nm), there is no signal-idler mixing and result of the equation (3.2) coincides with the raw gain calculation using equation (3.3). In the absence of an input probe, at wavelengths shorter than 1515 nm, the signal gain can be estimated based on the conversion efficiency using equation (2.33). However, this estimation do not consider the Raman contribution.

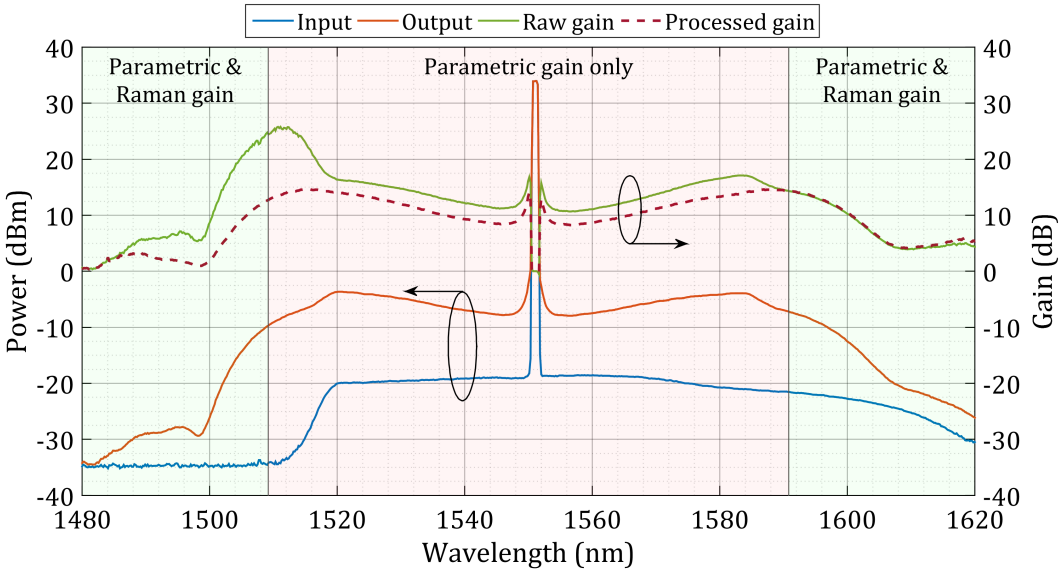

Figure 3.5. Experimental demonstration: the raw gain measurement is skewed by signal-idler mixing, the processed gain is free of distortion caused by signal-idler mixing.

3.2.3 Signal-signal interaction and pump depletion

Both FWM and stimulated Raman scattering can generate products of interaction between different probe frequencies, which are indistinguishable from the amplified probe itself and therefore their effect on measured gain cannot be compensated by numerical processing of the results. However, the power of these products scales with signal power, so their insignificance can be ensured by reducing the input probe power until the gain is independent of it. Reducing the input power also ensures the absence of pump depletion.

Figure 3.6 shows experimental gain spectra obtained as the input broadband probe (total power ~10 dBm) was attenuated by different amounts up to 18 dB. The HNLF length was 75 m, the pump wavelength was 1554 nm and the pump power was

5 W. An increased fibre length and high gain were used on purpose to invoke unwanted interactions for this demonstration. Gain distortion around the pump caused by unwanted FWM products is suppressed as the attenuation increases up to 15 dB. At the same time, the gain peak increases until the attenuation reaches 15 dB which indicates mitigation of pump depletion. Gain spectra obtained with attenuation of 15 dB and 18 dB converge indicating insignificance of remaining unwanted products and pump depletion. Overall, unwanted FWM, stimulated Raman scattering and pump depletion can be and should be mitigated by a broadband probe attenuation until the calculated gain spectra converge.

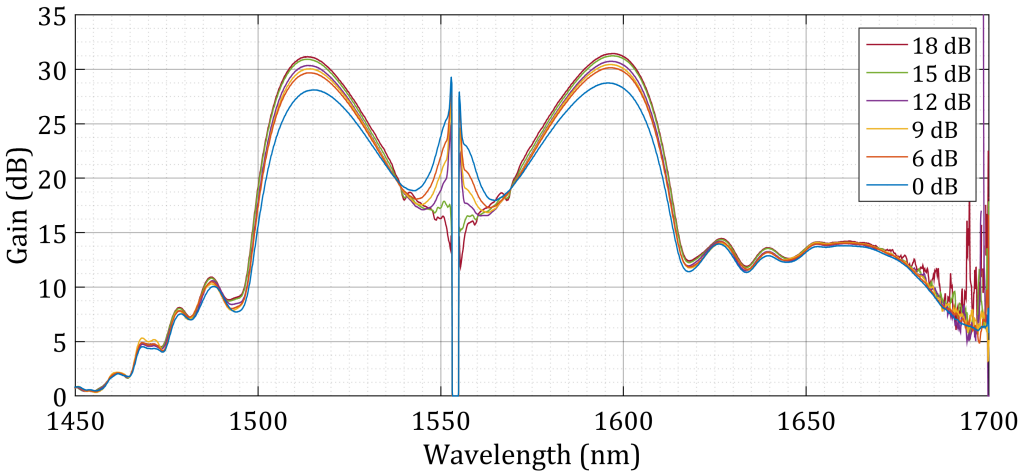

Figure 3.6. Experimental gain spectra for a variable SC attenuation levels (named in the legend). Attenuation by >15 dB dismisses unwanted products and pump depletion.

3.2.4 Polarised probe for gain spectrum measurement

Typically, when gain of a polarisation sensitive amplifier is measured using modulated signals or polarised narrowband probes, e.g. sourced from a tuneable laser, the probe polarisation is tuned to maximise gain. However, a polarised broadband probe is not suitable for a maximum gain measurement in such a way as illustrated in Figure 3.7 which shows input and output optical spectra of a polarised broadband probe obtained by passing a supercontinuum through a polariser. There is a significant ripple seen on the output spectrum because different frequencies possess different polarisations due to frequency dependent polarisation evolution in polarisation controllers, HNLF and other components [102]. Therefore, gain measurement using a polarised broadband probe does not allow a broadband gain measurement since measured gain can be interpreted only at the frequency where

output power was monitored during polarisation tuning. Consequently, it is necessary to use a *depolarised* broadband probe to perform broadband gain measurements. However, a gain of a depolarised broadband probe is averaged across all polarisation states which is usually not an interest of amplifier characterisation, so it is required to derive relations between gain of depolarised probe and maximum gain of polarised probe.

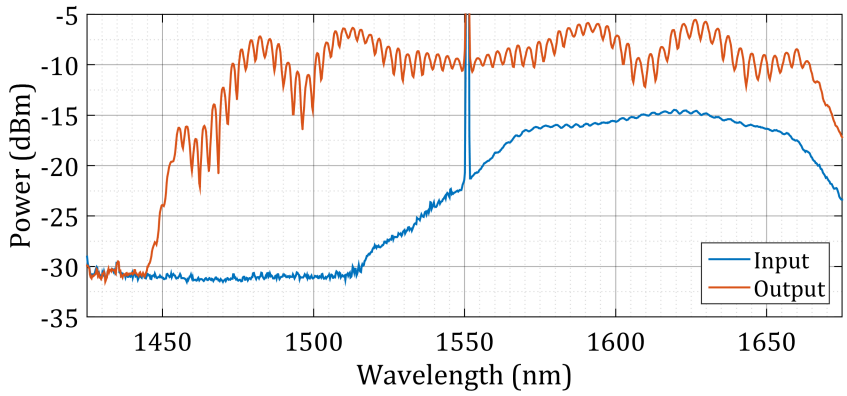

Figure 3.7. Experimental optical power spectrum of a polarised broadband probe at the FOPA output demonstrates an unsuitability of polarised broadband probes for a broadband gain measurement.

3.2.5 Depolarised probe for gain spectrum measurement

In this subsection results of experimental gain measurements using a supercontinuum (SC) acting as a depolarised broadband probe and a tuneable laser (TL) acting as a source of polarised narrow linewidth probe are analysed to derive equations linking the maximum TL gain with the SC gain. This is to enable finding of the maximum gain for polarised signals using experimental gain measurements employing a depolarised broadband probe.

Three representative configurations (1, 2 and 3) are considered in this analysis. They allow to examine different phase-matching and pump polarisation states as well as various combinations of parametric and Raman gains. All configurations utilize the same 50 m long HNLF with a fixed pump power of 5 W. In configuration 1, the pump wavelength is 1565 nm (~15 nm away from the ZDW) to restrict the parametric gain to a small region near the pump and examine the parametric and Raman gain independently. In configurations 2 and 3, the pump wavelength is tuned to 1551.4 nm as parametric gain spans over 100 nm in this case, thus allowing to observe a mixing of parametric and Raman gains provided by the same pump. In configurations 1 and 2 the pump polarisation is tuned to maximise the parametric gain ensuring linearity

of the pump polarisation (linear pump polarisation allows the highest FWM coupling efficiency [59]). In configuration 3 the pump polarisation is tuned to suppress the parametric gain peak, so it can be stated that the pump polarisation is not linear in this case. An overview of these configurations is shown in Table 1)

Table 1. Overview of considered configurations.

Configuration	1	2	3
Parametric gain bandwidth	Minimum	Maximum	Maximum
Parametric gain peak	Maximum	Maximum	Flattened

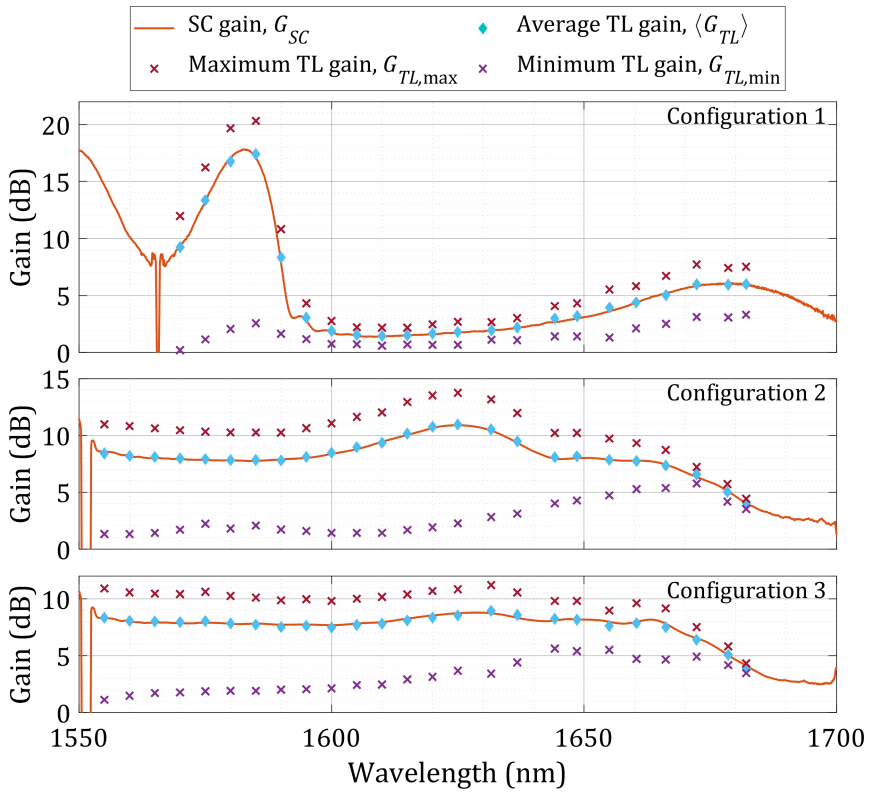

Figure 3.8. Comparison of experimental gain measurements for three representative FOPA configurations. G_{SC} (orange curve) is the SC gain processed to resolve signal-idler mixing; $G_{TL,max}$ (red crosses) and $G_{TL,min}$ (purple crosses) are the maximum and the minimum TL gain respectively; $<G_{TL}>$ (cyan diamonds) is the average of the maximum and the minimum TL gains.

Figure 3.8 shows comparison of experimental results obtained with a SC and a TL for amplifier configurations 1, 2 and 3. Experimentally measured SC gain processed using equation (3.2) is denoted as G_{SC} (orange curve). The maximum ($G_{TL,max}$, red crosses) and the minimum ($G_{TL,min}$, purple crosses) TL gains were measured as the

probe polarisation was adjusted through the full range at each examined frequency. The average TL laser gain (cyan diamonds)

$$\langle G_{TL} \rangle = \left(G_{TL,max} + G_{TL,min} \right)/2 \tag{3.4}$$

corresponds to the total gain which two polarisation multiplexed signals with gains $G_{TL,max}$ and $G_{TL,min}$ would receive in the examined amplifier.

An agreement between the average TL gain $\langle G_{TL} \rangle$ and the SC gain G_{SC} shows that considerations made in Subsections 3.2.2 and 3.2.3 were sufficient to ensure accurate gain measurement for both parametric and Raman gain regions. Therefore, gain measurements using a depolarised broadband probe can be used to find the total gain of polarisation multiplexed signals over wide bandwidth quickly and accurately. This is usually the main interest of *polarisation-diverse* amplifier characterisation.

However, a gain characterisation of *polarisation-sensitive* amplifiers is often required. This is also the case for the experimental FOPA optimisation performed in this chapter, where the maximum gain for polarised signals (essentially the maximum TL gain $G_{TL,max}$) is to be found based on gain measurements employing a SC and leading to finding a SC gain G_{SC}. The agreement between the average TL laser gain $\langle G_{TL} \rangle$ and the SC gain G_{SC} in all three configurations provides a relation linking the SC gain with the maximum TL gain $G_{TL,max}$, which is the main interest of further derivation:

$$G_{SC} \approx \langle G_{TL} \rangle = \left(G_{TL,max} + G_{TL,min} \right)/2 \tag{3.5}$$

The maximum TL gain $G_{TL,max}$ is to be found from equation (3.5) based on the experimentally measured SC gain G_{SC}. However, this requires a knowledge of the minimum TL gain $G_{TL,min}$. Note, that the minimum TL gain cannot be neglected in equation (3.5) as Figure 3.8 demonstrates that the minimum TL gain can be comparable with the maximum TL gain, especially for large detuning from the pump. One possible reason for the substantial minimum TL gain (meaning that any probe polarisation obtains a substantial amplification) at some frequencies is the presence of Raman orthogonal susceptibility. However, the Raman orthogonal susceptibility peaks at ~3 THz (~25 nm) detuning from the pump in silica [71], so this does not explicitly explain the increase of the minimum TL gain seen for larger TL detuning from the pump. Instead the significant increase of the minimum TL gain ~100 nm away from the pump might be attributed to a relative rotation of the probe and the pump polarisation states due to high-order birefringence [102].

A study of the exact reasons for the increase of the minimum TL gain at large detuning is beyond the scope of this work. Instead, it was found that the minimum TL gain can be approximated with a sufficient accuracy using a ratio between the minimum and the maximum TL gains (note, gains are expressed in dB):

$$R = G^{dB}_{P-NP,min} / G^{dB}_{P-NP,max} \tag{3.6}$$

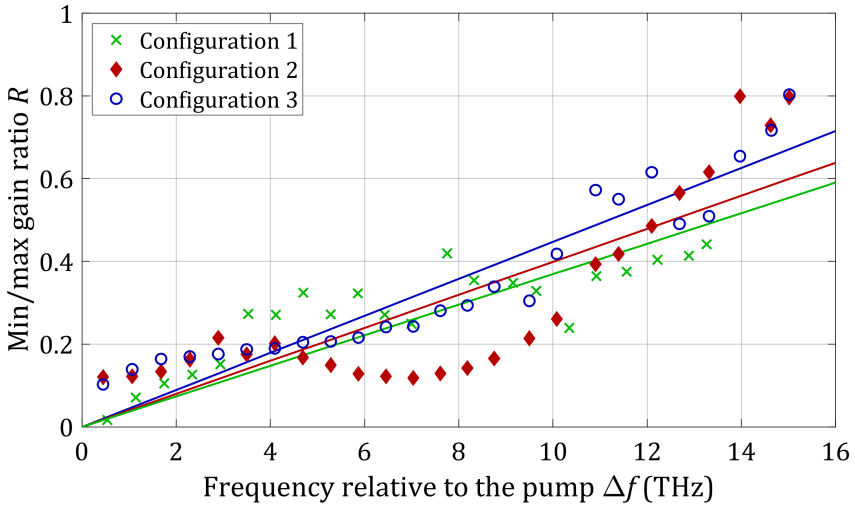

Figure 3.9. Gain ratio R calculated based on experimental measurements for three examined FOPA configurations. Crosses, diamonds and circles are calculated values. Lines are fitted for each configuration.

Figure 3.9 shows the ratio R calculated using equation (3.6) and plotted versus TL detuning from the central FOPA frequency (coincides with the pump frequency in single pump FOPA) for every TL gain measurement. The gain ratio R was fitted with straight lines described by equation $R = k_R \Delta f$, where k_R is the slope of the fitting line, for every examined amplifier configuration. It is found that the values of k_R for all examined amplifier configurations are close to each other. It is therefore suggested to use the average slope of three configurations $\langle k_R \rangle = 0.0409\ \mathrm{THz}^{-1}$ to approximate the ratio R for broadband gain spectrum measurements in FOPA employing the same HNLF in following subsections. An approximate value of the ratio $R(\Delta f)$ can be used to rewrite equation (3.6) in linear units as follows:

$$G_{TL,min} = \left(G_{TL,max}\right)^{R}. \tag{3.7}$$

Equation (3.7) is then to be substituted into equation (3.5) to obtain an equation:

$$2G_{SC} = G_{TL,max} + \left(G_{TL,max}\right)^{R}, \tag{3.8}$$

which can be solved numerically to find the maximum TL gain $G_{TL,max}$ based on experimentally measured SC gain G_{SC}. In other words this allows to derive the maximum gain for polarised signals across a wide range using a single measurement of SC gain.

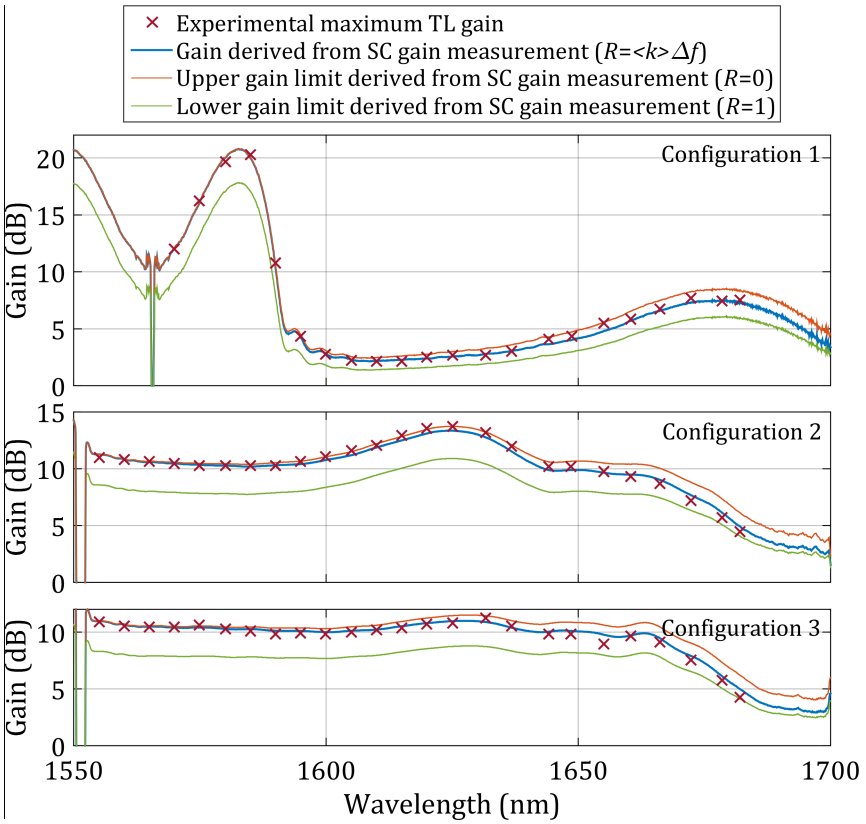

Figure 3.10. Comparison of experimental gain measurements using a tuneable laser (red crosses) and using a depolarised broadband probe after polarisation effects are accounted for with an approximation $R = \langle k_R \rangle \Delta f$ (blue line). Orange and green lines are derived from an experimental gain measurement using a depolarised broadband probe and assume extreme cases: $R = 0$ – no gain for orthogonal signal polarisation, and $R = 1$ – all signal polarisations obtain the same gain.

3.2.6 Estimation of the measurement error

The suggested approximations of the gain ratio R using a straight line and the fitting line slope k_R using an averaged value might look very rough. This subsection evaluates the measurement error introduced by these approximations and demonstrates that these approximations are sufficient.

Figure 3.10 shows a comparison of the experimentally measured maximum TL gain (red crosses) and the maximum TL gain derived from the experimentally measured SC gain as described in the previous subsection (blue curve). A good

agreement between the two measurement techniques is observed. The standard deviation between them is ~0.3 dB. It proves that the described approach relying on gain measurement employing a SC allows the maximum gain of polarised signals to be found over a wide bandwidth and various amplifier configurations with high accuracy.

A rough estimation of the maximum gain for polarised signals can also be made without performing an approximation of the gain ratio R requiring a few TL measurements. The ratio R can take values from 0 to 1 as follows from its definition (equation (3.6)), so the solution of equation (3.8) in terms of the maximum gain for polarised signals $G_{TL,max}$ is in a range from G_{SC} to $2G_{SC} - 1$ in all cases. This restricts the maximum gain for polarised signals within a band which is less than 3 dB wide, thus allowing its rough estimation with an error <1.5 dB. The <3 dB band for rough gain estimation is restricted by orange and green curves at Figure 3.10 which are derived from an experimentally measured SC gain using gain ratio values $R = 0$ and $R = 1$ respectively.

3.3 FOPA gain spectrum optimisation and characterisation

In this section FOPA gain spectrum is experimentally optimised in terms of pump wavelength, pump power and fibre length to obtain a broadband flat FOPA gain spectrum. All gain measurements are performed using a broadband gain spectrum measurement technique using a supercontinuum as an input probe as explained in Section 3.2. Then, a 60 Gbps QPSK signal at three different wavelengths across the L band is amplified using this FOPA to demonstrate a viability of the demonstrated FOPA for signal amplification. The work described in this section has been published in [31, 32]. This section relies on the same set of experimental data as [32], but provides extra details and discussion.

The key idea of the FOPA optimisation in this section is an accurate tuning of pump wavelength whilst employing short HNLF lengths of 25 and 50 m. The key advantage of a HNLF length decrease is reduction of dispersion parameters drift along the fibre allowing a better control of gain spectrum shape through pump wavelength tuning [103]. Another important advantage of HNLF decrease is an increase of the stimulated Brillouin scattering threshold allowing to increase a pump power [26]. Two HNLF lengths have been examined to evaluate an improvement provided by a shorter HNLF length.

It was found that the broadest and the flattest FOPA gain spectrum is achieved when pump wavelength is tuned very close to the ZDW (in a range of 0.1 nm). In this case a phase-matched gain is avoided, instead an almost equally phase-mismatched gain is demonstrated over wide bandwidth. It has been proved that the 25 m HNLF is capable to provide lower GV than the 50 m HNLF. Additionally, it has been shown that within a phase-mismatched parametric gain can be seamlessly merged with a forward Raman gain provided by the same parametric pump to enhance a total FOPA gain bandwidth. As a result a record flat and broad unfiltered single pump Raman-enhanced FOPA gain of 9.2±0.7 dB over a continuous range of 104 nm (12.2 THz) on one side of the pump has been demonstrated with a potential for further improvement. A viability of such FOPA for signal amplification is confirmed by demonstrating an amplified 60 Gbps QPSK signal penalty of <1 dB for received $Q^2 < 14$ dB as compared to a back-to-back unamplified configuration.

3.3.1 Pump wavelength tuning

Figure 3.11 shows experimental FOPA gain spectra obtained for the (a) 25 m and (b) 50 m fibres at 5 W pump power for pump wavelength varied in a range from 1550 nm to 1556 nm. Gain spectra are plotted versus frequency relative to the pump to avoid a shift between curves that would arise within the wavelength domain.

The total observed gain bandwidth was >28 THz. The gain spectra are asymmetric due to substantial Raman gain forming an independent of pump frequency gain peak in the range -15…-10 THz, which is not mirrored on the high frequency side [70]. As a result, the gain spectra spans over >16 THz on the Stokes side (left-hand side of the plots) and is restricted by a maximum of ~12 THz on the anti-Stokes side. A further gain spectrum optimisation concentrates therefore on the Stokes side, because it provides a wider gain bandwidth.

The gain spectra obtained with the pump wavelengths λ_p = 1551.8 nm for the 25 m fibre and λ_p = 1551.4 nm for the 50 m fibre (highlighted in Figure 3.11) possess an almost constant gain in a large area around the pump. As a result they have the lowest gain variation (GV) across the parametric gain window compared to other gain spectra obtained with corresponding fibre lengths. Moreover, the bandwidths of these gain spectra stretch over 10 THz allowing them to merge with the Raman gain peak without a gap. Therefore, the pump wavelengths λ_p = 1551.8 nm (25 m) and λ_p = 1551.4 nm (50 m) may be considered the optimal pump wavelengths.

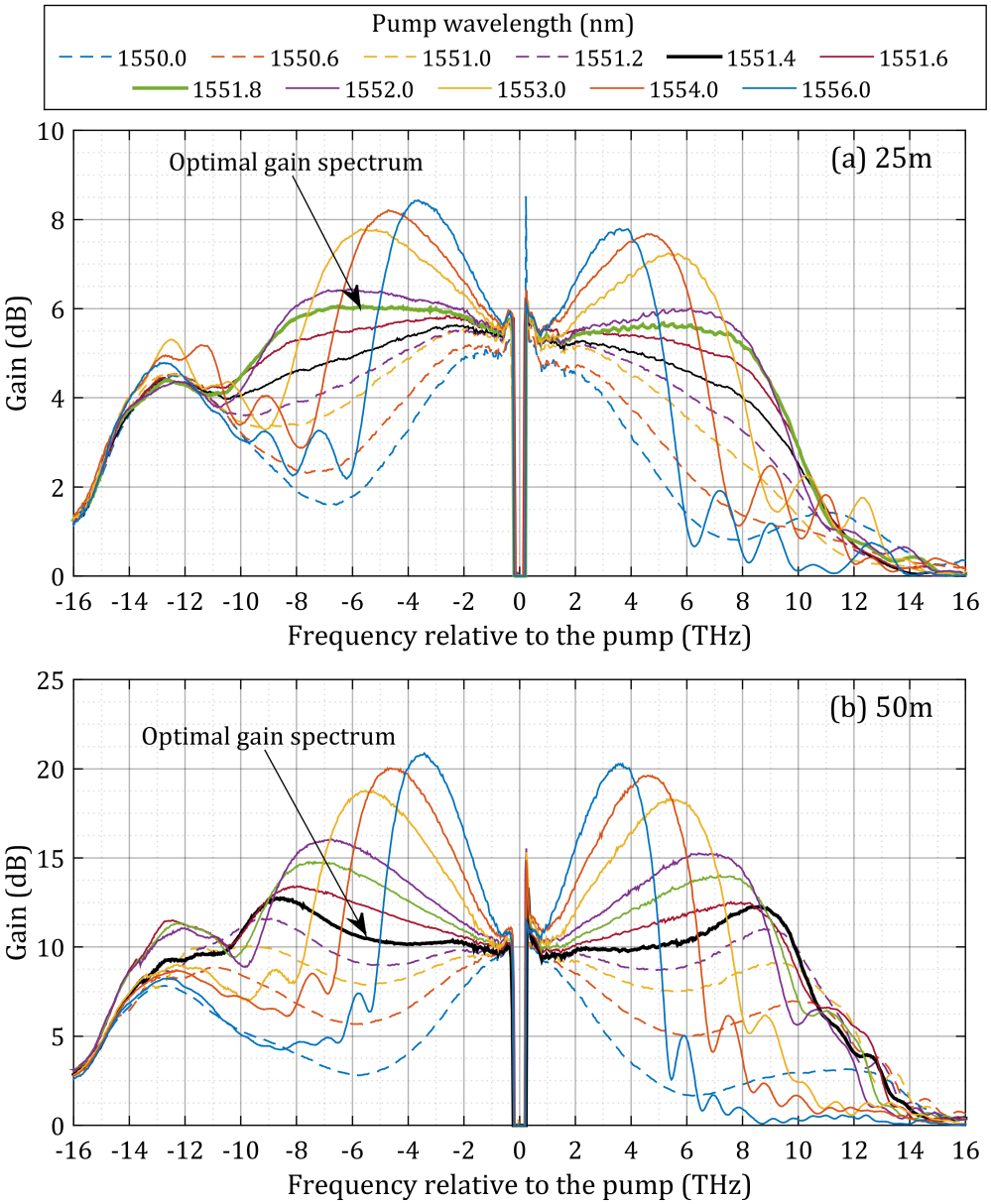

Figure 3.11. Experimental FOPA gain spectra for a range of pump wavelengths (named in the legend) and a pump power of 5 W for a) 25 m and b) 50 m HNLF.

To help understand the relationship of these optimal pump wavelengths to the ZDW of each HNLF, Figure 3.12 displays both experimental and theoretical FOPA gain curves as the pump is tuned about the optimal values. The theoretical gain is plotted using equations (2.32) and (2.33) and the datasheet HNLF parameters listed in Subsection 3.1.1, which were fine tuned in terms of the fibre nonlinear coefficient γ. It was found that the nonlinear coefficient needs to be set to 14 $W^{-1} \cdot m^{-1}$ to allow for

matching of experimental and simulated gain magnitudes. Note that the nonlinear coefficient was additionally scaled by a factor of 8/9 to account for polarisation averaging in randomly birefringent fibre (see Subsection 2.3.1). For the theoretical curves, ZDW is set to the experimentally-obtained optimal pump wavelength for each fibre.

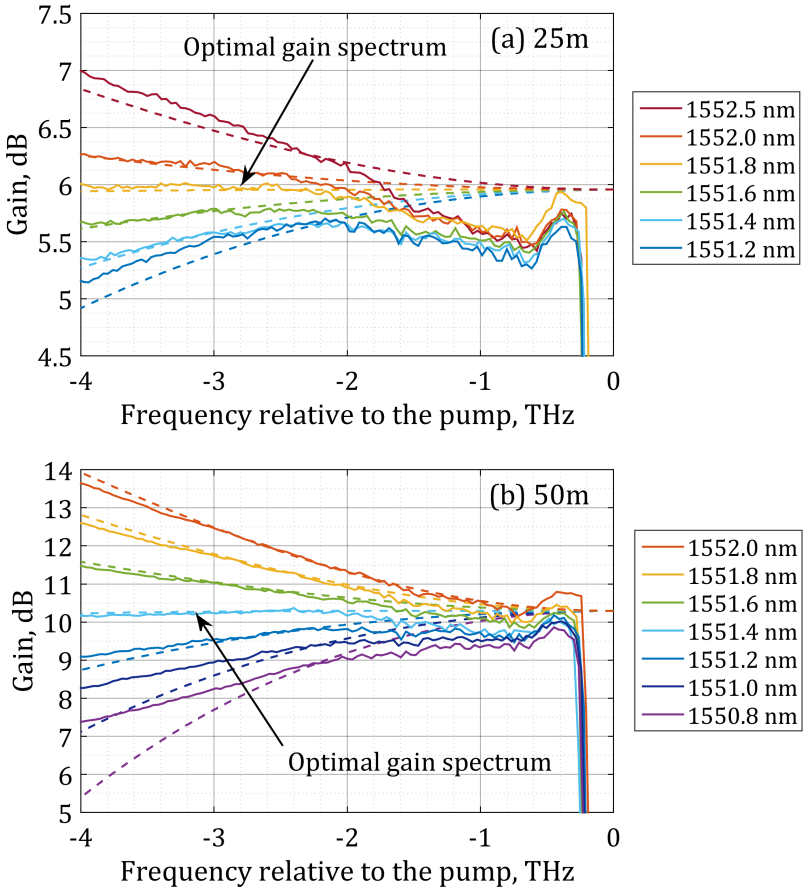

Figure 3.12. Theoretical (dashed) and experimental (solid) FOPA gain spectra for a) 25 m and b) 50 m fibres. Theoretical gain spectra assume a ZDW of a) 1551.8 nm and b) 1551.4 nm. Pump wavelengths are shown in the corresponding legends.

It can firstly be seen that the experimental results close to the pump (0-2 THz) are distorted and need to be discounted from this analysis – the distortion is due to imperfect filtering of residual ASE from the pump EDFA (shown at Figure 3.13). The gradient of the theoretical gain curves can be seen to change from positive to negative as the pump wavelength is tuned from wavelengths longer than the ZDW (anomalous dispersion) to shorter (normal dispersion). Generally good agreement between experiment and theory is seen in the 2-4 THz range which strongly implies that the optimal pump wavelength is close (within measurement granularity and error) to the

ZDW of each fibre. Therefore the ZDW for the 25 m and 50 m fibres is estimated to equal 1551.8±0.1 nm and 1551.4±0.1 nm respectively. It should be noted that at frequencies extending beyond 4 THz there is a significant divergence of the theory from experimental observation which is attributed primarily to insufficient knowledge of the HNLF dispersion profile, impact of polarisation effects and the Raman contribution.

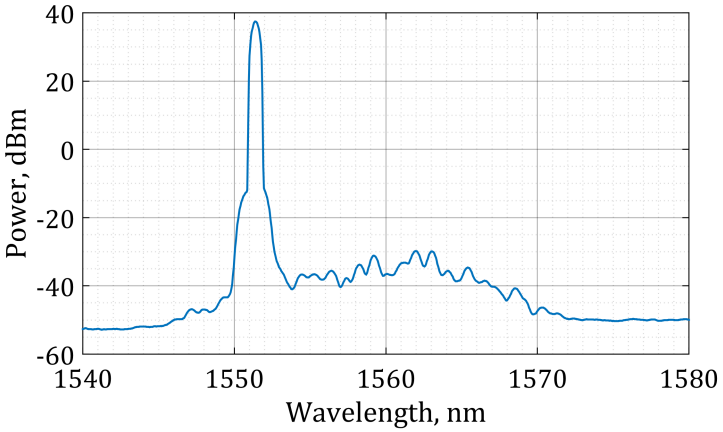

Figure 3.13. Parametric pump and a residual ASE noise measured experimentally without input signal/probe at the input of the HNLF.

Overall, the performed pump wavelength tuning leads to three conclusions. First, the main contribution to GV is provided by an exponential phase-matched gain, so the flattest gain spectrum is achieved when the phase-matched peak gain is as suppressed as possible. Second, the maximum parametric gain bandwidth can be attained when the pump wavelength is very close to the fibre ZDW (within 0.1 nm). This observation contradicts a FOPA gain spectrum analysis (single-polarisation) described in Subsection 2.2.3, supposedly due to a combination of effects not included in this model: Raman gain contribution, polarisation effects and longitudinal parameters fluctuations. Consequently, an advanced theoretical model is required to verify if this observation is applicable for fibres with particular parameters only and what are these parameters. Third, forward Raman gain induced by the parametric pump can enhance an overall gain spectrum bandwidth (has been demonstrated in [8]).

It should be noted that this experiment was performed before it was found that the frequency dependent ratio R between the minimum and the maximum gain needs to be considered during processing of gain spectrum measurements to obtain accurate results (see Subsections 3.2.5 and 3.2.6). Therefore, the original gain spectrum processing was performed essentially assuming $R = 0$, i.e. no gain for signals

orthogonal with the pump. Using this inaccurate gain spectrum processing it was concluded that the optimal pump wavelength for the 25 m fibre is λ_p = 1551.6 nm, so all measurements with 25 m HNLF in following sections were performed using this pump wavelength. In this thesis the results of these measurements are provided being processed in the most accurate up-to-date way and these results can clearly be improved using the actual optimal pump wavelength λ_p = 1551.8 nm. Since both the difference introduced by the processing of results and the use of the sub-optimal pump wavelength λ_p = 1551.6 nm in the 25 m HNLF essentially introduce a gain spectrum tilt, it is viewed that the 25 m HNLF gain spectra obtained with the sub-optimal pump wavelength λ_p = 1551.6 nm and the gain ratio $R = 0$ represent an achievable potential for gain spectra with λ_p = 1551.8 nm. Further for convenience, the sub-optimal pump wavelength of the 25 m fibre λ_p = 1551.6 nm, which is used in all experiments, is called optimal.

3.3.2 Pump power tuning

Figure 3.14 shows gain spectra obtained for both fibres using the optimal pump wavelengths for a range of pump powers from 4 W to 9 W. It shows that increasing the pump power above 5 W for the 50 m fibre causes an exponential growth of the gain peak, which is deleterious to GV. This does not occur in the 25 m fibre as it can be seen that an increase of the pump power up to 9 W provides a flat gain of 9.2±0.7 dB over bandwidth of 104 nm (12.2 THz). Additionally, as it was explained above the potential gain spectrum in the 25 m HNLF with the pump wavelength λ_p = 1551.8 nm is shown by broken curve and suggests gain of 9.6±0.5 dB over bandwidth of 111 nm (12.8 THz).

It should be noted that although the examined pump powers may be considered high, if the amplifier is to be used to amplify typical telecoms signals across the full band then total signal output powers will be in the Watt region. This implies that any next-generation wideband optically pumped amplifier will require multi-Watt pumps.

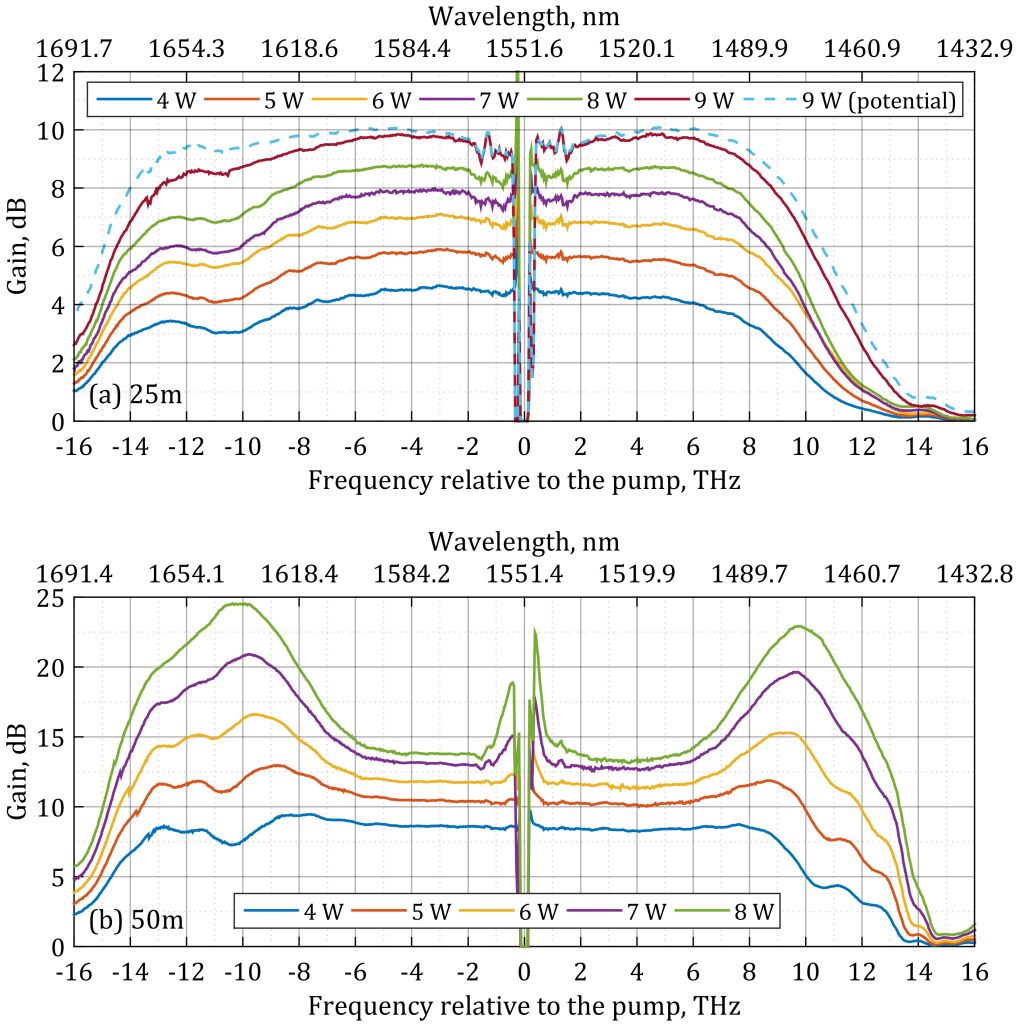

Figure 3.14. Experimental FOPA gain spectra for a series of pump power values (named in the corresponding legends) for optimal pump wavelengths in a) 25 m HNLF (λ_p = 1551.6 nm) and b) 50 m HNLF (λ_p = 1551.4 nm).

3.3.3 Merge of Raman and parametric gains

Within silica fibre, the Raman gain coefficient is much lower than the phase-matched parametric gain coefficient [11]. This experiment demonstrates however that phase-mismatched parametric gain can be at the same level as the Raman gain. Figure 3.15 shows that the magnitude of the parametric phase-matched gain (the normalised mismatch parameter $= 1$, see subsection 2.2.3 for details) is indeed impossible to match with the Raman gain magnitude. However, parametric phase-mismatched gain ($K = 0$) has an intersection point with Raman gain. The gain value corresponding to the intersection depends on Raman fractional strength f_R. It should be noted that although the demonstrated relation between parametric and Raman gains is

fundamental, it is not accurate as it does not consider a combined effect of parametric and Raman gain, polarisation effects, etc. Nevertheless, Raman gain lines corresponding to high Raman fractional strength at Figure 3.15 show a good agreement with Figure 3.14: Raman and parametric gains are matched up to ~10 dB and Raman gain exceeds phase-mismatched parametric gain above the 10 dB level. Figure 3.15 implies that it might be possible to match Raman and parametric gain at higher gain level, but this would require a fibre with low f_R, which is not typical for HNLF.

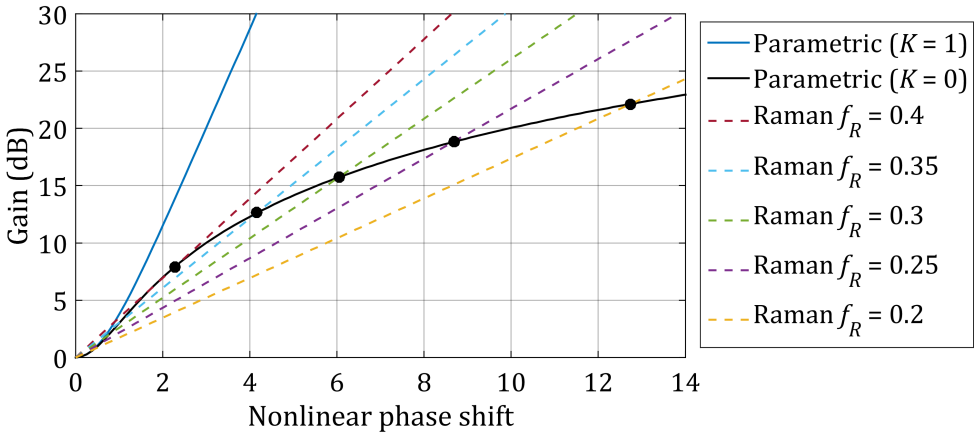

Figure 3.15. Theoretical parametric and Raman gains as a function of nonlinear phase shift γPL. Phase-matching and Raman fractional strengths are varied.

Overall, if the parametric gain roll-off is countered by a corresponding rise of the Raman gain, they can be utilised together to keep the overall GV low with overall gain bandwidth ~13 THz defined by the Raman response.

3.3.4 Comparison of fibre lengths performance

A direct comparison of the two fibres for equivalent gain levels is shown in Figure 3.16, where the 25 m fibre was pumped with twice the power compared to the 50 m to match their gains. For the higher 9 dB gain case, the 50 m fibre spectrum exhibits a small peak which is not observed in the 25 m fibre. In the case of 6 dB gain this peak is not evident, but the GV is still higher for the 50 m fibre. This is due to the reduced pump power (2.5 W) causing a reduction in parametric gain bandwidth which produces a gap between the parametric and Raman bands 10 THz away from the pump. Overall, the 25 m fibre shows less GV for the same gain value in both cases for two reasons. First, there are less longitudinal fluctuations of dispersion parameters in the shorter fibre. Additionally, a higher pump power used in the

shorter fibre length leads to an advantage of wider parametric gain bandwidth whilst keeping gain level and gain variation on the similar level. This stems from the fact that the parametric gain bandwidth scales with γP whilst gain magnitude scales with γPL. However, the total gain bandwidth is the same for both fibres as in these cases the total gain bandwidth was defined by the gain spectrum bandwidth enhancement by the Raman gain.

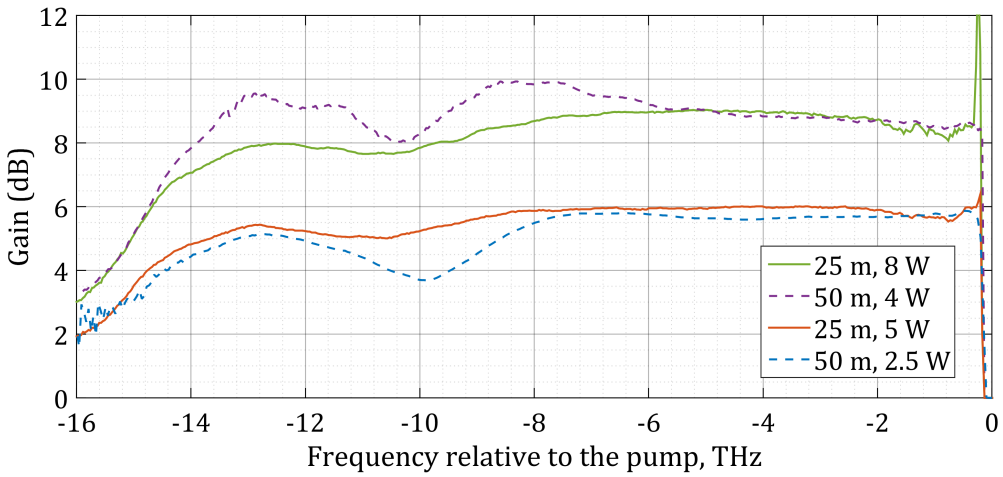

Figure 3.16. Comparison of experimental FOPA gain spectra obtained at optimal pump wavelengths with 50 m (λ_p = 1551.4 nm) and 25 m (λ_p = 1551.6 nm) fibres for equal gain level. The legend shows a fibre length and a pump power.

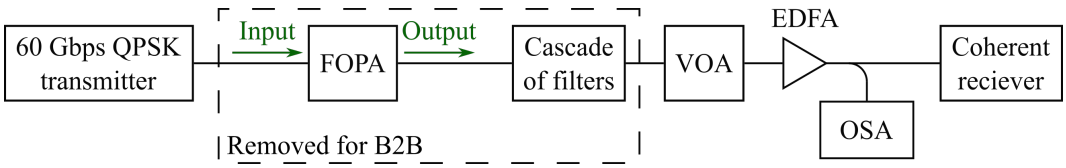

Figure 3.17. Experimental setup for signal amplification evaluation.

3.3.5 Experimental signal amplification

To ascertain the suitability of the demonstrated FOPA for use within telecommunication applications, the quality of single-polarisation 60 Gbps QPSK signal amplified by the FOPA was compared with the quality of the same signal without amplification at three wavelengths of 1570 nm, 1586 nm and 1600 nm. The examined wavelength range was limited only by the test equipment used for analysis. The experimental setup is shown at Figure 3.17. A 60 Gbps QPSK transmitter was connected to the input of the FOPA experimental setup described earlier in Subsection 3.1.1. The FOPA employed a 25 m HNLF, pump power of 8 W and pump

wavelength of 1551.6 nm which provided a signal amplification by ~9 dB at all examined wavelengths. The output from the FOPA experimental setup was passed through a cascade of filters to remove the pump and an idler. The amplified signal optical signal-to-noise ratio (OSNR) was tuned by passing the signal through a variable optical attenuator (VOA) and then amplifying by an L band EDFA. The EDFA was set to provide a fixed output signal power of 13 dBm. The signal power and OSNR before the coherent receiver were monitored using an OSA connected via a tap coupler. For the evaluation of an unamplified signal performance the FOPA and the cascade of filters were removed from experimental the setup to obtain a back-to-back (B2B) configuration. The received OSNR was measured with a resolution bandwidth of 0.1 nm and varied from 10 dB to 20 dB. Each signal was coherently detected and digitally sampled using a real-time oscilloscope with 80 GHz sampling rate. Offline standard digital signal processing was used to count bit errors and to estimate a Q^2 value from the constellation when no bit errors were measured.

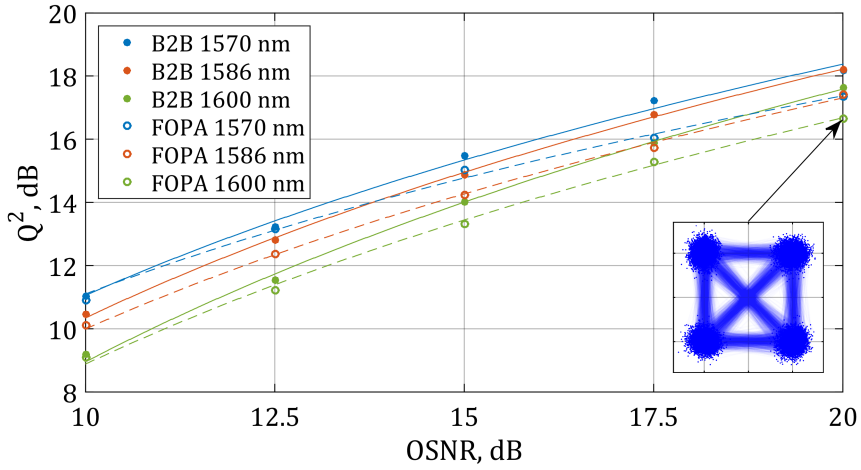

Figure 3.18. Experimental comparison of 60 Gbps QPSK signal performance in B2B configuration and after ~9 dB amplification by FOPA for a range of signal wavelengths named in the legend. Inset is an example constellation for the amplified signal.

The performance of signals amplified by FOPA was compared with the B2B unamplified performance and is plotted in Figure 3.18. The degradation of the B2B performance with increased wavelength is attributed to the wavelength dependent response of the transmitter modulator. OSNR penalty of the amplified signal relative to B2B was subsequently calculated and plotted in Figure 3.19. Since there was no measurement points with exactly the same value of Q^2 for both B2B and FOPA configurations, a linear interpolation of Q^2 versus OSNR was used to calculate OSNR

penalty. It should be noted that the lines of Figure 3.18 and Figure 3.19 are merely best fits for visual guidance and have no physical relevance. The error in the penalty calculation was estimated to be 0.5 dB. OSNR penalties below 1 dB are observed for $Q^2 \leq 14$ dB, which are attributed primarily to dithering and noise transfer from the pump [104]. OSNR penalties at 1586 nm and 1600 nm are almost the same. OSNR penalty at 1570 nm for $Q^2 \leq 15$ dB is measured to be smaller, but the difference is within measurement error. The reason for the large increase of OSNR penalty seen at 1570 nm for $Q^2 > 15$ dB is unclear, but is speculated to be due to residual ASE noise from the EDFA amplifying the pump [12].

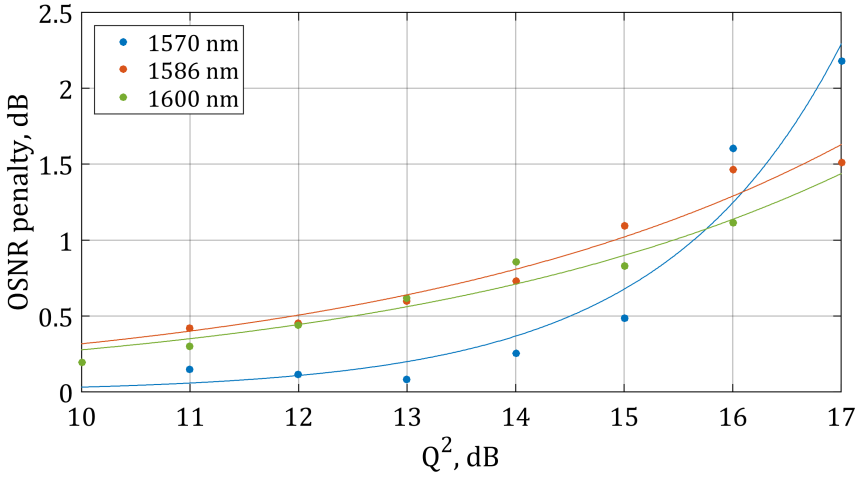

Figure 3.19. Experimentally measured OSNR penalty introduced to 60 Gbps QPSK signal by ~9 dB amplification in FOPA as compared to B2B configuration for a range of signal wavelengths shown in the legend.

3.3.6 Summary

A single pump, high-power and short-length FOPA was experimentally optimised in terms of gain spectral bandwidth and GV. It was found that parametric gain may be stretched over 11 THz with GV below 1 dB. This allows extension of the gain spectrum by merging the parametric spectrum with a forward Raman gain spectrum provided by the same pump. It was shown that the 25 m fibre provides a superior GV compared to 50 m for the same gain value and bandwidth and that optimal GV is achieved when the pump wavelength is tuned to the fibre ZDW. This was confirmed by theoretical gain calculations up to 4 THz from the pump. A record flat gain of 9.2±0.7 dB in a range of 104 nm (12.2 THz) was demonstrated on single side of the FOPA central frequency with a 25 m of dispersion-stable HNLF and pump power of 9 W. Moreover, there is a

potential to improve this result in every aspect by an optimal choice of pump wavelength and to achieve a gain of 9.6±0.5 dB in a range of 111 nm (12.8 THz). This amplifier was also proved to be suitable for signal amplification as OSNR penalty less than 1 dB was observed for 60 Gbps QPSK L band signals for received Q^2 below 14 dB.

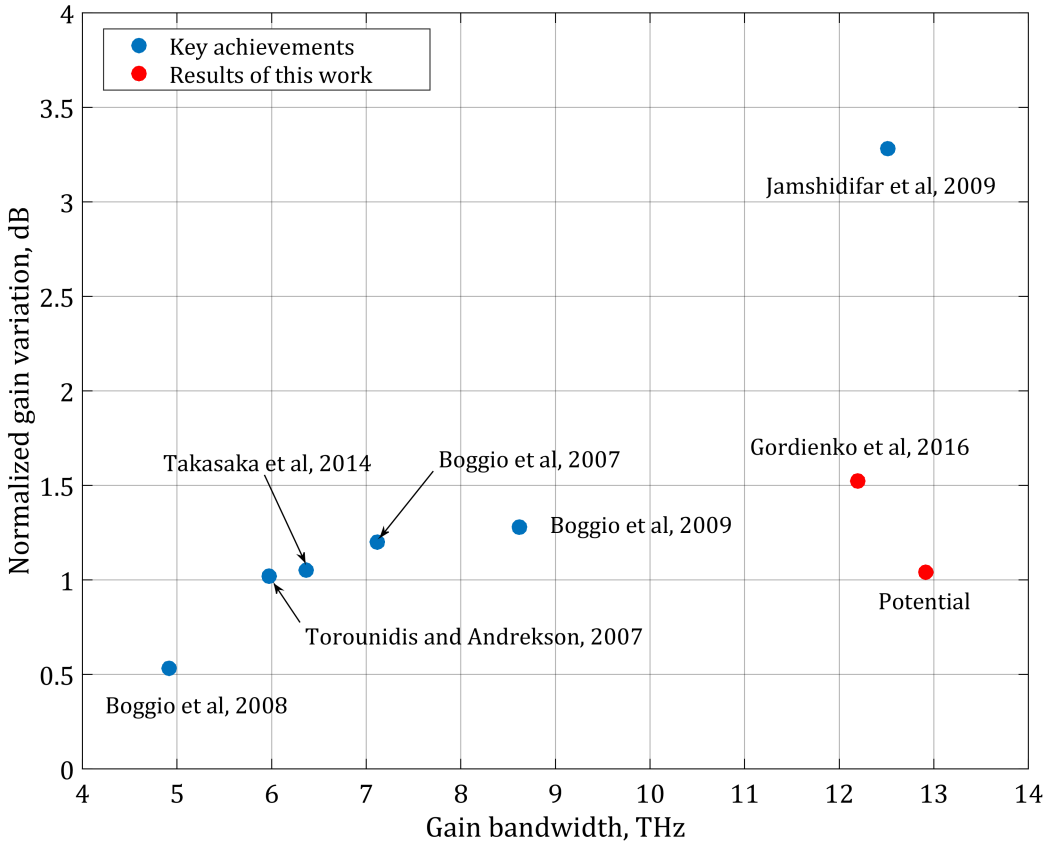

Figure 3.20. Normalised GV (per 10 dB gain) vs gain bandwidth on one side of the FOPA central frequency. Blue dots correspond to achievements quoted in this chapter. Red dot correspond to the gain spectra reported in this chapter (see Figure 3.14(a), 9 W).

Figure 3.20 visually displays the demonstrated FOPA gain spectrum in context with the state-of-the-art achievements discussed in the Chapter 3 introduction. Note, only gain spectra obtained with continuous pump(s) were considered. GV normalised per 10 dB gain is introduced in this figure to perform a fair comparison of FOPAs with different gain. Figure 3.20 shows that previous works has showed a solid trend of significant GV increase with a gain bandwidth. In contrast, the FOPA gain spectrum demonstrated in this work strongly outperforms this trend. The normalised GV was decreased by more than a factor of 2 when compared to the similar gain bandwidth achievement. The bandwidth of flat FOPA gain spectrum (3 dB GV per typical 20 dB

gain) was expanded by more than 3 THz. Moreover, there is still a significant potential for improvement.

Although the demonstrated FOPA gain might not be considered large (~10 dB), the low normalized GV implies that two or three such FOPA can be cascaded to achieve a required gain magnitude over a wide bandwidth whilst keeping a low total GV. This work is therefore a promising step towards an ultra-wideband, low GV FOPA for future broadband systems.

4 ADVANCED FOPA GAIN SPECTRUM ENGINEERING

An ultra-wide (>12 THz) flat FOPA gain spectrum has been demonstrated in the previous chapter. However, it was found that the gain variation (GV) increase with gain significantly accelerates when gain exceeds ~10 dB over wide bandwidth. Therefore, it was suggested that a typically required by optical communications net gain of >20 dB might be obtained by cascading of flat gain spectra of ~10 dB. Cascading is viewed as a way to significantly increase a broadband flat gain on the cost of a little increase of the normalised GV. Consequently, a GV decrease is more important than a gain magnitude increase if the cascading approach is to be implemented.

Section 4.1 demonstrates a novel gain spectrum shaping technique allowing to further decrease a GV of the FOPA gain spectra demonstrated in Chapter 3. This technique has allowed to reach a GV <1 dB over 102 nm bandwidth whilst leaving a possibility for a further GV improvement. Section 4.2 introduces an approach of cascading to allow for a broadband, low GV and, importantly, high gain. A potential of the FOPA cascading is estimated to allow for 20 dB gain wit GV of 3 dB over >100 nm bandwidth.

4.1 Parametric gain spectrum shaping by pump polarisation

It has been shown previously that the single pump FOPA gain spectrum can be modified by tuning signal polarisation [8]. However, it is not practical to tune signal polarisation for gain spectrum shaping. In this section it is shown that GV can be substantially improved by using a pump polarisation as an optimisation parameter. Thus, GV of broadband gain spectra demonstrated in Section 3.3 and spanning over a >100 nm bandwidth was improved from 2 dB and 3 dB to 1 dB. Note, the best obtained gain spectrum demonstrated in Section 3.3 (9.2±0.7 dB over 104 nm) was not considered in this section due to difficulties associated with using such a high pump power. It is suggested that the observed gain spectrum shape dependency on pump polarisation originate from a high-order birefringence and simulations supporting this suggestion are performed in this section. The work described in this section has been published in [33]. This section relies on the same set of experimental data as [33], but provides extra details and discussion.

4.1.1 Experimental results

An experimental setup described in Section 3.1 and a broadband gain measurement technique described in Section 3.2 are used in this subsection. Figure 4.1(a) demonstrates the gain spectra obtained with a 50 m fibre length and a pump power of 5 W. These are exactly the gain spectrum curves discussed in Subsections 3.2.5 and 3.2.6 (named configurations 2 and 3), so the same measurement results are available with a TL measurement too. The maximum gain (blue curve) features a 3 dB high hump around 1625 nm which makes a significant contribution to overall GV. Tuning the pump polarisation while observing the supercontinuum gain spectrum using the optical spectrum analyser allows to obtain a much flatter gain spectrum (orange curve). The peak around 1625 nm is suppressed in this gain spectrum, so the GV is decreased by ~2 dB and a gain of 10.5±0.5 dB over 102 nm (11.9 THz) bandwidth is demonstrated.

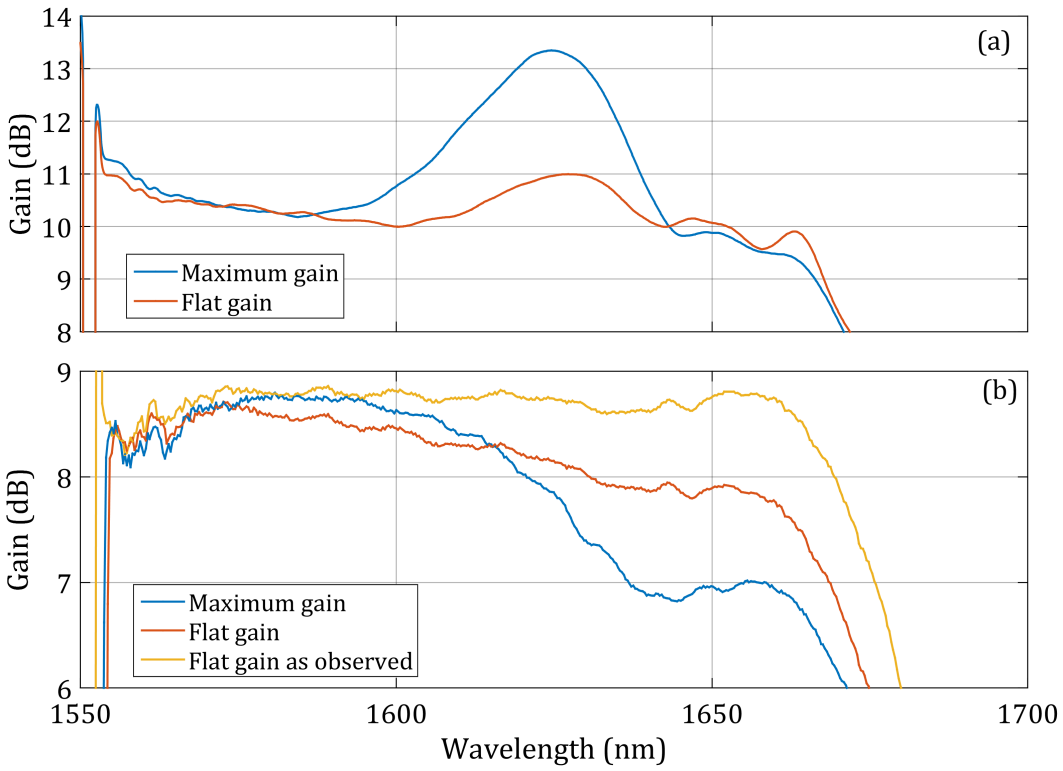

Figure 4.1. Experimental gain spectra obtained in (a) 50 m long fibre with pump power of 5 W and (b) 25 m long fibre with pump power of 8 W. Pump polarisation was tuned to maximize (blue) or to flatten (orange) gain. Yellow curve corresponds to flat gain spectrum processing using $R = 0$ (see Subsection 3.2.5).

Similarly, Figure 4.1(b) demonstrates gain spectra obtained in the 25 m length fibre with a pump power of 8 W. Pump polarisation tuning to maximise parametric gain peak leads to gain spectrum with ~2 dB GV in a range between the pump and 1665 nm. However, by tuning the pump polarisation a GV was decreased by 1 dB and a gain of 8.2±0.5 dB over 110 nm bandwidth was obtained.

It should be noted that the gain spectra presented at Figure 4.1 are processed using the approximation $R = \langle k_R \rangle f$ providing an accurate gain measurement result (Subsection 3.2.6). However, this experiment was performed assuming $R = 0$ because it was before it was found that the linear approximation $R = \langle k_R \rangle f$ is required to perform accurate broadband gain spectrum measurement. Therefore, although the result presented here is still demonstrating the concept, the demonstrated improvement is not the best achievable. The yellow curve at Figure 4.1(b) shows the result of optimisation while assuming $R = 0$ and targeting a flat broadband gain. It was possible to obtain the targeted gain spectrum shape with a ripple of only ±0.1 dB. An ease of gain spectrum shape amending by tuning pump polarisation and a proximity of resulting gain spectrum shape to the targeted shape (even though it was not an optimal target) imply that the gain spectrum shape similar to the yellow curve (8.7±0.1 dB over 100 nm) can be achieved for real if a suitable pump wavelength is used (see Subsection 3.3.1).

The supercontinuum (SC) polarisation is evenly distributed across all Poincare sphere within an optical spectrum analyser measurement time as discussed in Subsection 3.1.2. Therefore, the measured SC gain is averaged across all signal polarisations. Moreover, a pump polarisation is averaged over the entire Poincare sphere in randomly birefringent fibre. In this case, the measured SC gain is averaged across both signal and pump polarisations, so it should be insensitive to the input pump polarisation. However, the maximum gain for polarised signals derived from the experimentally measured SC gain and shown at Figure 4.1 clearly demonstrate dependency on the input pump polarisation. For further investigation of the gain spectrum dependency on pump polarisation the SC gain itself (averaged across all signal polarisations) is discussed rather than the maximum gain for polarised signals derived from the SC gain. Figure 4.2 shows experimentally measured SC gain spectra for four fibre lengths. Pump polarisation for each fibre length is tuned to minimise (broken lines) and to maximise gain (solid lines). Figure 4.2 shows that three fibre lengths, 25 m, 50 m and 75 m long, exhibit a pump polarisation sensitivity increasing

with an offset from the pump until Raman gain starts to dominate over parametric gain (~1650 nm). A possible explanation to this behaviour is a high-order birefringence, which effect increases with offset from the pump and eventually dominates over the effect of polarisation randomisation. On the other hand, the 100 m fibre shows little pump polarisation sensitivity. The only difference (except length) between the 100 m fibre and the three other fibre lengths is that the 100 m fibre is wound on a reel, while shorter fibres are coiled without a reel. The winding stress introduces a substantial polarisation mode dispersion (PMD) as compared to relaxed fibres. Therefore, a possible conclusion is that short fibres without winding stress do not exhibit enough random birefringence to average an effect of high-order birefringence, while the 100 m fibre possessing higher PMD introduces much more randomisation.

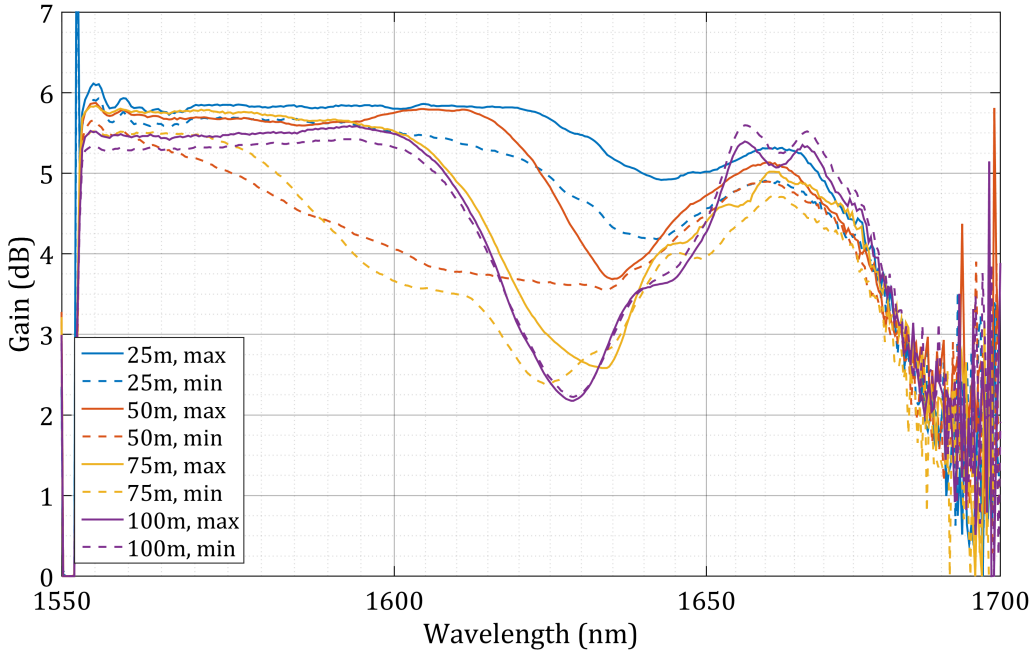

Figure 4.2. Experimental gain spectra obtained in fibre lengths from 25 m to 100 m (named in the legend). Pump wavelength was set close to the zero dispersion wavelength of each fibre length. Pump power was scaled to ensure the same gain level. For each fibre pump polarisation was tuned to maximise (solid curves) and minimise (broken curves) the suoercontinuum gain.

4.1.2 Simulations

To help verify the hypothesis that the observed pump polarisation impact on gain spectral shape is due to wavelength dependent birefringence, proof-of-concept simulations have been undertaken using a dual polarisation numerical model of the

nonlinear Schrodinger equation (NLSE) solutions employing the split-step Fourier method. Details on the simulation are provided in Appendix 1. A pump and a large number of probes were propagated through highly nonlinear fibre (HNLF) possessing the datasheet values of the HNLF, pump power of 10 W and HNLF length of 25 m.

Four cases of the fibre refractive index birefringence have been considered. First, no birefringence. Second, a linear birefringence. Third, a linear birefringence, whilst the birefringence axis undergo a random walk over the Poincare sphere. Fourth, a tilted birefringence, whilst the birefringence axis undergo a random walk over the Poincare sphere. For this simulation a beat length $L_B = 5$ m at the pump wavelength has been used. A random rotation of birefringence axes was performed every 1 cm (the simulation step) by a random angle with a standard deviation of $\sigma = \pi/100$. The sequence of incremental axes rotations along the fibre was the same in all simulations. A realistic tilt value of $\Delta\beta_1 = 0.002$ ps/m was derived by a frequency differentiation of birefringence occurring due to fibre core ellipticity [105]. These data are summarized in Table 2.

Table 2. Overview of simulated cases of birefringence.

Case	Beat length, m	Standard deviation of axes rotation, rad	Birefringence tilt, ps/m
No birefringence	$L_B = 0$	$\sigma = 0$	$\Delta\beta_1 = 0$
Linear birefringence	$L_B = 5$	$\sigma = 0$	$\Delta\beta_1 = 0$
Random linear birefringence	$L_B = 5$	$\sigma = \pi/100$	$\Delta\beta_1 = 0$
Random tilted birefringence	$L_B = 5$	$\sigma = \pi/100$	$\Delta\beta_1 = 0.002$

The simulation was concerned about finding a depolarised gain to compare it with the experimentally measured SC gain. The total simulated bandwidth was 50 THz and the number of simulated frequencies was 65536. Each frequency point contained a randomly polarised probe with a power of -60 dBm. A depolarised gain at every simulated frequency was found as an average gain over neighbouring 300 frequencies (probe polarisation is different at each of these frequencies, whilst gain dependency on frequency is negligible on this scale). Low probe power (-60 dBm per frequency) ensures that gain saturation and signal-signal interaction are negligible (Subsection 3.2.3). The obtained simulated depolarised gain was processed in the same way as experimental depolarised gain to resolve signal-idler mixing and polarisation effects (as described in Section 3.2).

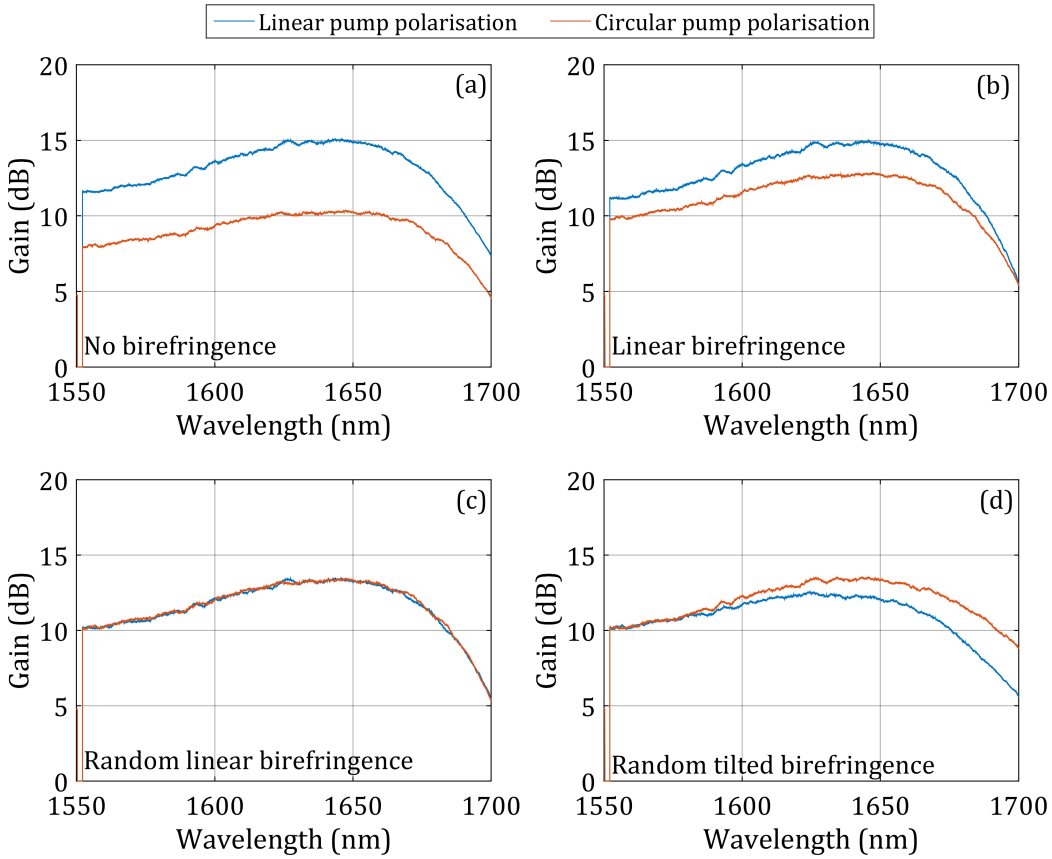

Figure 4.3. Simulated depolarised probe gain spectra obtained for four cases of fibre birefringence described in Table 2 and for two input pump polarisations: linear polarisation aligned to one of the principal axes (blue) and circular polarisation (orange).

Figure 4.3 shows simulated SC gain spectra for four cases of birefringence and two pump polarisation states: a linear polarisation aligned to one of the principal axes and a circular polarisation. Figure 4.3(a) demonstrates that in absence of birefringence a signal gain averaged across many signal polarisations shows a strong dependence on pump polarisation. This is because pump maintains its polarisation along all fibre and the linearly polarised pump suggests higher gain coefficient than the circularly polarised pump [59].

Linear birefringence causes a circularly polarised pump to go through a series of elliptic, linear and circular polarisations (Subsection 2.1.5). Therefore, the simulated SC gain for circular pump polarisation is averaged across these pump polarisations and is different from the no birefringence case (Figure 4.3(b)). The simulated SC gain with the linear pump polarisation is the same as in the no birefringence case, because this pump polarisation is aligned to one of the principal axes and is not affected by linear birefringence.

A random rotation of birefringence axes causes pump polarisation to randomly walk over all the Poincare sphere. Consequently, with a sufficient randomisation a SC gain spectrum is independent of the input pump polarisation as shown at Figure 4.3(c). This result is qualitatively similar to the experimentally observed gain spectrum with the 100 m fibre at Figure 4.2.

In the case of tilted random birefringence there is a divergence between gain spectra obtained with different input pump polarisation, which increases with signal offset from the pump (Figure 4.3(d)). It should be noted that the random birefringence allows for a pump polarisation insensitive gain near the pump. Among all simulated birefringence cases this behaviour is the only one qualitatively similar to the experimental observations with fibre lengths of 25, 50 and 75 m. Therefore, the hypothesis that a high-order birefringence is an origin of the game spectrum shaping using the pump polarisation should be a good starting point for a more advanced investigation.

4.1.3 Summary

It has been experimentally demonstrated that pump polarisation can be used as an additional degree of freedom to reduce the GV of a single pump FOPA by up to 2 dB. As a result, a gain of 10.5±0.5 dB over 102 nm bandwidth has been demonstrated. Additionally, it was predicted that it would be possible to achieve a GV of only 0.2 dB over >100 nm bandwidth.

Proof of concept simulations imply that the observed gain sensitivity to pump polarisation arises due to high-order birefringence, even if gain is expected to be polarisation-insensitive assuming a fibre with a random linear birefringence. This phenomenon was observed only in short fibres with low PMD and the pump near the zero dispersion wavelength. It is suggested that it arises in fibres where random birefringence is not sufficient to average an effect of high-order birefringence.

The observed phenomenon can be used in a more general sense than GV decrease, for example to design a gain spectrum shape which compensates for an attenuation slope. However, high-order birefringence can also introduce an undesirable polarisation dependent gain in broadband FOPAs. Therefore, an effect of high order birefringence on FOPA gain needs to be studied in more details as the state-of-the-art vector FOPA theory neglects high-order birefringence [59].

4.2 FOPA cascading

It has been suggested to cascade low gain FOPA stages to achieve high gain as it is difficult to maintain low GV for gains >10 dB. The cascading consists in implementation of two or more consecutive independent FOPA gain stages. Independency of gain stages implies that the phase mismatch accumulated in one stage is not transferred to the following stage. In other words, each stage must have no idlers at the input. Therefore, the FOPA cascading suggests to implement a few consecutive FOPA stages whilst idlers are removed (filtered) after each stage. In practice idlers can be removed by using a band splitter. For the best performance a new pump can be used in each stage, but for the best power efficiency the residual pump from one stage can be reused in another stage given that its power is sufficient.

The idea of cascaded FOPA has been briefly introduced in [34] and is discussed in details in this section. A performance of cascaded FOPA is compared with single-stage FOPA through simulations. Then, an achievable cascaded FOPA gain spectrum is estimated and prospects of FOPA cascading are discussed.

4.2.1 Simulations

An advantage of cascading for FOPA gain spectrum and an impact of the idler removal are illustrated using single-polarisation split step Fourier method simulations neglecting Raman. A pump power of 10 W and fibre parameters listed in experimental setup description (Subsection 3.1.1) were used in these simulations. The pump frequency was shifted from the zero dispersion frequency by 20 GHz into the anomalous dispersion side to obtain a broadband flat gain spectrum. Three cases were considered: a single 25 m fibre, a single 50 m fibre, and two consecutive 25 m fibres with a filter to remove idlers between them. If the filter between two consecutive 25 m fibres is removed, this case becomes an equivalent of a single 50 m fibre.

The purple and the green curves at Figure 4.4 show gain spectra obtained in 25 m and 50 m long fibres respectively. The 50 m fibre suggests an improvement of the minimum gain over the 10 THz bandwidth by ~5 dB as compared to the 25 m fibre. However, the GV over this bandwidth is substantially increased from ~1 dB to ~5 dB. On the contrary, two independent FOPA stages employing 25 m fibres suggest essentially double gain and double GV as compared to the single stage (yellow curve). Although the pump power and the total fibre length are the same in two 25 m stages and in the single 50 m stage, two 25 m stages suggest ~5 dB higher gain and ~3 dB

lower GV over 10 THz bandwidth than the single 50 m stage. Additionally, this simulation proves that the idlers removal indeed makes gain stages independent and leads to a simple summation of the stages' gain spectra.

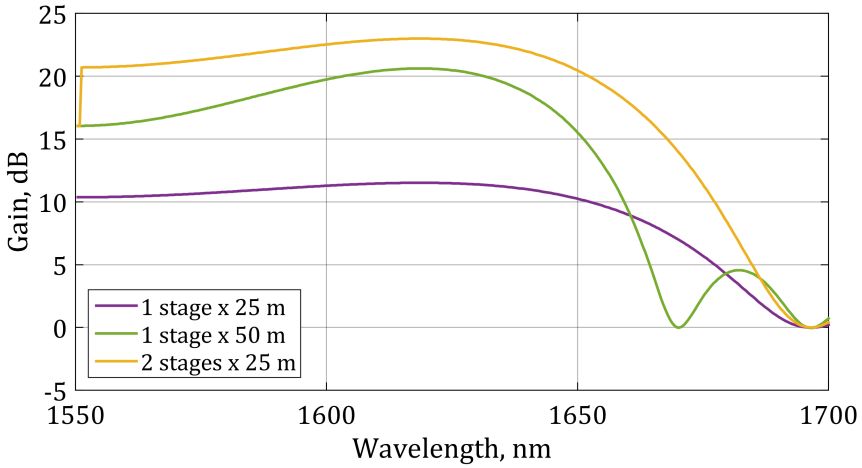

Figure 4.4. Simulated FOPA gain spectra to demonstrate an advantage of cascading for FOPA.

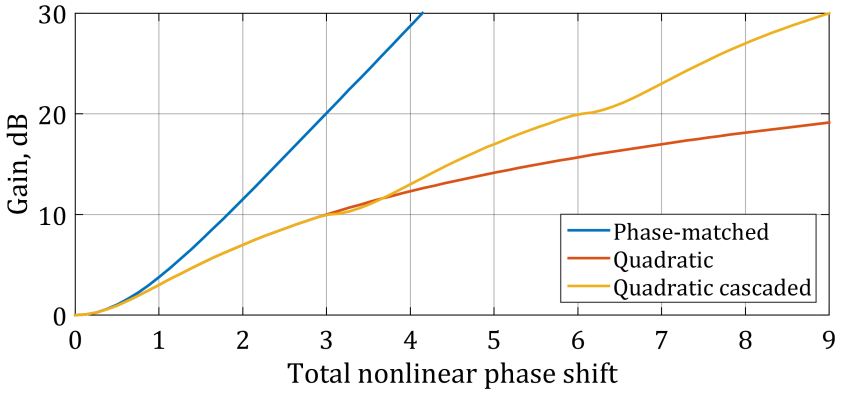

Figure 4.5. Gain calculated as a function of nonlinear phase-shift in three cases: phase-matched (K = 1), quadratic (K = 0) and quadratic with idlers removal every 10 dB of gain.

Figure 4.5 shows quadratic FOPA gain (normalised mismatch parameter K = 0) calculated as a function of nonlinear phase shift in cases of a single stage and an idlers removal every 10 dB. Phase-matched gain (K = 1) is shown for reference. Quadratic gain is a key interest here because it has been shown in the previous chapter that a flat quadratic gain can be achieved over very wide bandwidth with low GV. Figure 4.5 demonstrates that the cascading indeed allows to substantially increase gain of FOPA operating in the quadratic gain regime. The reason for this is that by the end of the first stage a significant phase mismatch is accumulated, so a further increase of gain

is slowed down. It appears to be advantageous to periodically remove idlers and to generate new ones to reset phase-matching.

4.2.2 Practical considerations for FOPA cascading

It has been demonstrated from the theoretical point of view that an employment of a few consecutive low gain stages allows for a higher gain with lower GV than a single high gain stage. In this subsection a practical potential of FOPA cascading is discussed.

Two suggested configurations of cascaded FOPA are shown at Figure 4.6. The configuration with pump reuse is energy efficient, but the pump power in the second stage is reduced due to mid-stage loss. On the other hand, the configuration without pump reuse requires a separate pump source for each fibre and potentially imposes higher mid-stage loss on signals due to an additional WDM coupler, but allows to obtain an optimal performance of each stage.

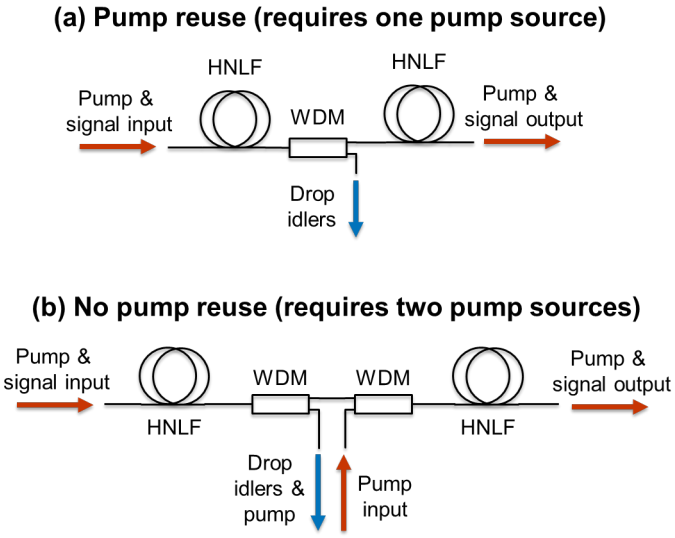

Figure 4.6. Suggested configurations of cascaded FOPA: (a) with pump reuse and (b) without pump reuse.

The resulting gain spectrum for each configuration can be estimated using experimentally measured gain spectra. For assessment of the configuration reusing the pump it is suggested to use gain spectrum measurement results for a range of pump powers in the 25 m HNLF (Figure 3.14(a)). Therefore, it is assumed that the 9 W pump is used and each stage employs a 25 m HNLF. Mid stage loss due to idler removal are assumed to be 0.5 dB. Then, the second stage pump power is reduced to ~8 W. The resulting gain spectrum is then estimated as a sum of gain spectra obtained in the 25 m HNLF using pump powers of 9 W and 8 W and reduced by 0.5 dB due to

mid-stage loss. Experimental gain spectra per stage and the estimated cascaded gain spectrum are shown at Figure 4.7. The cascaded gain of 16.4±1.6 dB over 106 nm (12.3 THz) bandwidth suggests a significant GV improvement against the best previously reported gain spectrum comparable in terms of both bandwidth and total gain value: 16.8±2.8 dB over 110 nm (12.5 THz) bandwidth [8].

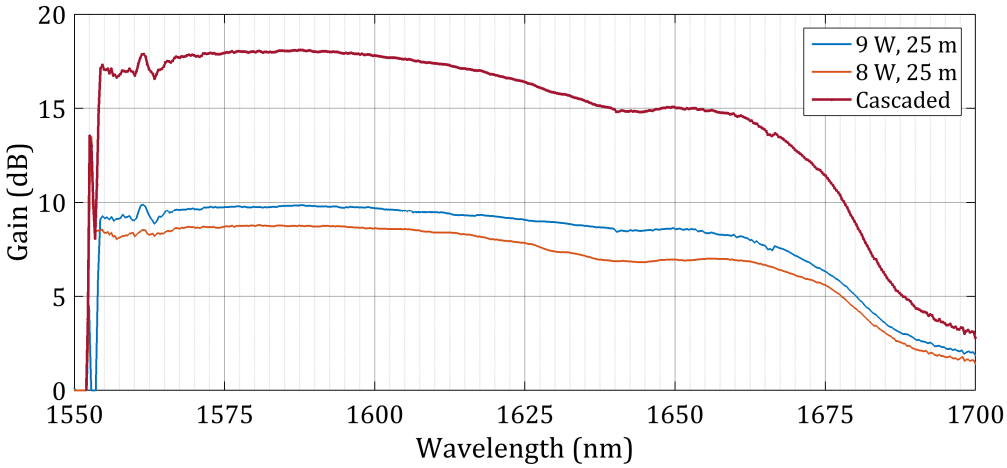

Figure 4.7. Estimated cascaded gain spectrum with pump reuse based on experimentally measured gain spectra with pump powers of 9 W and 8 W in the 25 m long HNLF.

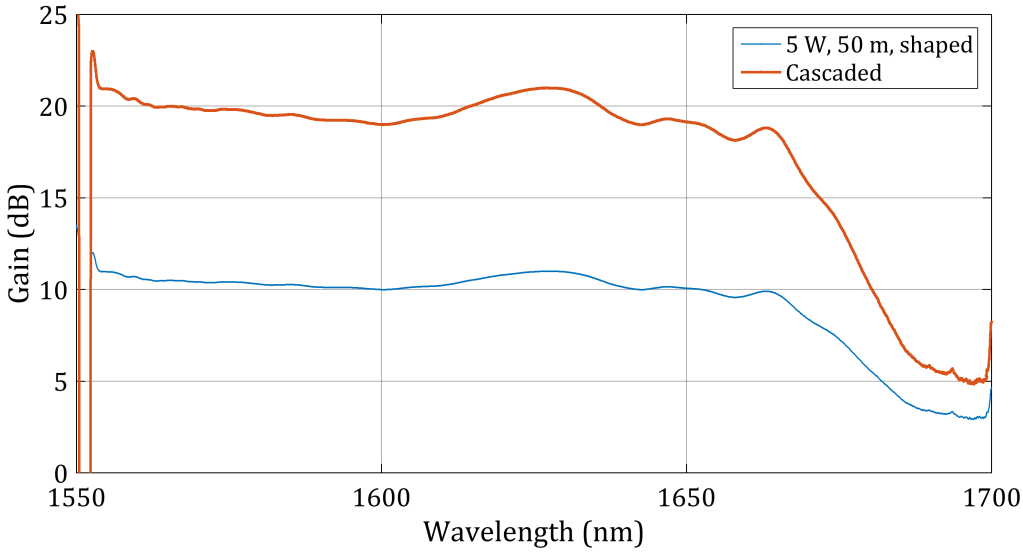

Figure 4.8. Estimated cascaded gain spectrum without pump reuse based on experimentally measured gain spectrum with pump power of 5 W and in the 50 m long HNLF and using gain spectrum shaping by pump polarisation.

For the best result a configuration without pump reuse is assessed. A gain spectrum measured with pump power of 5 W in the 50 m HNLF and shaped by pump

polarisation (Figure 4.1) is chosen to be a gain per stage. Signal loss between stages due to idler removal and a coupling with a pump are assumed to be 1 dB. The resulting cascaded gain spectrum is shown at Figure 4.8. It suggests gain of 19.6±1.4 dB over 114 nm (13.3 THz) bandwidth – a truly superior result.

4.2.3 Summary and discussion

It has been suggested that cascading of ~10 dB gain stages with low GV allows to scale GV almost linearly with gain in contrast to single stage FOPAs which GV grows rapidly for gain >10 dB. An estimation based on experimentally measured gain spectra per stage has shown that the typically aimed by discrete amplifiers gain of ~20 dB can be achieved using cascaded FOPA over the record bandwidth of 114 nm (13.3 THz) with a GV below 3 dB. Moreover, it was predicted in this work that GV < 1 dB per ~10 dB gain stage can be achieved (Subsection 4.1.1). This allows for even lower GV and/or higher overall gain of cascaded FOPA over >100 nm bandwidths.

In addition, the concept of FOPA cascading matches the trends of amplifier development. The recently suggested four-fibre loop for polarisation-insensitive FOPA [66] essentially implies FOPA cascading. Additionally, an implementation of two-stage EDFAs has shown an advantage of placing dispersion compensating modules, gain flattening filters and other equipment in between stages. It is viewed that the future FOPA development will undoubtedly rely on cascading.

5 RAMAN-AMPLIFIED PARAMETRIC PUMP AND ITS USE IN FOPA AND OPTICAL PHASE CONJUGATION

FOPA research progress although significant has been almost entirely performed in or around the C band. This is because state-of-the-art FOPAs require an EDFA to produce a pump of sufficient power (≥1 W) and quality, having narrow linewidth and low noise [13]. Even though a parametric pump situated within the EDFA gain window can still provide FOPA gain spreading well beyond the C band [32], the ability to generate a pump for FOPA in other spectral regions is vital for a flexible FOPA operation across the whole low-loss transmission window.

Several approaches to produce a parametric pump outside the C band have been previously reported with various degrees of success: semiconductor optical amplifiers have been used at ~1310 nm [106], Ytterbium-doped fibre amplifiers (YDFA) at ~1050 nm [91], and high power wavelength conversion from the C and L bands to ~1650 nm and ~1480 nm respectively using an additional FOPA [54]. These are notable papers highlighting the need for high power parametric pumps outside the EDFA-band, but each possessed some limitations constraining FOPA development. Semiconductor devices cover a wide wavelength range, but provide insufficient power for good FOPA performance (17.5 dBm in [106]). YDFA operation range is outside the low loss window for silica and is far from the optical communications' regions of interest. Using wavelength conversion for pump generation significantly degrades energy efficiency as compared to EDFA and cannot offer full wavelength flexibility as it is still bound by the EDFA.

The key pump in FOPAs is therefore almost always amplified using a high power EDFA which restricts the wavelength range to the Erbium gain spectrum. It is surprising that, to the best of my knowledge, Raman amplification or generation of a pump for FOPA has not been explored in the literature up to now. Raman lasers are known to be able to provide a high power (>1 W) in a sufficiently narrow bandwidth for FOPA (i.e. <5 GHz) [107–110]. However, works focusing on a narrow linewidth Raman sources do not explore a number of amplified wave's characteristics critical for FOPA pumping and therefore do not make it clear if such sources can be used to pump FOPA. Additionally, all these works rely on a single-order pumping by Ytterbium doped fibre lasers, so there is no evidence of their wavelength flexibility.

This chapter explores the suitability of Raman-amplified pumps for FOPA and other parametric applications. In Section 5.1 a discrete Raman amplifier is used to produce a pump power sufficient for use in a FOPA (up to 1.5 W). The Raman-amplified pump quality is examined to demonstrate its suitability for use in a FOPA. The Raman amplifier architecture and a non-resonant nature of Raman gain [111] ensure that such amplifier can be designed to operate anywhere in the silica transmission window with similar performance. In Section 5.2 the obtained Raman-amplified pump is subsequently employed in a FOPA to produce gain bandwidth of >35 nm or peak gain of 24.9 dB. To the best of my knowledge it is the first demonstration of a FOPA utilising a Raman-amplified pump. As a proof-of-principle, this demonstration is performed within the C band, but it is clearly extendable beyond this range if a suitable Raman laser and FOPA gain fibre are sourced. Finally, in Section 5.3 a wideband EDFA-free Raman-assisted optical phase conjugation (RA-OPC) is performed within the Raman amplifier gain fibre itself. In contrast to previous works on RA-OPC [112, 113], the main focus of this work is Raman amplification of the low input power parametric pump to achieve a broadband RA-OPC performance requiring high parametric pump power (0.5–1 W). As a result a conversion efficiency >0 dB has been demonstrated over >60 nm.

5.1 Raman-amplified parametric pump and its characterisation

In this section an ability of a seeded high gain discrete Raman amplifier to produce a pump suitable for FOPA and other parametric applications is examined. First, a range of available fibres is tested as a Raman gain fibre and parametric pumps obtained in each fibre are briefly characterised. Then, the parametric pump amplified in the best performing fibre among tested is examined in detail in terms of qualities critical for FOPA performance, such as linewidth, optical signal-to-noise ratio (OSNR) and relative intensity noise (RIN). Power efficiency, polarisation and wavelength flexibility are also discussed.

5.1.1 Experimental setup

Figure 5.1 shows the experimental setup of a Raman amplifier for a parametric pump. A continuous single-polarisation parametric pump seed was generated from a 100 kHz linewidth tuneable laser (TL) operating in the C band with a maximum power

of 40 mW (16 dBm). The parametric pump seed was passed through a phase modulator (PM) which was driven by three radio frequency (RF) tones with frequencies 100, 320 and 980 MHz to mitigate stimulated Brillouin scattering (SBS) [19]. The parametric pump seed was then passed to the Raman amplification stage.

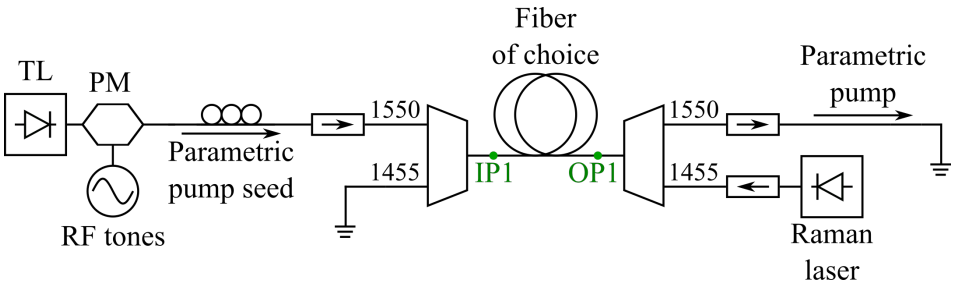

Figure 5.1. Experimental setup of discrete Raman amplifier for parametric pump amplification and characterisation.

A range of readily available fibres of various types and lengths were tested as a gain medium in the Raman amplifier to find the most suitable. These were: standard single mode fibre (SSMF), dispersion compensating fibre (DCF), dispersion shifted fibre (DSF) and highly nonlinear fibre (HNLF). The fibre-under-test was backward-pumped using a randomly polarised Raman fibre laser operating at 1455 nm and of ~5 W maximum output power [114]. The amplified parametric pump and the Raman pump were multiplexed and demultiplexed using two 1455/1550 WDM couplers. Isolators were employed as indicated in Figure 5.1 to stop back-reflections.

Power measurements and the Raman-amplified parametric pump characterisation were performed using two calibrated bidirectional 1% couplers placed at the ends of the gain fibre (points IP1 and OP1 at Figure 5.1) and connected to an optical spectrum analyser (OSA) and a RIN measurement kit via an optical switch.

5.1.2 Raman gain fibre testing

A range of fibres is tested to find a Raman gain fibre suitable for producing a high power pump for FOPA. The fibre testing was performed using a parametric pump seed wavelength of 1550 nm, parametric pump seed power of 7.6 mW (8.8 dBm) at the input of the gain fibre (IP1), and a coupled Raman pump power of 3.2 ± 0.1 W at OP1.

Figure 5.2 summarises the output parametric pump power, gain, insertion loss, backscattered power and remnant Raman pump power for a range of tested fibres. A power of >1 W (30 dBm) is targeted as is typically required for parametric applications such as FOPA. The power of the parametric pump Rayleigh backscatter is measured for each fibre to perform an initial comparison of the fibres' susceptibility to double Rayleigh backscattering known to be a performance limiting factor in high gain Raman amplifiers due to multi-path interference [115]. The minimal SBS was indirectly confirmed for all fibres by observing the SBS peak to be lower than the Rayleigh peak at IP1 (not shown at Figure 5.2). The amount of remnant Raman pump power indicates if the tested fibre is too short or too long.

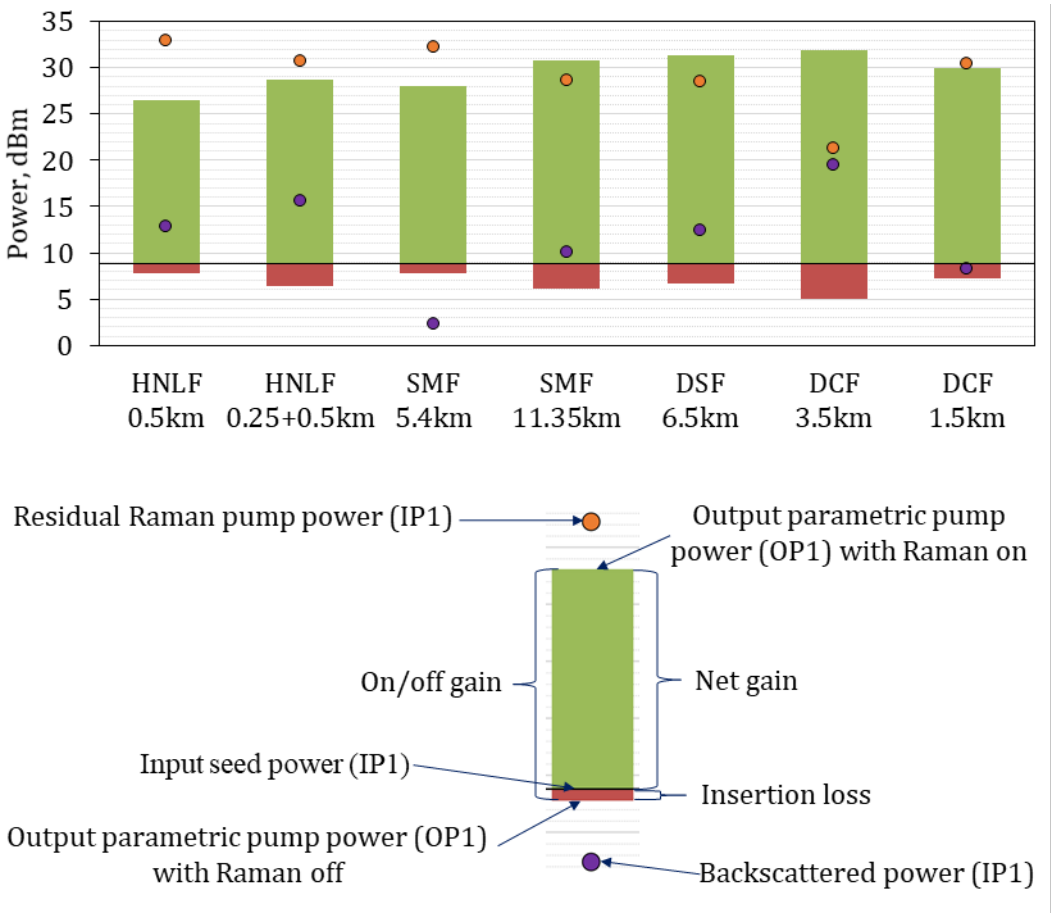

Figure 5.2. Summary of fibres tested in Raman amplifier.

For HNLF, the lengths available were insufficient to reach a high parametric pump power, leaving over 1 W remnant Raman pump power. In addition, as compared with the other fibres tested, the backscattered power in HNLF was higher and the gain limited by multi-path interference is therefore expected to be lower. The 5.4 km SSMF

was too short to provide enough gain. The 11.35 km SSMF and the 6.5 km DSF allowed for the parametric pump power of 1.2 W (30.8 dBm) and 1.35 W (31.3 dBm) respectively. These two fibres caused a significant Raman pump depletion leaving ~0.7 W of remnant Raman pump power. DSF showed superior gain-to-attenuation ratio than SSMF as DSF provided more gain and lower insertion loss than SSMF (SSMF is almost twice longer than DSF). On the other hand the DSF had higher Rayleigh backscattering than SSMF. Consequently, the choice between DSF and SSMF is reduced to a trade-off between the parametric pump power and an impact of the multi-path intereference. The 3.5 km DCF demonstrated the highest output parametric pump power of ~1.6 W (32 dBm) and the lowest remnant Raman pump power of ~130 mW. However, it also incurred the worst backscattered to output power ratio among all fibres, so a very high multi-path interference is expected in this case. The 1.5 km DCF conversely produced an output parametric pump power of 1 W (30 dBm) with low backscatter, which implies that DCF is competitive with SSMF and DSF in terms of performance, but the lengths tested were less optimal.

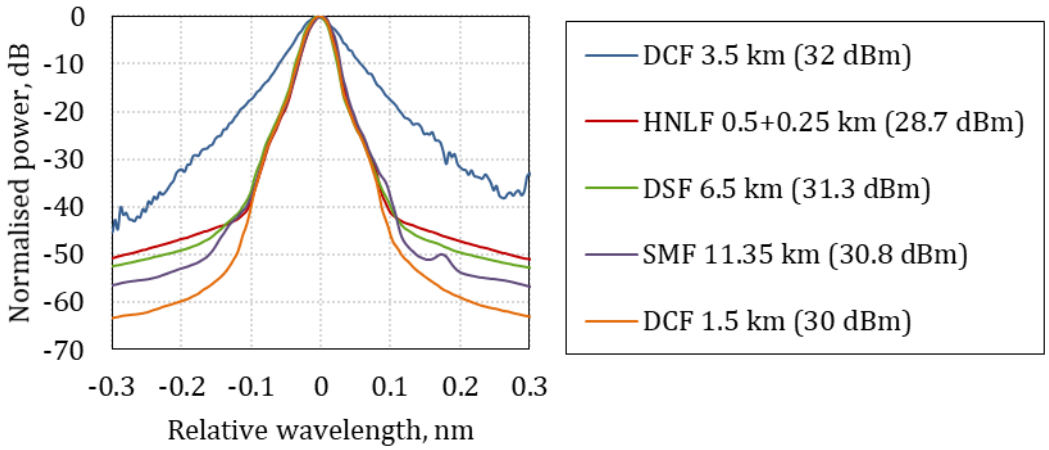

Figure 5.3. Comparison of experimental parametric pump spectra (normalised for visual aid) at the output of tested Raman gain fibres. Output parametric pump powers are shown in brackets.

Figure 5.3 shows comparison of output parametric pump spectra for fibres which showed the highest output parametric pump power. The power is normalised to the peak for each case to perform comparison of the noise level. It can be seen that the noise level around the pump correlates with the measured backscattered power shown in Figure 5.2. The 3.5 km DCF fibre is indeed unsuitable for a parametric pump amplification due to a severe parametric pump broadening and an overwhelming level of noise generated around the parametric pump. The 6.5 km DSF was concluded

to be an optimal Raman gain fibre for a parametric pump amplification as it provided the second highest output parametric pump power and an adequate level of noise and backscatter.

5.1.3 Pump characterisation

In this subsection the previously chosen 6.5 km DSF was used as a Raman amplifier gain fibre. The parametric pump seed wavelength was by default set to 1566 nm which is suitable for a FOPA using a HNLF with the zero dispersion wavelength of 1565 nm. The parametric pump seed power was maximised and measured to be 9.3 mW (9.7 dBm) at IP1. Figure 5.4 shows the output parametric pump power (OP1) versus input Raman pump power (OP1). The highest achieved Raman-amplified parametric pump power was ~1.5 W (31.7±0.1 dBm) at OP1. Essentially the same power level was observed over a range of >15 nm as shown by the inset plot of Figure 5.4. The absence of a distinctive gain peak as well as a nonlinear dependence of the measured gain on the Raman pump power is due to strong Raman pump depletion. SBS was not limiting the maximum parametric pump power as the maximum backscattered power was only 15 mW (11.9 dBm) at IP1.

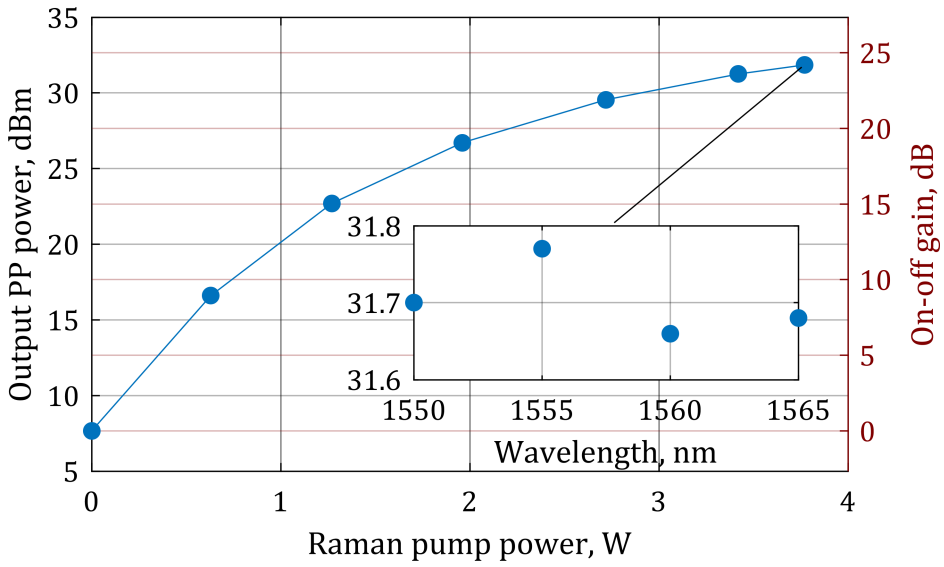

Figure 5.4. Experimentally measured output parametric pump power (OP1) and on-off gain versus Raman pump power (OP1). The maximum output parametric pump power versus wavelength is shown inset.

Figure 5.5 shows RIN spectra [116] of the parametric pump seed at the output of the tuneable laser and of the 1.5 W Raman-amplified parametric pump. The amplified parametric pump RIN was ~-138 dB/Hz up to 70 MHz, falling below -140 MHz for

higher frequencies. The two spikes observed around 73 MHz are a result of dithering tone mixing. Overall, the Raman amplification has introduced a ~10 dB/Hz RIN penalty compared to the tuneable external cavity laser, however the measured RIN level is suitable for parametric applications at the cost of a small signal penalty [82].

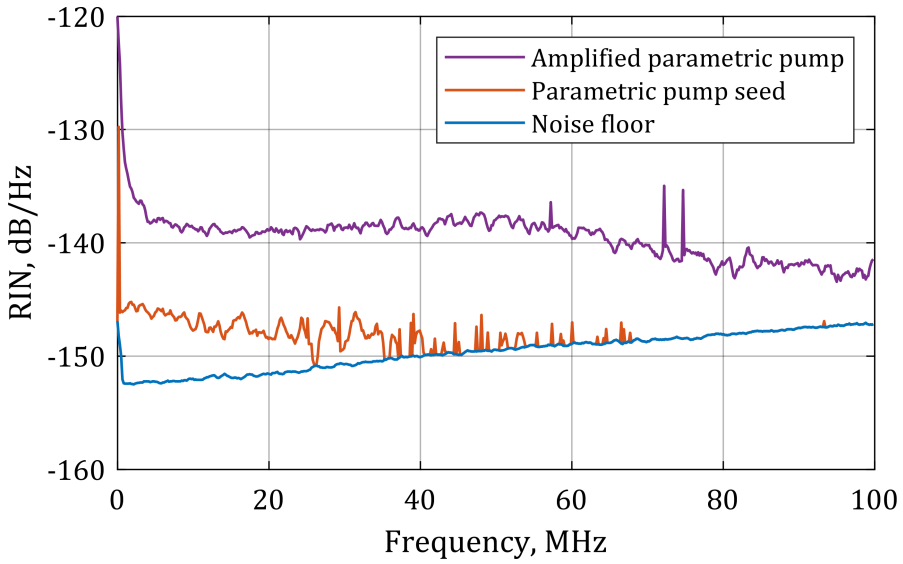

Figure 5.5. Comparison of experimental RIN for the parametric pump seed and the 1.5 W Raman-amplified parametric pump.

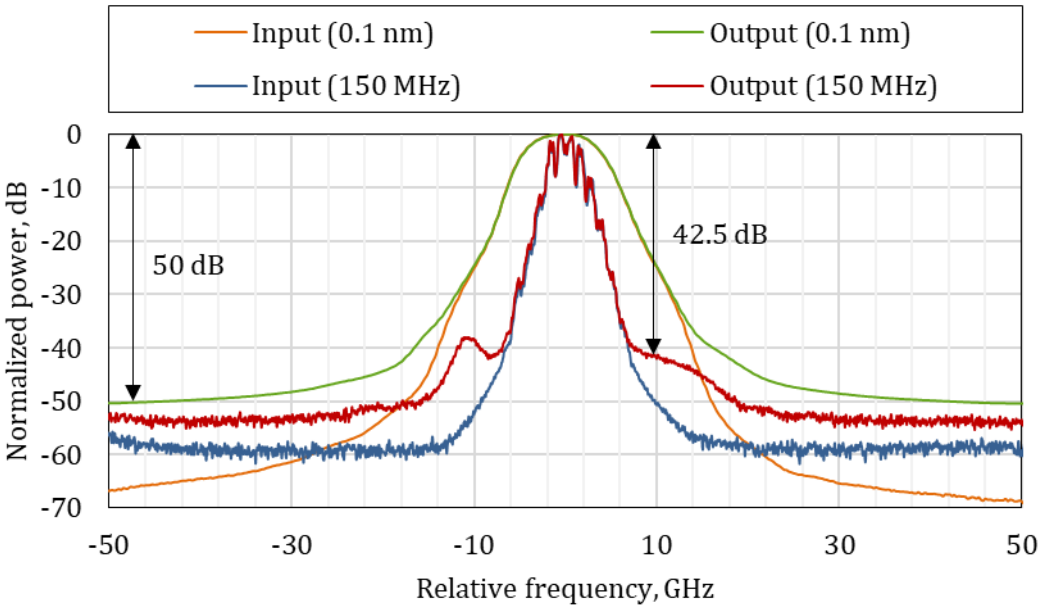

Figure 5.6. Input (IP1) and output (OP1) normalised power spectra of the Raman-amplified parametric pump. OSA resolution is 150 MHz or 0.1 nm. The input and output parametric pump powers are 9.7 dBm and 31.7 dBm.

Figure 5.6 shows power spectra of the parametric pump at the input and the output of the Raman amplifier for OSA resolutions of 150 MHz and 0.1 nm. The power of each plot is normalised to aid visual comparison. Note that the noise floor for the 150 MHz measurements is due to OSA instrument noise rather than optical noise. The multiple spikes at the top of the 150 MHz spectra are due to dithering of the parametric pump. The full width at half-maximum of the parametric pump is ~3.7 GHz. It can be seen that the output parametric pump spectrum with resolution of 150 MHz is undistorted above the noise level of ~-40 dB. The noise localised around the parametric pump is presumably a result of the multi-path interference. The output OSNR measured with resolution of 0.1 nm was ~50 dB. This measurement does not account for noise located near the parametric pump, but measures the Raman amplified spontaneous emission (ASE) noise.

5.1.4 Discussion and summary

Raman pumps identical to the one employed in this experiment are commercially available anywhere in a wavelength range 1200–1600 nm [114]. There is a wide range of narrow linewidth lasers to seed the Raman amplifier at arbitrary wavelength too. The equivalent of the characterised parametric pump can therefore be obtained using the described discrete Raman amplifier architecture over a whole low-loss window of modern fibres (~1310–1625 nm) [117].

Since a seeded Raman amplifier rather than a random Raman laser was used, the polarisation properties of the Raman-amplified parametric pump are defined mostly by the parametric pump seed, likewise, in the case of an EDFA-amplified parametric pump.

The optical power efficiency achieved in this experiments was ~30% as a 5 W Raman pump was used to produce a 1.5 W parametric pump at OP1. The electrical efficiency of the demonstrated Raman amplifier was therefore roughly equivalent to that of an EDFA: i.e. a parametric pump power of 1.5 W was achieved in the Raman amplifier pumped by a Raman laser with a datasheet maximum power consumption of 70 W [114], while the power consumption of a 2 W EDFA from the same supplier was found to be 80 W [118].

Overall, a 1.5 W parametric pump was obtained using a Raman amplifier with efficiency comparable to EDFA. The linewidth of 3.7 GHz was on purposely introduced by dithering and not affected by Raman amplification. Such linewidth is typically used in FOPA to mitigate SBS. Energy efficiency and polarisation properties match those of

EDFA-amplified parametric pumps. The RIN reflecting an impact of pump-noise transfer and multi-path interference was on the level of ~-138 dB/Hz, and the signal to Raman ASE noise ratio was -50 dB. These values correspond to small signal penalties and show that although discrete Raman amplifiers' performance cannot compare with EDFA, the enabled FOPA pump wavelength flexibility is worth this trade-off.

5.2 FOPA employing Raman-amplified pump

It has been shown in Section 5.1 that a Raman-amplified parametric pump can be an energy efficient and wavelength flexible alternative to EDFA-amplified parametric pumps. In this section a FOPA employing a Raman-amplified pump is therefore demonstrated for the first time to the best of my knowledge.

5.2.1 Experimental setup

The experimental setup of FOPA employing Raman-amplified pump is shown in Figure 5.7. A seeded discrete Raman amplifier was implemented to boost a parametric pump power to 1.5 W at OP1 as described in Section 5.1. The parametric pump was consequently coupled with a continuous probe via a 1% coupler and passed through a FOPA gain fibre. The 100 kHz linewidth continuous probe, used to characterise FOPA gain, was sourced from a C band tuneable laser (TL) and passed through a polarisation controller (PC) before coupling with the parametric pump. The gain spectrum measurement technique described in Section 3.2 could not be implemented here as the only available Raman laser required for supercontinuum generation was employed in this experiment to pump the Raman amplifier.

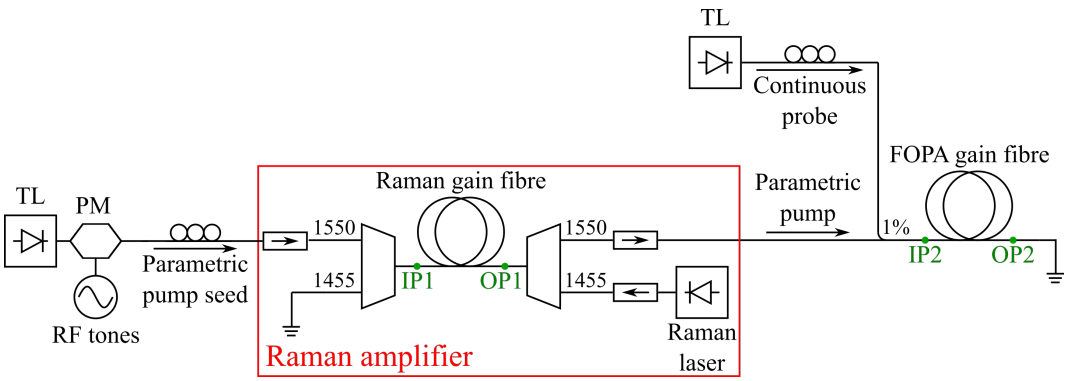

Figure 5.7. Experimental setup of FOPA employing a Raman-amplified pump.

The 0.5 km HNLF was used as a FOPA gain fibre. The HNLF zero dispersion wavelength was $\lambda_0 \sim 1565$ nm and fibre nonlinearity was $\gamma \sim 8$ W^{-1}km^{-1}. Additional two calibrated bidirectional 1% couplers connected to an OSA through an optical switch were added at the ends of FOPA gain fibre (points IP2 and OP2 at Figure 5.7) to perform power measurements.

5.2.2 Results and discussion

Figure 5.8 shows the FOPA gain spectrum achieved when using the Raman amplified parametric pump at two different wavelengths: 1566 nm and 1565.3 nm. The parametric pump power at IP2 was 1 W (30.1 dBm) due to 1.6 dB component insertion loss between the power measurement points OP1 and IP2. Depending on the parametric pump wavelength, the peak parametric gain was reaching 24.9 dB or spanning over an EDFA-equivalent 35 nm bandwidth with a minimum gain of 11.4 dB.

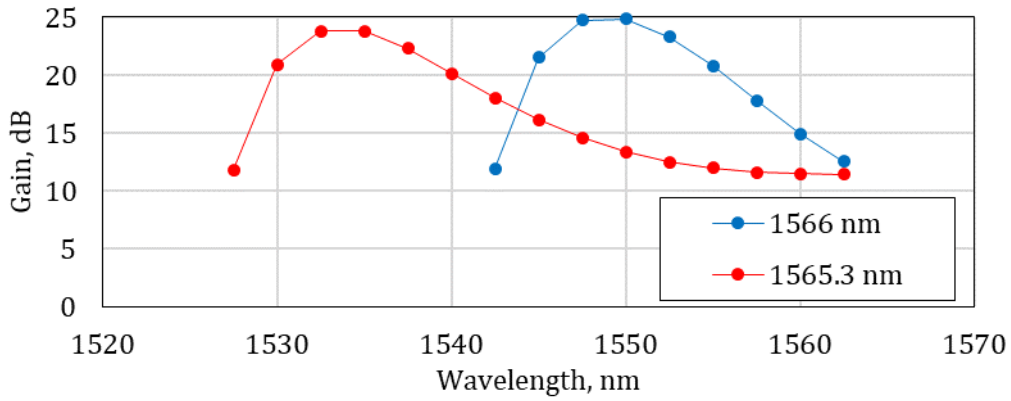

Figure 5.8. Experimental FOPA gain spectra obtained with the Raman-amplified parametric pump tuned to wavelength of 1566 nm (blue dots) or 1565.3 nm (red dots).

Figure 5.9 shows power spectra at the input and output of the FOPA (IP2 and OP2) for pump wavelength of 1565.3 nm and an example probe wavelength of 1536 nm (OSA resolution was 0.1 nm). A spike at the input around 1596 nm is caused by a double reflection/scattering of an idler generated within FOPA. The spike is >30 dB lower than the input probe and >50 dB lower than the idler output, so it can be neglected. A probe OSNR in this example both at the input and the output was 34 dB. FOPA did not have a noticeable impact on the probe OSNR as it was limited by Raman ASE noise transmitted from the Raman amplifier along with the parametric pump and then amplified in FOPA together with the probe. The side lobes around the parametric pump were also generated within the Raman amplifier gain fibre (DSF is prone to four

wave mixing) and further amplified within the FOPA. For the best performance, a narrow passband filter therefore need to be used on the Raman-amplified parametric pump before coupling it with a signal to remove a Raman ASE noise and unwanted four wave mixing products generated within the Raman amplifier. However, an additional filter in this experiment would introduce an attenuation causing an intolerable for this demonstration parametric pump power decrease.

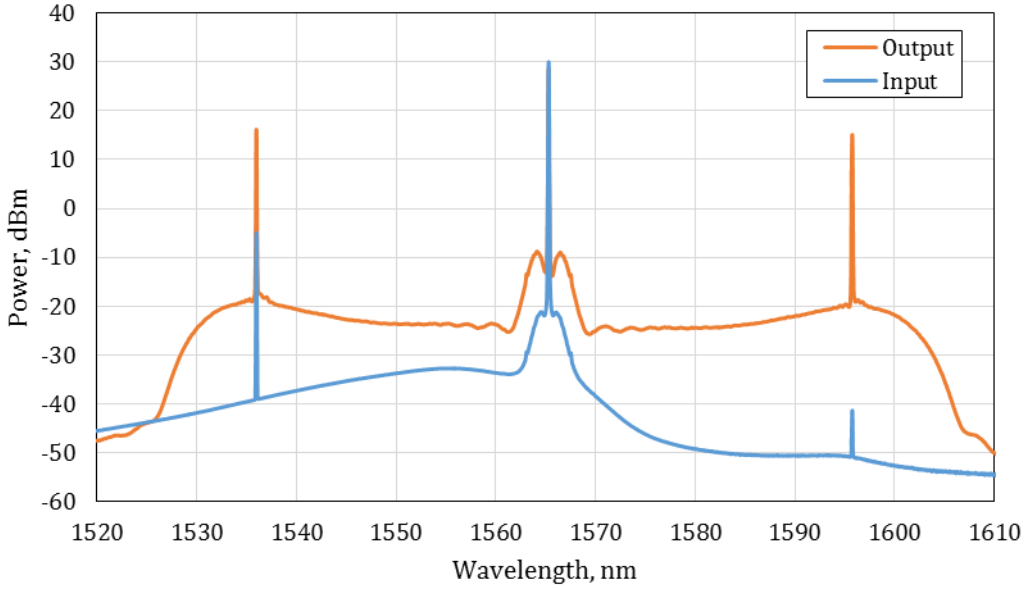

Figure 5.9. Example power spectra at the input and output of FOPA employing a Raman-amplified parametric pump.

The discrete Raman amplifier was operated in this experiment as a standalone black box replacing an EDFA or other amplifier, so it can be used with any existing FOPA configuration [25, 54, 106] or technique [33, 63, 94]. The major difference between using an EDFA and a discrete Raman amplifier is a need to mitigate SBS in a Raman gain fibre to achieve high output powers within narrow linewidth. Note, that if dithering is not required and not desirable for a parametric device utilizing a Raman-amplified pump, a core radius varying [79] or strained fibre [77] could be used to mitigate SBS since Raman gain is not bound by dispersion, which is affected by these techniques.

Overall, the results obtained here demonstrate that a Raman-amplified pump can be used in a FOPA and related applications in an identical way to an EDFA-amplified pump, while granting the pump wavelength flexibility. Although Raman amplifiers can provide a gain at arbitrary wavelengths themselves, it can be seen that FOPAs

employing Raman-amplified pump have a potential for higher and broader gain than discrete Raman amplifiers.

5.3 Wideband optical phase conjugation employing low input pump power

Given that FOPA employing a Raman-amplified pump enables long-haul signal transmission outside of C and L bands, other fibre optical communication subsystems might also need to be upgraded for operation beyond common C and L bands. In particular, as of current state-of-the-art a promising technique of optical phase conjugation (OPC) is relying on EDFA as heavily as FOPA does. It is therefore in the context of this chapter to examine a wavelength flexible wideband OPC employing a Raman-amplified pump. It is implied that the wavelength flexibility can be granted if a parametric pump for OPC is generated using a wavelength unrestricted Raman gain [111] and a low power seed which can be obtained anywhere in potential transmission bands.

Raman-assisted optical phase conjugation (RA-OPC) has been shown to be a promising technique due to many improvements as compared to the conventional OPC. Conversion efficiency has been shown to improve by >10 dB which is larger than the Raman gain employed in this RA-OPC [112, 119]. Q factor improvement by 2 dB has been demonstrated in RA-OPC as compared to OPC [120]. Conversion bandwidth improvement by >10 nm has also been demonstrated in RA-OPC [113]. However, all these works utilise moderate Raman gains (<8 dB), so they either rely on EDFA for the parametric pump amplification or demonstrate low conversion efficiency <-10 dB. This section focuses on implementation of high Raman gain (up to 17 dB) within RA-OPC to allow for the EDFA removal from the setup and to enable OPC for spectral regions outside of the C band with high conversion efficiency over wide bandwidth and negligible SBS whilst keeping the parametric pump linewidth narrow <150 MHz (linewidth measurement is limited by OSA resolution).

5.3.1 Concept of EDFA-free optical phase conjugation

The parametric pump amplified by Raman in Section 5.1 and implemented in FOPA in Section 5.2 could in principle be used for OPC too except this parametric pump was dithered to avoid SBS in both the Raman amplifier and the FOPA. It was necessary

because SBS causes a significant parametric pump RIN increase [76], which is then transferred to amplified/conjugated signals [82]. However, using a similarly dithered parametric pump for OPC applications would cause a significant distortion of the generated phase-conjugate (idler) [84].

The most common technique to mitigate SBS in OPC devices is using two counter-phase dithered parametric pumps which can mutually compensate for dither transfer from parametric pumps to idlers [121, 122]. Therefore, EDFA-free OPC can be performed using two Raman-amplified counter-phase dithered parametric pumps. However, performing an experiment with two parametric pumps is outside the scope of this thesis. Instead, the maximum achievable undithered parametric pump power within the Raman amplifier is examined in this section and consequently an undithered parametric pump is used to demonstrate a single pump EDFA-free RA-OPC within the Raman gain fibre itself. The operation principle for this is shown in Figure 5.10 whereby a signal and a parametric pump seed are injected into the same Raman gain fibre. The parametric pump is Raman amplified to provide wide bandwidth OPC, while the signal and the generated idler/conjugate are additionally boosted by the Raman to drastically improve the conversion efficiency [12]. The key is that the parametric pump reaches high power only near the end of the Raman gain fibre, so it does not invoke significant SBS.

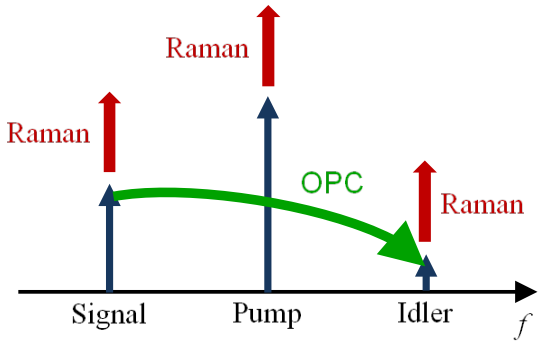

Figure 5.10. Principle of operation of EDFA-free RA-OPC.

Additionally, it has been reported that a digital signal processing of the received idler may offer some compensation for one-tone dither transfer to a phase-conjugate [123]. Therefore, a one-tone dithered parametric pump is examined and implemented for EDFA-free RA-OPC too.

5.3.2 Experimental setup

The experimental setup performing a parametric pump amplification and a RA-OPC at the same time within a high gain Raman amplifier is shown in Figure 5.11. It was essentially the discrete Raman amplifier shown in Figure 5.1 with an additional tuneable laser (TL) coupled through a 1% coupler. The additional 100 kHz linewidth TL was used to generate a 100 kHz linewidth continuous probe for conversion efficiency and OSNR measurements.

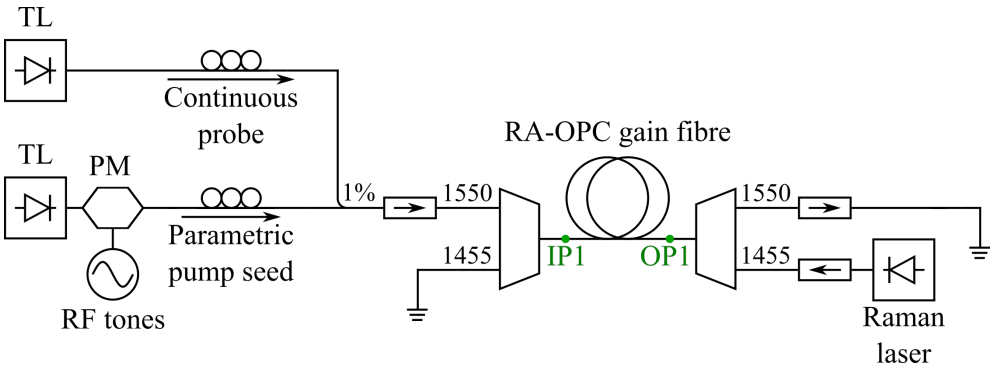

Figure 5.11. Experimental setup of EDFA-free RA-OPC.

Among all available fibres only the 6.5 km DSF and the 0.5 km HNLF were considered to be used as a gain fibre for RA-OPC, because the gain fibre zero dispersion wavelength was required to be in C band, where the experiment was performed. Eventually, the 0.5 km HNLF was used as a gain fibre due to too low SBS threshold of the 6.5 km DSF as explained in Subsection 5.3.3.

The parametric pump seed wavelength was 1565.3 nm as it showed the largest FOPA gain bandwidth whilst using the same 0.5 km HNLF. The continuous probe was tuned through C and L bands for RA-OPC characterisation. The parametric pump seed and the continuous probe power at IP1 were 9.3 mW (9.7 dBm) and 0.01 mW (-20 dBm) respectively. The output powers of the parametric pump and phase-conjugates were measured at OP1.

5.3.3 Raman amplification of pump within optical phase conjugator

Because of the impact of dithering on the single pump OPC process, any Raman amplifier gain fibre for this experiment should provide high Raman gain, while being short enough to let the amplified parametric pump through without incurring significant SBS. The 6.5 km DSF was therefore not appropriate for this functionality as the maximum undithered output parametric pump power (OP1) was only ~23 mW

(13.6 dBm). Any power above this level was reflected back due to SBS. The maximum *useable* parametric pump power would be even smaller as SBS increases RIN long before full back reflection. In this context, a parametric pump power <23 mW is not enough for a wideband OPC operation.

The 0.5 km HNLF conversely had a much higher SBS threshold than the 6.5 km DSF due to its shorter length. RIN measurements were performed to find the maximum SBS-free output parametric pump power, which was adjusted by tuning Raman pump laser power and thus changing a Raman amplifier gain [76]. The parametric pump amplification to 23.6 dBm with and without tones and to 26.8 dBm with one tone provided the same parametric pump RIN level (Figure 5.12). No changes to RIN, while the output parametric pump power and a number of tones are being changed, mean that SBS was negligible in these three cases. In contrast, the undithered parametric pump amplification to 24.4 dBm caused a substantial RIN increase over the previous cases indicating arise of SBS.

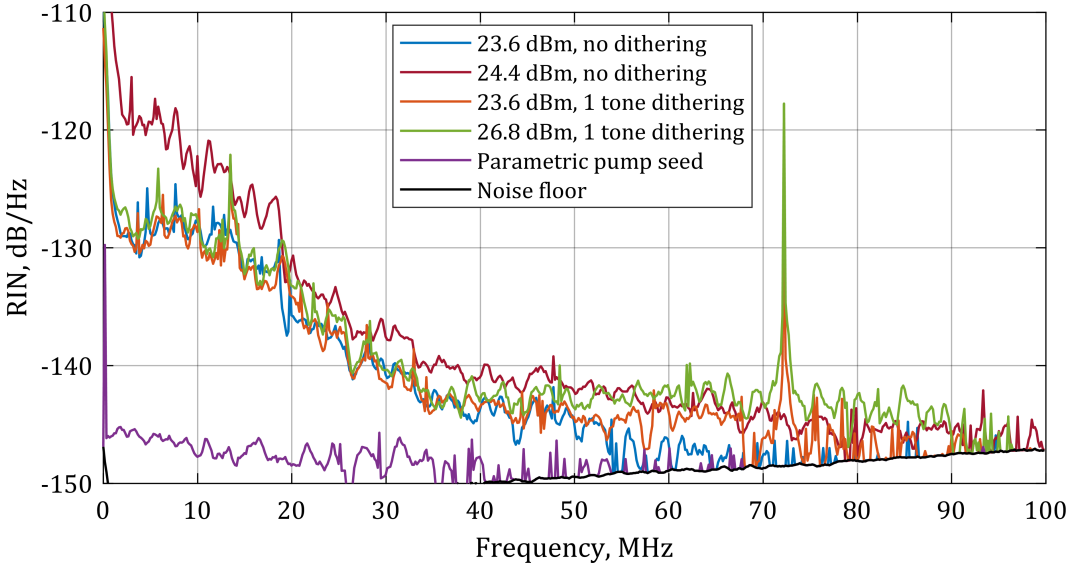

Figure 5.12. Experimental RIN of the parametric pump at the RA-OPC output for varied Raman gain and dithering on/off; the legend shows corresponding output parametric pump powers. RIN of the parametric pump seed is shown for comparison.

Overall, the 0.5 km HNLF was selected as the gain fibre for the EDFA-free RA-OPC as it allowed to boost a parametric pump power to 230 mW (23.6 dBm) or 480 mW (26.8 dBm) at OP1 using no or one-tone dithering respectively without inducing SBS. The corresponding coupled Raman pump laser power at OP1 was 3 W and 3.9 W respectively. RA-OPC is characterised below for these two cases of parametric pump

amplification. Note, that this setup could also have been used to pump a separate (not Raman-assisted) OPC device. The one-tone parametric pump power of 26.8 dBm was limited by the maximum Raman gain and could have been increased if higher Raman pump power had been available to provide more gain.

5.3.4 Characterisation of EDFA-free optical phase conjugator

The RIN of both undithered and one-tone dithered parametric pumps amplified in the 0.5 km HNLF was ~-128 dB/Hz for frequencies below ~15 MHz (Figure 5.12). It is presumably attributed to multi-path interference. On the other hand, the amplified parametric pump RIN is approaching RIN of the parametric pump seed source as frequency increases. Therefore, overall signal penalty due to RIN is expected to be low as high RIN is localised in a narrow range of low frequencies.

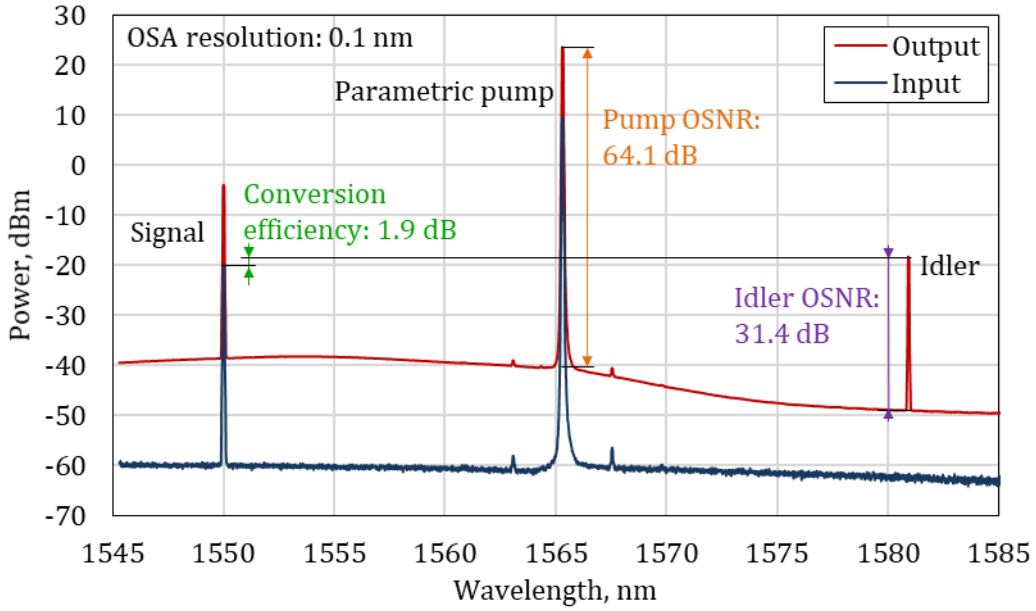

Figure 5.13. An example experimental optical spectra at the input (IP1) and the output (OP1) of the RA-OPC showing the undithered parametric pump, a signal and the corresponding generated idler.

Figure 5.13 shows an example experimental optical spectra at the input (IP1) and the output (OP1) of the RA-OPC for a signal at 1550 nm and the undithered parametric pump. The internal conversion efficiency of 1.9 dB was measured as a ratio between idler power at the output of HNLF and signal power at the input of HNLF. The signal polarisation was tuned to maximise the idler power before the conversion efficiency measurement. The parametric pump OSNR of 64.1 dB was measured as a ratio between an output parametric pump power and an output noise power at the pump

wavelength within OSA resolution bandwidth of 0.1 nm. High performance FOPA have been demonstrated with a similar parametric pump OSNR value [13]. An idler OSNR of 30.9 dB was measured as a ratio between output idler power (signal on) and optical noise power (signal off). It was confirmed that the presence of the signal did not affect optical noise level as the optical noise in this experiment is attributed mainly to Raman ASE noise.

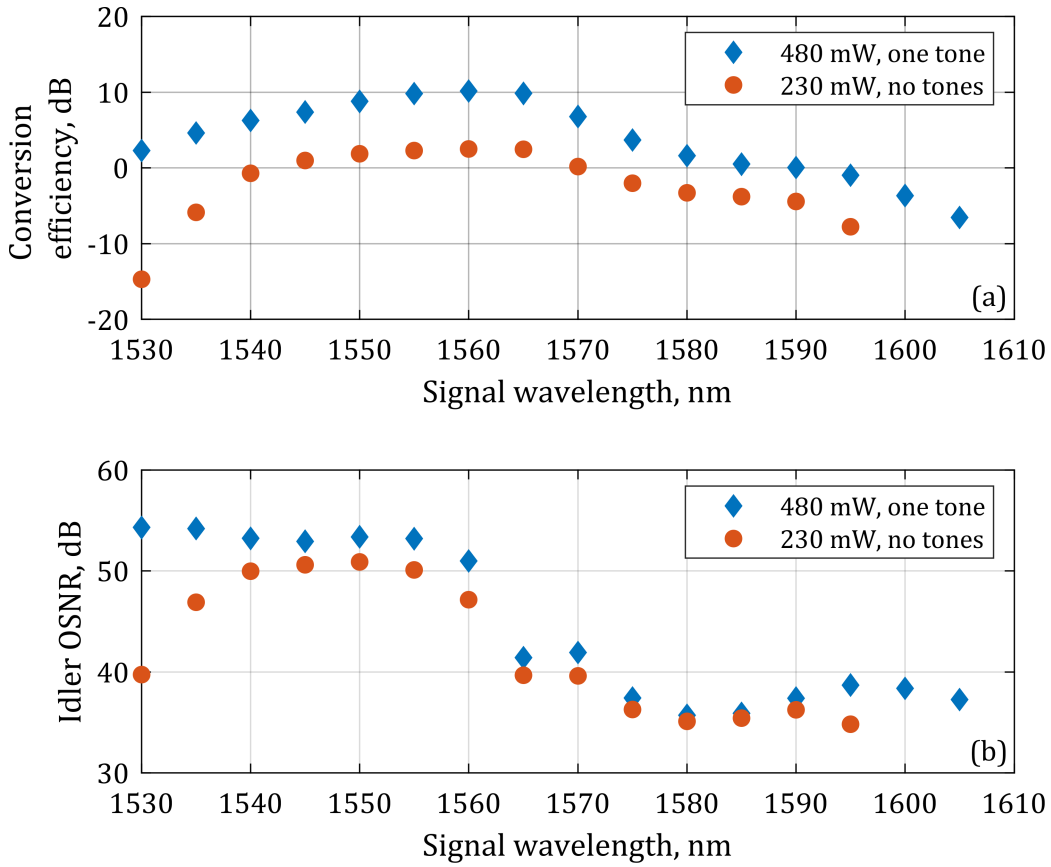

Figure 5.14. Experimental measurements of (a) internal conversion efficiency and (b) idler OSNR (adjusted for an input signal power of 0 dBm) for RA-OPC performed within the Raman amplifier under two pumping levels allowing for output parametric pump power of 480 mW (dithered with one tone) and 230 mW (not dithered).

The internal conversion efficiency was then measured for a range of signal wavelengths 1530–1605 nm with a step of 5 nm (Figure 5.14(a)). The measurement was performed for two scenarios: with one tone dithering or no dithering of the parametric pump seed and the Raman pump power of 3.9 W or 3 W at OP1 leading to the parametric pump power of 480 mW or 230 mW at OP1 respectively without observing SBS. A positive internal conversion efficiency was achieved without

dithering for signals in a 25 nm range 1545–1570 nm and with dithering for signals in a 60 nm range 1530–1590 nm. The highest conversion efficiency has constituted 2.5 dB without dithering and 10.2 dB with dithering. It was achieved for signals around 1560 nm where the *signals* benefited from the maximum Raman gain. Figure 5.15 shows the output optical spectrum (OP1) with signal off whereas the peak of Raman ASE noise in a range 1550–1560 indicates the region of the highest Raman gain. Conversion efficiency in the opposite direction (from L band to C band) was ~5-10 dB lower as the *idlers* benefit less from the Raman gain since they are generated later along the fibre.

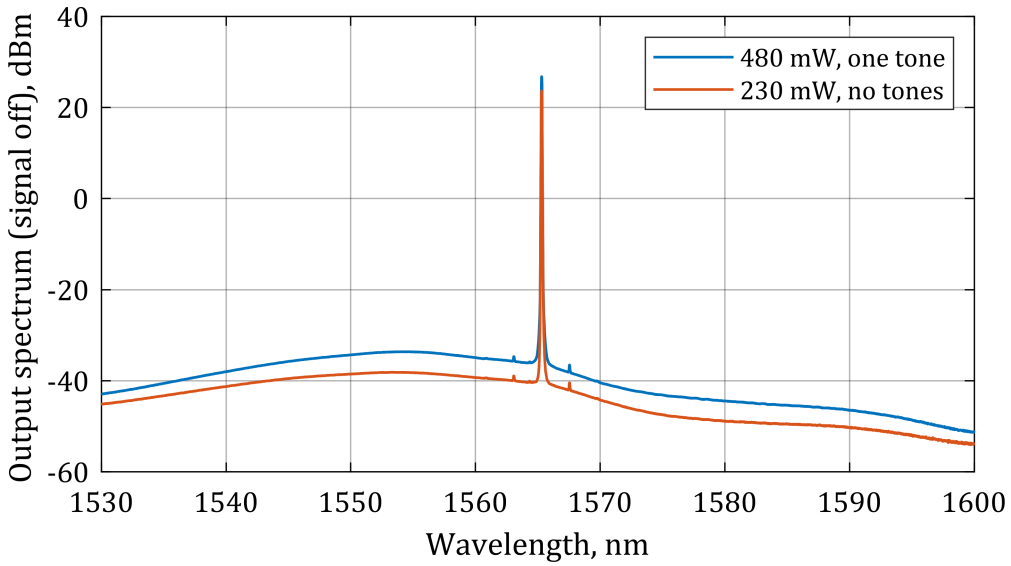

Figure 5.15. Experimental optical spectrum at the output of RA-OPC (OP1) with signal off for two dithering levels corresponding SBS-free pumping levels and consequently output parametric pump powers of 230 mW and 480 mW. It shows the Raman ASE noise distribution for OSNR calculation and additionally indicates the region with the highest Raman gain.

In Figure 5.13 the idler OSNR was calculated as $P_i - P_{ASE}$, where P_i and P_{ASE} are the idler and the Raman ASE noise powers [dBm]. Since $P_i = P_s + G_i$, where P_s is the input signal power [dBm] and G_i is the conversion efficiency, the idler OSNR can be calculated using equation (5.1). The result of this calculation is shown in Figure 5.14(b), where the idler OSNR is the difference between the measured conversion efficiency G_i (Figure 5.14(a)) and the Raman ASE noise power P_{ASE} at the idler wavelength (Figure 5.15) plus signal power P_s = 0 dBm (IP1).

$$OSNR_{idler} = P_s + G_i - P_{ASE} \tag{5.1}$$

The highest idler OSNR is observed when signals are in the C band and idlers are consequently in the L band since in this range the conversion efficiency is at its highest, while Raman ASE noise is low. Consequently the idler OSNR exceeds 50 dB in a ~15 nm range of signal wavelengths 1540–1555 nm without dithering and in >30 nm range of signal wavelengths 1530–1560 nm with dithering.

5.3.5 Discussion

Phase-conjugation with a positive conversion efficiency means transparent RA-OPC operation as the output power of phase-conjugates is not less than the input signal power. Wide bandwidth of transparent operation, >25 nm without dithering and >60 nm with one-tone dithering. Taking into account results of idler OSNR measurement in this proof-of-concept experiment, the internal conversion efficiency G_i > 1 dB with OSNR >50 dB has been demonstrated over at least 10 nm without dithering, and conversion efficiency G_i > 2.3 dB with OSNR >51 dB over at least 30 nm with one-tone dithering allowing OPC of an almost entire C band with a high OSNR.

It should be noted that in both cases the highest conversion efficiency and the highest idler OSNR were taking place in strongly overlapping regions. This was possible because the pump was located ~110 nm (~14.5 THz) away from the Raman pump, at the edge of the Raman gain peak. Consequently, signals situated close to the Raman gain peak and supplied with the most amplification produced idlers in the low Raman gain region with low ASE noise. An optimisation employing both parametric pump and Raman laser wavelength tuning is presumably able to broaden an overlap of high conversion efficiency and high idler OSNR ranges.

The key outcome of this experiment is achieving wideband OPC while using low power parametric pump seed (~10 mW at the RA-OPC input in this experiment) not requiring to employ EDFA within the system. This opens up OPC to wavelengths outside of the EDFA gain bands however, if this is not the requirement, an EDFA could be used to increase the parametric pump seed power and thus further improve performance. Overall, the suggested architecture is beneficial for high conversion efficiency single pump OPC unrestricted by the EDFA operation range.

5.4 Summary

It has been demonstrated that a discrete high output power Raman amplifier is suitable for amplification of a narrow linewidth pump suitable for use in a FOPA. A

parametric pump was amplified by Raman to achieve a power of 1.5 W and was subsequently used to pump a conventional FOPA without the use of any EDFA. In principle, this system can be redesigned to operate in any wavelength range where Raman gain is available. A peak FOPA gain of 24.9 dB was demonstrated using this technique as well as amplification over 35 nm with a minimum gain of 11.4 dB.

Additionally, a narrow linewidth undithered/one-tone dithered parametric pump was boosted by a Raman amplifier to a power of 230 mW/480mW without incurring significant SBS to be used in dithering-affected parametric processes, e. g. OPC (it is assumed that one-tone dithering can be compensated for using a digital signal processing). An EDFA-free RA-OPC has been consequently demonstrated within the Raman amplifier gain fibre itself. In this case, besides the conversion efficiency boost by the Raman gain, the Raman amplification of parametric pump allowed a positive internal conversion efficiency wideband operation over >25 nm range without using dithering or over >60 nm with one-tone dithering.

These results expand the potential for parametric devices including amplifiers, phase-conjugators, wavelength convertors, etc. to operate at arbitrary wavelengths. FOPA employing a Raman-amplified parametric pump can be used to provide a high gain over wide bandwidth anywhere in a low loss window of modern zero-water peak 'dry' fibres spanning from 1260 nm to 1625 nm [117] to get extra transmission bandwidth. Considering FOPA being able to provide >10 THz gain bandwidth as discussed in Chapter 3 the WDM transmission capacity can be multiplied. Alternatively, FOPA employing a Raman-amplified parametric pump can be used to supply high gain around the 1300 nm low-loss window of SSMF which is attractive for FOPA implementation using existing fibre links.

A presumed optical communications expansion beyond C and L bands would require an improved wavelength flexibility from many modern technologies. Nonlinearity compensation through OPC is one of them, so EDFA-free RA-OPC can be a way of implementation OPC for next generation optical communications. Finally, a wavelength conversion which can be performed OPC or FOPA alike is to surely benefit from central wavelength flexibility.

6 CONCLUSION AND FUTURE WORK

6.1 Conclusion

In this thesis, a range of innovative techniques has been demonstrated and investigated to make FOPA an enabling technology for significant expansion of the bandwidth available for WDM transmission. The main focuses of this thesis have been an improvement of unfiltered flat FOPA gain bandwidth and an enabling of FOPA gain at arbitrary wavelengths.

The boundaries of flat FOPA gain bandwidth has been expanded by implementation of following approaches and findings. An ultra-short highly nonlinear fibres down to 25 m length have been employed. It has been proved that the fibre length decrease allows to improve gain bandwidth and flatness due to a mitigation of longitudinal fluctuations of zero dispersion wavelength (ZDW), an increase of the stimulated Brillouin scattering (SBS) threshold and a higher pump power used to reach a particular gain magnitude. The pump wavelength placed in proximity of ZDW was found to provide the broadest and the flattest gain. The achieved parametric gain bandwidth of ~11 THz and the quadratic law of the gain increase in this case has allowed for flat FOPA gain spectrum enhancement by merging ranges of mostly parametric gain and mostly forward Raman gain invoked by the parametric pump. It has been demonstrated that cascading of independent ~10 dB gain stages is more advantageous than a single high gain FOPA when aiming for a broadband high gain with low gain variation. Therefore, it is the best to restrict gain per independent FOPA by ~10 dB. It has been shown that an independency of consecutive stages can be achieved by removing idlers between them. Additionally, a technique of broadband gain spectrum shaping via pump polarisation has been explored and demonstrated to allow for a 2 dB gain variation reduction and potentially to achieve as low gain variation as 0.2 dB over >100 nm bandwidth. Overall, a record flat gain of 10.5±0.5 dB over 102 nm (11.9 THz) bandwidth has been demonstrated. It is estimated that cascading of such stages can allow for a gain of ~20 dB with a gain variation below 3 dB over ~110 nm bandwidth on a single side of the FOPA central frequency.

This thesis has addressed the FOPA operation range restriction imposed by reliance of FOPA pump amplification on EDFA. An EDFA-free FOPA has been demonstrated in this thesis to unleash the FOPA potential to operate in arbitrary

wavelength range. It has been shown that a sufficiently high power (>1 W) pump suitable for FOPA can be obtained using a discrete Raman amplifier. The pump suitability consist in narrow linewidth, high optical signal-to-noise ratio, low relative intensity noise and single polarisation. An energy efficiency of pump amplification by Raman was found to be similar to this of EDFA. In addition, an EDFA-free optical phase conjugation (OPC) has been demonstrated. A proof-of-concept experiment has allowed for a decent performance with conversion efficiency >1 dB over >10 nm bandwidth with OSNR >30 dB. Assuming a digital signal processing to compensate for one tone dithering the proof-of-concept experiment has demonstrated OPC of almost a whole C band (bandwidth of at least 30 nm) with conversion efficiency >2.3 dB and OSNR >51 dB. This approach not only has a potential of competitive OPC performance, but suggests full wavelength flexibility necessary for OPC implementation in optical communications expanding outside of C and L bands. Moreover, the demonstrated EDFA-free OPC setup can also be used for wavelength conversion to significantly expand its implementation flexibility via extending a range of central wavelength choice.

Overall, whilst FOPA features a great potential of a virtually unlimited bandwidth and an arbitrary wavelength operation, it is difficult to realise this potential in practice. This thesis has significantly developed this potential and advanced the state-of-the-art performance by demonstrating a range of techniques leading to a record bandwidth and flatness of FOPA gain spectra and by demonstrating a FOPA which operation range is not bound by reliance on EDFA. These achievements are viewed as a step towards significant extension of bandwidth available for signal transmission via implementation of broadband FOPA.

6.2 Future work

Although a significant progress has been made there is a way to go to enable FOPA implementation outside of a lab. This defines two main directions of future FOPA development. First, the demonstrated ultra-wide gain FOPA is to be realised in a polarisation-insensitive configuration whilst delivering high net gain. Second, a broadband high gain FOPA is to be demonstrated in spectral regions yearning for high gain amplifiers suitable for WDM signals amplification, e.g. around ~1310 nm.

The first experiment is therefore to implement FOPA stages supplying ~10 dB flat gain over ~100 nm bandwidth in the four-fibre loop polarisation-insensitive scheme

and to amplify polarisation-multiplexed WDM signals over full bandwidth. This experiment would aim to achieve ~15 dB polarisation-insensitive net gain (assuming 5 dB insertion loss) with GV of ~2 dB over a record bandwidth up to 100 nm. On condition that sufficiently low signal penalties will be achieved, this amplifier would be able to compete with EDFA by amplification of a C+L bands equivalent at once. The polarisation dependent gain is not expected to limit performance of such FOPA, because looped architectures have proved themselves to provide stably low polarisation dependent gain imposing little signal penalties. It is also viewed that implementation of ultra-short fibre lengths and the four-fibre loop architecture is sufficient to mitigate the nonlinear crosstalk, so the main impact on signal quality is expected to be imposed by the pump dithering. If dithering is indeed to become the FOPA limiting factor, a study of SBS mitigation techniques for FOPA should come into focus.

The second experiment would be to demonstrate high FOPA gain around 1310 nm using a Raman-amplified pump and a standard single mode fibre. Besides discrete amplification it would be possible to perform a distributed amplification. Both operation regimes might be attractive for passive optical networks and data centre networks.

APPENDIX 1. SIMULATION OF VECTOR PROPAGATION MODEL.

This appendix describes a simulation of the vector model FOPA. A symmetrised split step Fourier method [57] is used, so propagation of each step length Δz contains three stages: a linear propagation by half step $\Delta z/2$, an implementation of nonlinear interaction at the middle of step over the whole step length of Δz and a linear propagation by a further half step $\Delta z/2$.

A.1. Basis

A circular basis is used, because the nonlinear length in FOPA $L_{NL} = 1/\gamma P$, where γ is the nonlinear coefficient and P is the pump power, can be very short (~10 m) and therefore comparable with the beat length. In this method the electrical field is represented as a superposition of right- and left-hand circularly polarised components u_R and u_L respectively. Before the simulation the input field in the Jones basis is transformed to the circular basis as follows:

$$\begin{pmatrix} u_R(0) \\ u_L(0) \end{pmatrix} = \frac{1}{\sqrt{2}} \cdot \begin{pmatrix} 1 & i \\ i & 1 \end{pmatrix} \begin{pmatrix} u_x(0) \\ u_y(0) \end{pmatrix}, \tag{A.1}$$

where $(u_x(0) \quad u_y(0))^T$ is the input Jones vector and $(u_R(0) \quad u_L(0))^T$ is its representation in the circular basis. After the propagation by distance L the transformation back to the Jones basis is performed as follows:

$$\begin{pmatrix} u_x(L) \\ u_y(L) \end{pmatrix} = \frac{1}{\sqrt{2}} \cdot \begin{pmatrix} 1 & -i \\ -i & 1 \end{pmatrix} \begin{pmatrix} u_R(L) \\ u_L(L) \end{pmatrix}, \tag{A.2}$$

A.2. Linear propagation

A linear propagation by step Δz is performed in the spectral domain as follows:

$$\begin{pmatrix} \hat{u}_R(z+\Delta z) \\ \hat{u}_L(z+\Delta z) \end{pmatrix} = \begin{pmatrix} h_{11} & h_{12} \\ h_{21} & h_{22} \end{pmatrix} \begin{pmatrix} \hat{u}_R(z) \\ \hat{u}_L(z) \end{pmatrix} \tag{A.3}$$

where $\hat{u}_R$ and $\hat{u}_L$ are Fourier transforms of u_R and u_L, Δz is the propagated distance, and coefficients h_{11}, h_{12}, h_{21} and h_{22} are defined as

$$
\begin{aligned}
h_{11} &= \frac{1}{2}\cdot[(1+\sin 2\chi)\cdot h_a + (1-\sin 2\chi)\cdot h_b];\\
h_{12} &= \frac{-i}{2}\cdot(h_a - h_b)\cdot\cos(2\chi)\cdot\exp(2i\psi);\\
h_{21} &= \frac{i}{2}\cdot(h_a - h_b)\cdot\cos(2\chi)\cdot\exp(-2i\psi);\\
h_{22} &= \frac{1}{2}\cdot[(1-\sin 2\chi)\cdot h_a + (1+\sin 2\chi)\cdot h_b];
\end{aligned}
\tag{A.4}
$$

where 2ψ and 2χ are the longitude and the latitude of the principal eigenstate on the Poincare sphere, h_a and h_b are the linear propagation coefficients for two orthogonal eigenstates:

$$
\begin{aligned}
h_a &= \exp\{[-\alpha_a/2 + i\beta_a(\omega)]\cdot\Delta z\};\\
h_b &= \exp\{[-\alpha_b/2 + i\beta_b(\omega)]\cdot\Delta z\};
\end{aligned}
\tag{A.5}
$$

where α_a and α_b are the linear loss coefficients for orthogonal eigenstates, $\beta_a(\omega)$ and $\beta_b(\omega)$ are the frequency dependent propagation constants for orthogonal eigenstates.

A.3. Nonlinear interaction

An impact of nonlinear effects in circular basis is described by following equations:

$$
\begin{aligned}
\frac{du_R}{dz} &= i\frac{2\gamma}{3}\cdot(|u_R|^2 + 2\cdot|u_L|^2)\cdot u_R;\\
\frac{du_L}{dz} &= i\frac{2\gamma}{3}\cdot(|u_L|^2 + 2\cdot|u_R|^2)\cdot u_L;
\end{aligned}
\tag{A.6}
$$

where γ is the nonlinear coefficient. These equations are implemented by approximating an integral with the trapezoidal rule as suggested in [57]:

$$
\begin{aligned}
u'_R\left(z+\frac{\Delta z}{2}\right) &= u_R\left(z+\frac{\Delta z}{2}\right)\cdot\exp\left[\left(\frac{\frac{du_R(z)}{dz}}{u_R(z)} + \frac{\frac{du_R(z+\Delta z)}{dz}}{u_R(z+\Delta z)}\right)\cdot\frac{\Delta z}{2}\right] =\\
&= u_R\left(z+\frac{\Delta z}{2}\right)\times\\
\times\exp\left\{i\frac{\gamma\Delta z}{3}\cdot[|u_R(z)|^2 + 2\cdot|u_L(z)|^2 + |u_R(z+\Delta z)|^2 + 2\cdot|u_L(z+\Delta z)|^2]\right\},&
\end{aligned}
\tag{A.7}
$$

where $u_R(z+\Delta z/2)$ and $u'_R(z+\Delta z/2)$ are the optical field before and after accounting for the nonlinear interaction respectively. The equation for the left-hand circularly polarised component is the same as equation (A.7), but with indices R and L being swapped.

One of terms in the equation (A.7) is an optical field after the step propagation $u_R(z+\Delta z)$ which is not known at the middle of the step. Therefore, the step

propagation (including linear propagation) is performed iteratively. At the first iteration (iteration number is shown in brackets as a superscript) it is approximated that $u_R^{(1)}(z+\Delta z) = u_R^{(1)}(z)$. For the following iterations the field after the step is approximated with the previous iteration result: $u_R^{(N)}(z+\Delta z) = u_R^{(N-1)}(z+\Delta z)$. The step propagation is iterated until convergence. The convergence is verified by comparing a relative change of the optical field as a result of current iteration with the tolerance set:

$$tol > \frac{\left\| u_R^{(N)}(z+\Delta z) - u_R^{(N-1)}(z+\Delta z) \right\|^2 + \left\| u_L^{(N)}(z+\Delta z) - u_L^{(N-1)}(z+\Delta z) \right\|^2}{\left\| u_R^{(N)}(z+\Delta z) \right\|^2 + \left\| u_R^{(N)}(z+\Delta z) \right\|^2}, \quad \text{(A.8)}$$

where tol is the set tolerance and N is the number of the performed iteration. The current step propagation is considered to converge when equation (A.8) is satisfied. If convergence cannot be achieved after a reasonable number of iterations, the ither step size Δz is to be reduced, or the tolerance is to be relieved.

A.4. Verification

This model was compared with a known analytical solution to verify implementation of equations, polarisation averaging and signal polarisation scrambling. Figure A.1 shows gain spectra of signals linearly co-polarised with the pump in case of random linear birefringence described in Subsection 4.1.2 and Table 2 and shown at Figure 4.3(c). The green curve represent an analytical solution derived in [59] for this case and implemented as described in Subsection 2.3.1 on vector FOPA theory with coefficients $b = 8/9$ and $u = 16/9$. Blue curve is a result of the split step simulation whilst signals and the pump had the same linear polarisation at the input. Orange curve is the result of the split step simulation whilst signals were polarisation scrambled and the resulting gain was obtained as described in Subsection 3.2.5 on co-polarised gain measurement using a depolarised probe. Figure A.1 shows that the split step simulation agree with the most advanced existing analytic solution describing a case of random linear birefringence. This provides a confidence in using this model to explore the case of random tilted birefringence which is not described by any existing analytic solution.

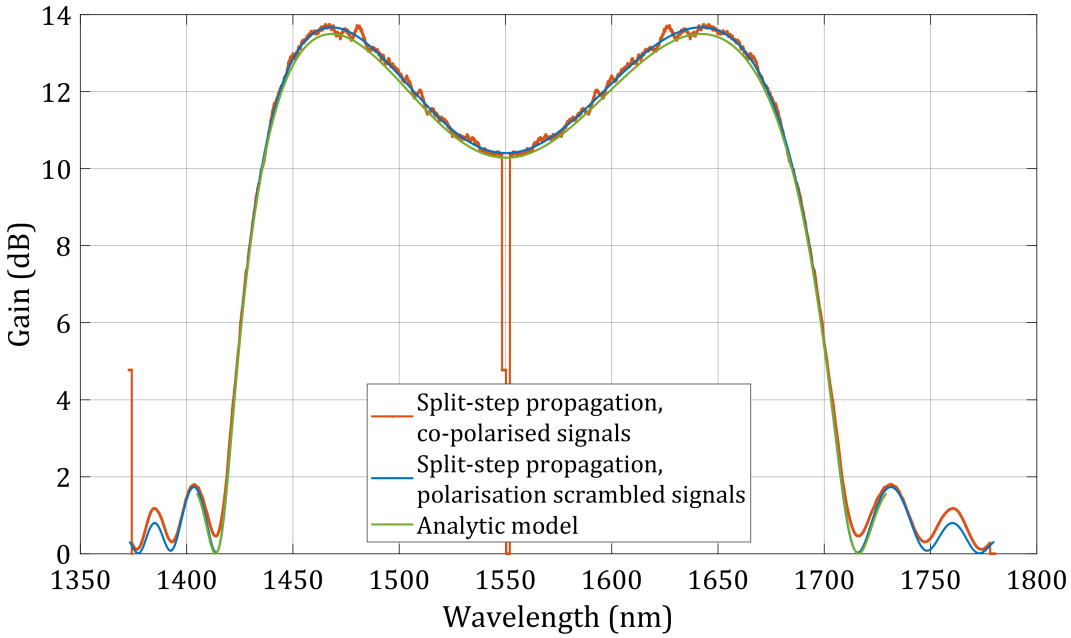

Figure A.1. Gain spectra obtained via dual polarisation split step simulation (orange and blue curves) show a good agreement with a known analytic solution (green curve). Orange curve is obtained using signals linearly co-polarised with the pump; blue curve is obtained using polarisation scrambled signals.

In addition, change of tolerance in range from 10^{-1} to 10^{-5} and change of step size in range from 0.005 m to 0.05 m have not induced any visual change of resulting gain spectrum. Therefore, the tolerance value of 10^{-5} and the step size of 0.01 m were considered to be sufficient for an accurate simulations. A change of the tolerance in so a wide range had no impact on the simulation result because in all cases the convergence was obtained within two iterations.

REFERENCES

[1] P. J. Winzer and D. T. Neilson, "From scaling disparities to integrated parallelism: a decathlon for a decade," *J. Light. Technol.*, vol. 35, no. 5, pp. 1099–1115, 2017.

[2] A. D. Ellis, J. Zhao, and D. Cotter, "Approaching the Non-Linear Shannon limit," *J. Light. Technol.*, vol. 28, no. 4, pp. 423–433, 2010.

[3] C. E. Shannon, "Communication in the presence of noise," *Proc. I.R.E.*, vol. 37, no. 1, pp. 10–21, 1949.

[4] F. Poletti, N. V. Wheeler, M. N. Petrovich, N. Baddela, E. N. Fokoua, J. R. Hayes, D. R. Gray, Z. Li, R. Slavík, and D. J. Richardson, "Towards high-capacity fibre-optic communications at the speed of light in vacuum," *Nat. Photonics*, vol. 7, no. 4, pp. 279–284, 2013.

[5] Z. Li, A. M. Heidt, J. M. O. Daniel, Y. Jung, S. U. Alam, and D. J. Richardson, "Thulium-doped fiber amplifier for optical communications at 2 μm," *Opt. Express*, vol. 21, no. 8, pp. 9289–9297, 2013.

[6] N. Simakov, Z. Li, Y. Jung, J. M. O. Daniel, P. Barua, P. C. Shardlow, S. Liang, J. K. Sahu, A. Hemming, W. A. Clarkson, S.-U. Alam, and D. J. Richardson, "High gain holmium-doped fibre amplifiers," *Opt. Express*, vol. 24, no. 13, pp. 13946–13956, 2016.

[7] Y. Emori, K. Tanaka, and S. Namiki, "100nm bandwidth flat-gain Raman amplifiers pumped and gain equalized by 12-wavelength-channel WDM laser diode unit," *Electron. Lett.*, vol. 35, no. 16, pp. 1355–1356, 1999.

[8] M. Jamshidifar, A. Vedadi, and M. E. Marhic, "Continuous-wave one-pump fiber optical parametric amplifier with 270 nm gain bandwidth," in *European Conference on Optical Communication (ECOC 2009)*, p. 1.1.4.

[9] M. E. Marhic, N. Kagi, T. Chiang, and L. G. Kazovsky, "Broadband fiber optical parametric amplifiers," *Opt. Lett.*, vol. 21, no. 8, pp. 573–575, 1996.

[10] R. Stolen and J. Bjorkholm, "Parametric amplification and frequency conversion in optical fibers," *IEEE J. Quantum Electron.*, vol. 18, no. 7, pp. 1062–1072, 1982.

[11] J. Hansryd, P. A. Andrekson, M. Westlund, J. Li, and P. O. Hedekvist, "Fiber-based optical parametric amplifiers and their applications," *IEEE J. Sel. Top. Quantum Electron.*, vol. 8, no. 3, pp. 506–520, 2002.

[12] Z. Tong, A. Bogris, M. Karlsson, and P. A. Andrekson, “Full characterization of the signal and idler noise figure spectra in single-pumped fiber optical parametric amplifiers,” *Opt. Express*, vol. 18, no. 3, pp. 2884–2893, 2010.

[13] A. Durécu-Legrand, C. Simonneau, D. Bayart, A. Mussot, T. Sylvestre, E. Lantz, H. Maillotte, Mussot, T. Sylvestre, E. Lantz, and H. Maillotte, “Impact of pump OSNR on noise figure for fiber-optical parametric amplifiers,” *IEEE Photonics Technol. Lett.*, vol. 17, no. 6, pp. 1178–1180, 2005.

[14] P. Kylemark, P. O. Hedekvist, H. Sunnerud, M. Karlsson, and P. A. Andrekson, “Noise characteristics of fiber optical parametric amplifiers,” *J. Light. Technol.*, vol. 22, no. 2, pp. 409–416, 2004.

[15] C. J. Mckinstrie and S. Radic, “Phase-sensitive amplification in a fiber,” *Opt. Express*, vol. 12, no. 20, pp. 4973–4979, 2004.

[16] Z. Tong, C. Lundström, P. A. Andrekson, C. J. McKinstrie, M. Karlsson, D. J. Blessing, E. Tipsuwannakul, B. J. Puttnam, H. Toda, and L. Grüner-Nielsen, “Towards ultrasensitive optical links enabled by low-noise phase-sensitive amplifiers,” *Nat. Photonics*, vol. 5, no. 7, pp. 430–436, 2011.

[17] R. Malik, A. Kumpera, M. Karlsson, and P. A. Andrekson, “Demonstration of ultra wideband phase-sensitive fiber optical parametric amplifier,” *Photonics Technol. Lett. IEEE*, vol. 28, no. 2, pp. 175–177, 2016.

[18] J. L. Blows and S. E. French, “Low-noise-figure optical parametric amplifier with a continuous-wave frequency-modulated pump,” *Opt. Lett.*, vol. 27, no. 7, pp. 491–493, 2002.

[19] T. Torounidis, P. A. Andrekson, and B. E. Olsson, “Fiber-optical parametric amplifier with 70-dB gain,” *IEEE Photonics Technol. Lett.*, vol. 18, no. 10, pp. 1194–1196, 2006.

[20] M. E. Marhic, “Introduction,” in *Fiber Optical Parametric Amplifiers, Oscillators and Related Devices*, New York: Cambridge University Press, 2008, pp. 1–8.

[21] S. Watanabe, S. Kaneko, and T. Chikama, “Long-haul fiber transmission using optical phase conjugation,” *Opt. Fiber Technol.*, vol. 2, no. 2, pp. 169–178, 1996.

[22] G. A. Nowak, Y.-H. Kao, T. J. Xia, M. N. Islam, and D. Nolan, “Low-power high-efficiency wavelength conversion based on modulational instability in high-nonlinearity fiber,” *Opt. Lett.*, vol. 23, no. 12, pp. 936–938, 1998.

[23] M. E. Marhic, K. K. Y. Wong, and L. G. Kazovsky, “Fiber optical parametric amplifiers with linearly or circularly polarized waves,” *J. Opt. Soc. Am. B*, vol. 20, no. 12, pp. 2425–2433, 2003.

[24] S. Takasaka and R. Sugizaki, “Polarization insensitive fiber optical parametric amplifier using a SBS suppressed diversity loop,” in *Optical Fiber Communication Conference (OFC 2016)*, p. M3D.4.

[25] M. F. C. Stephens, M. Tan, V. Gordienko, P. Harper, and N. J. Doran, “In-line and cascaded DWDM transmission using a 15dB net-gain polarization-insensitive fiber optical parametric amplifier,” *Opt. Express*, vol. 25, no. 20, pp. 24312–24325, 2017.

[26] J. B. Coles, B. P.-P. Kuo, N. Alic, S. Moro, C.-S. Bres, J. M. C. Boggio, P. A. Andrekson, M. Karlsson, and S. Radic, “Bandwidth-efficient phase modulation techniques for stimulated Brillouin scattering suppression in fiber optic parametric amplifiers,” *Opt. Express*, vol. 18, no. 17, pp. 18138–18150, 2010.

[27] M. E. Marhic, “Nonlinear crosstalk in fiber OPAs,” in *Fiber Optical Parametric Amplifiers, Oscillators and Related Devices*, New York: Cambridge University Press, 2008, pp. 281–302.

[28] M. Jamshidifar, A. Vedadi, and M. E. Marhic, “Reduction of four-wave-mixing crosstalk in a short fiber-optical parametric amplifier,” *IEEE Photonics Technol. Lett.*, vol. 21, no. 17, pp. 1244–1246, 2009.

[29] V. Gordienko, M. F. C. Stephens, and N. J. Doran, “Broadband Gain-Spectrum Measurement for Fiber Optical Parametric and Raman Amplifier,” *IEEE Photonics Technol. Lett.*, vol. 29, no. 16, pp. 1399–1402, 2017.

[30] V. Gordienko, M. F. C. Stephens, A. E. El-Taher, and N. J. Doran, “Novel broadband gain-specterum measurement technique for Raman and parametric amplifiers,” in *Optical Fiber Communication Conference (OFC 2017)*, p. W2A.11.

[31] V. Gordienko, M. F. C. Stephens, S. Takasaka, A. E. El-Taher, I. Phillips, W. Forysiak, R. Sugizaki, and N. J. Doran, “Demonstration of an ultra-flat Raman-enhanced fibre optical parametric amplifier (FOPA) with >110nm gain-bandwidth,” in *European Conference on Optical Communication (ECOC 2016)*.

[32] V. Gordienko, M. F. C. Stephens, A. E. El-Taher, and N. J. Doran, “Ultra-flat wideband single-pump Raman-enhanced parametric amplification,” *Opt. Express*, vol. 25, no. 5, pp. 4810–4818, 2017.

[33] V. Gordienko, M. F. C. Stephens, F. M. Ferreira, and N. J. Doran, “Gain spectrum shaping technique for one-pump fibre optical parametric amplifier (FOPA),” in *European Conference on Optical Communication (ECOC 2017)*, p. P1.SC1.16.

[34] V. Gordienko, M. Stephens, and N. Doran, “Towards Wide-Bandwidth Ultra-Flat FOPAs,” in *International Conference on Transparent Optical Networks (ICTON 2017)*, p. We.D5.1.

[35] G. P. Agrawal, “Introduction,” in *Nonlinear Fiber Optics*, 3rd ed., San Diego: Academic Press, 2001, pp. 1–30.

[36] Corning, “SMF-28 Ultra Optical Fiber,” 2014. [Online]. Available: https://www.corning.com/media/worldwide/coc/documents/Fiber/PI1424_11-14.pdf.

[37] ITU-T, “Recommendation G.652,” 2016. [Online]. Available: https://www.itu.int/rec/T-REC-G.652-201611-I/en.

[38] J. M. Senior and M. Y. Jamro, “Transmission characteristics of optical fibers,” in *Optical Fiber Communications Principles and Practice*, 3rd ed., Pearson Education Limited, 2009, pp. 86–169.

[39] M. E. Marhic, “Scalar OPA theory,” in *Fiber Optical Parametric Amplifiers, Oscillators and Related Devices*, New York: Cambridge University Press, 2008, pp. 31–77.

[40] J. M. Senior and M. Y. Jamro, “Optical fiber waveguides,” in *Optical Fiber Communications Principles and Practice*, 3rd ed., Pearson Education Limited, 2009, pp. 12–85.

[41] M. E. Marhic, “Properties of single-mode optical fibers,” in *Fiber Optical Parametric Amplifiers, Oscillators and Related Devices*, New York: Cambridge University Press, 2008, pp. 9–30.

[42] D. N. Payne and W. A. Gambling, “Zero material dispersion in optical fibres,” *Electron. Lett.*, vol. 11, no. 8, pp. 176–178, 1975.

[43] W. A. Gambling, H. Matsuura, and C. M. Ragdale, “Mode dispersion, material dispersion and profile dispersion in graded index single-mode fibers,” *IEE J. Microw. Opt. Acoust.*, vol. 3, no. 6, pp. 239–246, 1979.

[44] M. E. Marhic, K. K. Y. Wong, G. Kalogerakis, and L. G. Kazovsky, “Recent advances in the design and experimental implementation of fiber optical parametric amplifiers,” in *Proceedings of SPIE*, 2004, vol. 5623, pp. 691–704.

[45] B. P.-P. Kuo, J. M. Fini, L. Grüner-Nielsen, and S. Radic, "Dispersion-stabilized highly-nonlinear fiber for wideband parametric mixer synthesis," *Opt. Express*, vol. 20, no. 17, pp. 18611–18619, 2012.

[46] M. Hirano, T. Nakanishi, T. Okuno, and M. Onishi, "Broadband wavelength conversion over 193-nm by HNL-DSF improving higher-order dispersion performance," in *European Conference on Optical Communication (ECOC 2005)*, p. Th4.4.4.

[47] J. Hansryd, F. Dross, M. Westlund, P. A. Andrekson, and S. N. Knudsen, "Increase of the SBS threshold in a short highly nonlinear fiber by applying a temperature distribution," *J. Light. Technol.*, vol. 19, no. 11, pp. 1691–1697, 2001.

[48] K. K. Y. Wong, M. Marhic, and L. Kazovsky, "Temperature control of the gain spectrum of fiber optical parametric amplifiers," *Opt. Express*, vol. 13, no. 12, pp. 4666–4673, 2005.

[49] I. P. Kaminow, "Polarization in optical fibers," *IEEE J. Quantum Electron.*, vol. QE-17, pp. 15–22, 1981.

[50] K. Inoue and T. Mukai, "Signal wavelength dependence of gain saturation in a fiber optical parametric amplifier.," *Opt. Lett.*, vol. 26, no. 1, pp. 10–12, 2001.

[51] M. E. Marhic, "The optical gain spectrum," in *Fiber Optical Parametric Amplifiers, Oscillators and Related Devices*, New York: Cambridge University Press, 2008, pp. 110–145.

[52] M. E. Marhic, K. K. Y. Wong, and L. G. Kazovsky, "Wide-band tuning of the gain spectra of one-pump fiber optical parametric amplifiers," *IEEE J. Sel. Top. Quantum Electron.*, vol. 10, no. 5, pp. 1133–1141, 2004.

[53] M. E. Marhic, F. S. Yang, L. G. Kazovsky, and Y. Park, "Broadband fiber-optical parametric amplifiers and wavelength converters with low-ripple Chebyshev gain spectra," *Opt. Lett.*, vol. 21, no. 17, pp. 1354–1356, 1996.

[54] J. M. C. Boggio, S. Moro, E. Myslivets, J. R. Windmiller, N. Alic, and S. Radic, "155-nm continuous-wave two-pump parametric amplification," *IEEE Photonics Technol. Lett.*, vol. 21, no. 10, pp. 612–614, 2009.

[55] M. E. Marhic, "The nonlinear Shrodinger equation," in *Fiber Optical Parametric Amplifiers, Oscillators and Related Devices*, New York: Cambridge University Press, 2008, pp. 146–168.

[56] G. P. Agrawal, "Optical Solitons," in *Nonlinear Fiber Optics*, 3rd ed., San Diego: Academic Press, 2001, pp. 135–202.

[57] G. P. Agrawal, “Pulse propagation in fibers,” in *Nonlinear Fiber Optics*, 3rd ed., San Diego: Academic Press, 2001, pp. 31–62.

[58] A. S. Y. Hsieh, G. K. L. Wong, S. G. Murdoch, S. Coen, F. Vanholsbeeck, R. Leonhardt, and J. D. Harvey, “Combined effect of Raman and parametric gain on single-pump parametric amplifiers,” *Opt. Express*, vol. 15, no. 13, pp. 8104–8114, 2007.

[59] M. E. Marhic, “Vector OPA theory,” in *Fiber Optical Parametric Amplifiers, Oscillators and Related Devices*, New York: Cambridge Univ. Press, 2008, pp. 78–109.

[60] K. K. Y. Wong, M. E. Marhic, K. Uesaka, and L. G. Kazovsky, “Polarization-independent two-pump fiber-optical parametric amplifier,” *IEEE Photonics Technol. Lett.*, vol. 14, no. 7, pp. 911–913, 2002.

[61] H. Hu, R. M. Jopson, A. H. Gnauck, M. Dinu, S. Chandrasekhar, C. Xie, and S. Randel, “Parametric amplification, wavelength conversion, and phase conjugation of a 2.048-Tbit/s WDM PDM 16-QAM signal,” *J. Light. Technol.*, vol. 33, no. 7, pp. 1286–1291, 2015.

[62] K. K. Y. Wong, M. E. Marhic, K. Uesaka, and L. G. Kazovsky, “Polarization-independent one-pump fiber-optical parametric amplifier,” *IEEE Photonics Technol. Lett.*, vol. 14, no. 11, pp. 1506–1508, 2002.

[63] M. F. C. Stephens, V. Gordienko, and N. J. Doran, “20 dB net-gain polarization-insensitive fiber optical parametric amplifier with >2 THz bandwidth,” *Opt. Express*, vol. 25, no. 9, pp. 10597–10609, 2017.

[64] M. F. C. Stephens, M. Tan, I. D. Phillips, S. Sygletos, P. Harper, and N. J. Doran, “114Tb/s DP-QPSK WDM polarization-diverse optical phase conjugation,” *Opt. Express*, vol. 22, no. 10, p. 11840, 2014.

[65] M. Jazayerifar, I. Sackey, R. Elschner, T. Richter, L. Molle, P. W. Berenguer, C. Schubert, K. Jamshidi, and K. Petermann, “Impact of Brillouin backscattering on signal distortions in single-fiber diversity loop based polarization-insensitive FOPAs,” *J. Light. Technol.*, vol. 35, no. 19, pp. 4137–4144, 2017.

[66] M. F. C. Stephens, V. Gordienko, and N. J. Doran, “Reduced crosstalk, polarization insensitive fiber optical parametric amplifier (PI FOPA) for WDM applications,” in *Optical Fiber Communication Conference (OFC 2018)*, p. W3D.4.

[67] E. Desurvire, “Fundamentals of noise in optical fiber amplifiers,” in *Erbium-doped fiber amplifiers principles and applications*, New Jersey: John Wiley & Sons Inc., 2002, pp. 65–153.

[68] K. Rottwitt and P. Tidemand-Lichtenberg, “Material response in the frequency domain, susceptibility tensors,” in *Nonlinear Optics Principles and Applications*, CRC Press, 2015, pp. 63–86.

[69] G. P. Agrawal, “Stimulated Raman scattering,” in *Nonlinear Fiber Optics*, 3rd ed., San Diego: Academic Press, 2001, pp. 298–354.

[70] R. H. Stolen, W. J. Tomlinson, H. A. Haus, and J. P. Gordon, “Raman response function of silica-core fibers,” *J. Opt. Soc. Am. B*, vol. 6, no. 6, p. 1159, 1989.

[71] Q. Lin and G. P. Agrawal, “Raman response function for silica fibers,” *Opt. Lett.*, vol. 31, no. 21, pp. 3086–3088, 2006.

[72] G. P. Agrawal, “Stimulated Brillouin Scattering,” in *Nonlinear Fiber Optics*, 3rd ed., San Diego: Academic Press, 2001, pp. 355–388.

[73] D. A. Fishman and J. A. Nagel, “Degradations due to stimulated Brillouin scattering in multigigabit intensity-modulated fiber-optic systems,” *J. Light. Technol.*, vol. 11, no. 11, pp. 1721–1728, 1993.

[74] M. O. van Deventer and A. J. Boot, “Polarization properties of stimulated Brillouin scattering in single-mode fibers,” *J. Light. Technol.*, vol. 12, no. 4, pp. 585–590, 1994.

[75] P. Narum, A. L. Gaeta, M. D. Skeldon, and R. W. Boyd, “Instabilities of laser beams counterpropagating through a Brillouin-active medium,” *J. Opt. Soc. Am. B*, vol. 5, no. 3, pp. 623–628, 1988.

[76] J. Zhang and M. R. Phillips, “Modeling intensity noise caused by stimulated Brillouin scattering in optical fibers,” in *Conference on Lasers and Electro-Optics (CLEO 2005)*, p. CMH6.

[77] N. Yoshizawa and T. Imai, “Stimulated Brillouin scattering suppression by means of applying strain distribution to fiber with cabling,” *J. Light. Technol.*, vol. 11, no. 10, pp. 1518–1522, 1993.

[78] R. Engelbrecht, M. Mueller, and B. Schmauss, “SBS shaping and suppression by arbitrary strain distributions realized by a fiber coiling machine,” *2nd IEEE LEOS Winter Top. WTM 2009*, no. 1, pp. 248–249, 2009.

[79] K. Shiraki, M. Ohashi, and M. Tateda, “Suppression of stimulated Brillouin scattering in a fibre by changing the core radius,” *Electron. Lett.*, vol. 31, no. 8, pp. 668–669, 1995.

[80] K. Tsujikawa, K. Nakajima, Y. Miyajima, and M. Ohashi, "New SBS suppression Fiber with uniform chromatic dispersion to enhance four-wave mixing," *IEEE Photonics Technol. Lett.*, vol. 10, no. 8, pp. 1139–1141, 1998.

[81] K. Shiraki, M. Ohashi, and M. Tateda, "SBS threshold of a fiber with a brillouin frequency shift distribution," *J. Light. Technol.*, vol. 14, no. 1, pp. 50–57, 1996.

[82] J. M. C. Boggio, A. Guimaraes, F. A. Callegari, J. D. Marconi, and H. L. Fragnito, "Q penalties due to pump phase modulation and pump RIN in fiber optic parametric amplifiers with non-uniform dispersion," *Opt. Commun.*, vol. 249, pp. 451–472, 2005.

[83] A. Durecu-Legrand, A. Mussot, C. Simonneau, D. Bayart, T. Sylvestre, E. Lantz, and H. Mailotte, "Impact of pump phase modulation on system performance of fibre-optical parametric amplifiers," *Electron. Lett.*, vol. 41, no. 6, 2005.

[84] F. S. Yang, M. E. Marhic, and L. G. Kazovsky, "CW fibre optical parametric amplifier with net gain and wavelength conversion efficiency >1," *Electron. Lett.*, vol. 32, no. 25, pp. 2336–2338, 1996.

[85] M. E. Marhic and G. K. P. Lei, "Hybrid fiber optical parametric amplifiers for broadband optical communication systems," in *International Conference on Transparent Optical Networks (ICTON 2014)*, p. TH.B2.4.

[86] J. M. C. Boggio, J. D. Marconi, S. R. Bickham, and H. L. Fragnito, "Spectrally flat and broadband double-pumped fiber optical parametric amplifiers.," *Opt. Express*, vol. 15, no. 9, pp. 5288–5309, 2007.

[87] J. M. C. Boggio, C. Lundström, J. Yang, H. Sunnerud, and P. A. Andrekson, "Double-pumped FOPA with 40 dB flat gain over 81 nm bandwidth," in *European Conference on Optical Communication (ECOC 2008)*, p. Tu.3.B.5.

[88] T. Torounidis and P. Andrekson, "Broadband single-pumped fiber-optic parametric amplifiers," *IEEE Photonics Technol. Lett.*, vol. 19, no. 9, pp. 650–652, 2007.

[89] J. Kim, Ö. Boyraz, J. H. Lim, and M. N. Islam, "Gain enhancement in cascaded fiber parametric amplifier with quasi-phase matching: Theory and experiment," *J. Light. Technol.*, vol. 19, no. 2, pp. 247–251, 2001.

[90] M. E. Marhic, F. S. Yang, M. Ho, and L. G. Kazovsky, "High-nonlinearity fiber optical parametric amplifier with periodic dispersion compensation," *J. Light. Technol.*, vol. 17, no. 2, pp. 210–215, 1999.

[91] C. Fourcade-Dutin, Q. Bassery, D. Bigourd, A. Bendahmane, A. Kudlinski, M. Douay, and A. Mussot, "12 THz flat gain fiber optical parametric amplifiers with dispersion varying fibers," *Opt. Express*, vol. 23, no. 8, pp. 10103–10110, 2015.

[92] J. Hansryd and P. A. Andrekson, "Broad-band continuous-wave-pumped fiber optical parametric amplifier with 49-dB gain and wavelength-conversion efficiency," *IEEE Photonics Technol. Lett.*, vol. 13, no. 3, pp. 194–196, 2001.

[93] L. Provino, A. Mussot, E. Lantz, T. Sylvestre, and H. Mailotte, "Broadband and flat parametric amplifiers with a multisection dispersion-tailored nonlinear fiber arrangement," *J. Opt. Soc. Am. B*, vol. 20, no. 7, pp. 1532–1537, 2003.

[94] S. Takasaka, Y. Taniguchi, M. Takahashi, J. Hiroshi, M. Tadakuma, H. Matsuura, K. Doi, and R. Sugizaki, "Quasi phase-matched FOPA with 50 nm gain bandwidth using dispersion stable highly nonlinear fiber," in *Optical Fiber Communication Conference (OFC 2014)*, p. W3E.2.

[95] M. F. C. F. C. Stephens, I. D. D. Phillips, P. Rosa, P. Harper, and N. J. J. Doran, "Improved WDM performance of a fibre optical parametric amplifier using Raman-assisted pumping," *Opt. Express*, vol. 23, no. 2, p. 902, 2015.

[96] Y. Taniguchi, J. Hiroishi, M. Takahashi, and R. Sugizaki, "Nonlinear optical fiber, nonlinear optical device, and optical signal processor," European Patent 1988411A1, 2008.

[97] A. E. El-Taher, J. D. Ania-Castañón, V. Karalekas, and P. Harper, "High efficiency supercontinuum generation using ultra-long Raman fiber cavities," *Opt. Express*, vol. 17, no. 20, pp. 17909–17915, 2009.

[98] J. Wang, S. Liang, Q. Kang, Y. Jung, S. Alam, and D. J. Richardson, "Broadband silica-based thulium doped fiber amplifier employing multi-wavelength pumping," *Opt. Express*, vol. 24, no. 20, pp. 23001–23008, 2016.

[99] S. A. Filatova, V. A. Kamynin, V. B. Tsvetkov, O. I. Medvedkov, and A. S. Kurkov, "Gain spectrum of the Ho-doped fiber amplifier," *Laser Phys. Lett.*, vol. 12, no. 9, 2015.

[100] S. V. Firstov, S. V. Alyshev, K. E. Riumkin, V. F. Khopin, A. N. Guryanov, M. A. Melkumov, and E. M. Dianov, "A 23-dB bismuth-doped optical fiber amplifier for a 1700-nm band," *Sci. Rep.*, vol. 6, p. 28939, 2016.

[101] J. L. Blows, "Design strategy for controlling four-wave mixing-induced crosstalk between channels in a fibre optical parametric amplifier," *Opt. Commun.*, vol. 236, pp. 115–122, 2004.

[102] W. Eickhoff, Y. Yen, and R. Ulrich, "Wavelength dependence of birefringence in single-mode fiber," *Appl. Opt.*, vol. 20, no. 19, pp. 3428–3435, 1981.

[103] F. Yaman, Q. Lin, S. Radic, and G. P. Agrawal, "Impact of dispersion fluctuations on dual-pump fiber-optic parametric amplifiers," *IEEE Photonics Technol. Lett.*, vol. 16, no. 5, pp. 1292–1294, 2004.

[104] M. F. C. Stephens, A. Redyuk, S. Sygletos, I. D. Phillips, P. Harper, K. J. Blow, and N. J. Doran, "The impact of pump phase-modulation and filtering on WDM signals in a fibre optical parametric amplifier," *Opt. Fiber Commun. Conf. (OFC 2015)*, p. W2A.43.

[105] J. D. Love, R. A. Sammut, and A. W. Snyder, "Birefringence in elliptically deformed optical fibres," *Electron. Lett.*, vol. 15, no. 20, pp. 615–616, 1979.

[106] X. Xu, T. I. Yuk, and K. K. Y. Wong, "Distributed parametric amplification at 1.3 μm in 25-km single-mode fiber," in *International conference on Photonics in Switching (PS)*, 2012.

[107] Y. Feng, L. Taylor, and D. B. Calia, "Multiwatts narrow linewidth fiber Raman amplifiers," *Opt. Express*, vol. 16, no. 15, pp. 10927–10932, 2008.

[108] J. Shi, S. Alam, and M. Ibsen, "Highly efficient Raman distributed feedback fibre lasers," *Opt. Express*, vol. 20, no. 5, pp. 5082–5091, 2012.

[109] C. Vergien, I. Dajani, and C. Robin, "18 W single-stage single-frequency acoustically tailored Raman fiber amplifier," *Opt. Lett.*, vol. 37, no. 10, pp. 1766–1768, 2012.

[110] L. Zhang, J. Hu, J. Wang, and Y. Feng, "Stimulated-Brillouin-scattering-suppressed high-power single-frequency polarization-maintaining Raman fiber amplifier with longitudinally varied strain for laser guide star," *Opt. Lett.*, vol. 37, no. 22, pp. 4796–4798, 2012.

[111] Y. R. Shen and N. Bloembergen, "Theory of stimulated brillouin and raman scattering," *Phys. Rev.*, vol. 137, no. 6A, pp. 1787–1805, 1965.

[112] D. A. Chestnut, C. J. S. De Matos, and J. R. Taylor, "Raman-assisted fiber optical parametric amplifier and wavelength converter in highly nonlinear fiber," *J. Opt. Soc. Am. B*, vol. 19, no. 8, pp. 1901–1904, 2002.

[113] S. H. Wang, L. Xu, P. K. A. Wai, and H. Y. Tam, "All-optical wavelength conversion using multi-pump Raman-assisted four-wave mixing," in *Optical Fiber Communication Conference (OFC 2007)*, p. OWQ1.

[114] IPG Photonics, "PYL-R and PYL-R2 Series." [Online]. Available: https://www.equipland.com/objects/catalog/product/extras/23753_pl.pdf.

[115] C. R. S. Fludger and R. J. Mears, “Electrical measurements of multipath interference in distributed Raman amplifiers,” *J. Light. Technol.*, vol. 19, no. 4, pp. 536–545, 2001.

[116] G. E. Obarski and P. D. Hale, “How to measure relative intensity noise in lasers,” *Laser Focus World*, vol. 35, no. 5, pp. 273–277, 1999.

[117] OFS, “AllWave® One Fiber - Zero Water Peak.” [Online]. Available: https://fiber-optic-catalog.ofsoptics.com/Asset/AllWave-One-Fiber-160-web.pdf.

[118] IPG Photonics, “EAR Series: Booster EDFA Amplifiers.” [Online]. Available: http://www.ipgphotonics.com/en/445/Widget/Booster+EDFA+Amplifiers+Datasheet.pdf.

[119] C. J. S. de Matos, D. A. Chestnut, P. C. Reeves-Hall, and J. R. Taylor, “Continuous-wave-pumped Raman-assisted fiber optical parametric amplifier and wavelength converter in conventional dispersion-shifted fiber,” *Opt. Lett.*, vol. 26, no. 20, p. 1583, 2001.

[120] C. H. H. Uang and C. H. S. Hu, “Raman-enhanced optical phase conjugator in WDM transmission systems,” vol. 27, no. 2009, pp. 439–442, 2015.

[121] K. K. Y. Wong, M. E. Marhic, and L. G. Kazovsky, “Phase-conjugate pump dithering for high-quality idler generation in a fiber optical parametric amplifier,” *IEEE Photonics Technol. Lett.*, vol. 15, no. 1, pp. 33–35, 2003.

[122] I. Sackey, F. Da Ros, T. Richter, R. Elschner, M. Jazayerifar, C. Meuer, C. Peucheret, K. Petermann, and C. Schubert, “Design and performance evaluation of an OPC device using a dual-pump polarization-independent FOPA,” in *European Conference on Optical Communication (ECOC 2014)*, p. Tu.1.4.4.

[123] R. Elschner, T. Richter, L. Molle, C. Schubert, and K. Petermann, “Single-pump FWM-wavelength conversion in HNLF using coherent receiver-based electronic compensation,” in *European Conference on Optical Communication (ECOC 2010)*, p. P3.17.